Alexandra Sofia Dias Lopes

Bachelor of Science in Biomedical Engineering

Bio-Radar Applications for Remote Vital Signs Monitoring

Dissertation submitted in partial fulfillment
of the requirements for the degree of

Master of Science in
Biomedical Engineering

Adviser: Professor Doctor Hugo Gamboa, Auxiliar Professor, NOVA University of Lisbon

Examination Committee

Chair: Doctor Paulo António Martins Ferreira Ribeiro, FCT-NOVA
Rapporteur: Doctor Luís Miguel Nunes Pereira, FCT-NOVA
Member: Doctor Hugo Filipe Silveira Gamboa, FCT-NOVA

FACULDADE DE CIÊNCIAS E TECNOLOGIA
UNIVERSIDADE NOVA DE LISBOA

November, 2020

Bio-Radar Applications for Remote Vital Signs Monitoring

This document was created using the (pdf)LaTeX processor, based on the "novathesis" template[1], developed at the Dep. Informática of FCT-NOVA [2].
[1] https://github.com/joaomlourenco/novathesis [2] http://www.di.fct.unl.pt

For the world, but especially to my mother.

Acknowledgements

First, I would like to thank my adviser, Professor Hugo Gamboa, for giving me the opportunity of developing this captivating and futurist work, to Daniel Osório for sharing ideas and experiences during this process, to my full-time reviewers: Joana and Wilson, and later on (but always on time) Rita and Bernardo, a big thanks for your availability and attention.

To my parents, Vanda and Rui. To my mother who never gave up on us, and to my dad, who even not knowing, gave me the opportunity to be whoever I wanted to be. To my sister: I am not buying you more books for review exchanges.

To all my colleagues and friends of the Biomedical Engineering 2015-2020 Class with who I shared the best memories of academic life. I am not mentioning your names because you are soooo many.

To everyone who joined me in new and challenging projects that cheated us countless sleep hours: To my friends of ANEEB, where together, we connected the entire biomedical engineering student community in one unique place; To my friends of NBN and ENEEB, which made NOVA university a more biomedical engineering friendly centre; To my wonder and hard workers Tec2Med friends and to my colleagues from C-mo who always shared with me the dedication and ambition to go further.

To my long time friends, who stay with me even when I was too busy for our "coffee times", and last but not the least, to my best quarantine and thesis buddies: my doggies Kiko and Micas.

My Knowledge is a Gaussian Curve.

Abstract

Nowadays, most vital signs monitoring techniques used in a medical context and/or daily life routines require direct contact with skin, which can become uncomfortable or even impractical to be used regularly. Radar technology has been appointed as one of the most promising contactless tools to overcome these hurdles. However, there is a lack of studies that cover a comprehensive assessment of this technology when applied in real-world environments. This dissertation aims to study radar technology for remote vital signs monitoring, more specifically, in respiratory and heartbeat sensing.

Two off-the-shelf radars, based on impulse radio ultra-wideband and frequency modulated continuous wave technology, were customized to be used in a small proof of concept experiment with 10 healthy participants. Each subject was monitored with both radars at three different distances for two distinct conditions: breathing and voluntary apnea. Signals processing algorithms were developed to detect and estimate respiratory and heartbeat parameters, assessed using qualitative and quantitative methods.

Concerning respiration, a minimum error of 1.6% was found when radar respiratory peaks signals were directly compared with their reference, whereas a minimum mean absolute error of 0.3 RPM was obtained for the respiration rate. Concerning heartbeats, their expression in radar signals was not as clear as the respiration ones, however a minimum mean absolute error of 1.8 BPM for heartbeat was achieved after applying a novel selective algorithm developed to validate if heart rate value was estimated with reliability.

The results proved the potential for radars to be used in respiratory and heartbeat contactless sensing, showing that the employed methods can be already used in some motionless situations. Notwithstanding, further work is required to improve the developed algorithms in order to obtain more robust and accurate systems.

Keywords: RADAR; IR-UWB; FMCW; Respiratory Rate; Heart Rate; Contactless.

Resumo

Atualmente, a maioria das técnicas usadas para a monitorização de sinais vitais em contexto médicos e/ou diário requer contacto direto com a pele, o que poderá tornar-se incómodo ou até mesmo inviável em certas situações. A tecnologia radar tem vindo a ser apontada como uma das mais promissoras ferramentas para medição de sinais vitais à distância e sem contacto. Todavia, são necessários mais estudos que permitam avaliar esta tecnologia quando aplicada a situações mais reais. Esta dissertação tem como objetivo o estudo da tecnologia radar aplicada no contexto de medição remota de sinais vitais, mais concretamente, na medição de atividade respiratória e cardíaca.

Dois aparelhos radar, baseados em tecnologia banda ultra larga por rádio de impulso e em tecnologia de onda continua modulada por frequência, foram configurados e usados numa prova de conceito com 10 participantes. Cada sujeito foi monitorizado com cada um dos radar em duas situações distintas: respirando e em apneia voluntária. Algoritmos de processamento de sinal foram desenvolvidos para detetar e estimar parâmetros respiratórios e cardíacos, avaliados através de métodos qualitativos e quantitativos.

Em relação à respiração, o menor erro obtido foi de 1,6% quando os sinais de radar respiratórios foram comparados diretamente com os sinais de referência, enquanto que, um erro médio absoluto mínimo de 0,3 RPM foi obtido para a estimação da frequência respiratória via radar. A expressão cardíaca nos sinais radar não se revelou tão evidente como a respiratória, no entanto, um erro médio absoluto mínimo de 1,8 BPM foi obtido para a estimação da frequência cardíaca após a aplicação de um novo algoritmo seletivo, desenvolvido para validar a confiança dos valores obtidos.

Os resultados obtidos provaram o potencial do uso de radares na medição de atividade respiratória e cardíaca sem contacto, sendo esta tecnologia viável de ser implementada em situações onde não existe muito movimento. Não obstante, os algoritmos desenvolvidos devem ser aperfeiçoados no futuro de forma a obter sistemas mais robustos e precisos.

Palavras-chave: RADAR; *IR-UWB*; *FMCW*; Frequência respiratória; Frequência cardíaca; Sem contacto.

Contents

List of Figures

List of Tables

Acronyms

AD	Arctangent Demodulation
ADC	Analog-to-Digital Converter
AE	Absolute Error
AM	Amplitude Modulation
API	Application Programming Interface
BCG	Ballistocardiography
BLE	Bluetooth
BPM	Beat per Minute
CFAR	Constant False Alarm Rate
CNN	Convolutional Neural Network
CSD	Complex Signal Demodulation
CVD	Cardiovascular Diseases
CW	Continuous Wave
CWT	Continuous Wavelet Transformation
CZT	Chirp Z-Transform
DC	Direct Current
DSP	Digital Signal Processing
ECG	Electrocardiography
EEMD	Ensemble Empirical Mode Decomposition
EMD	Empirical Mode Decomposition
EMG	Electromyography
ETSI	European Telecommunications Standards Institute
FCC	Federal Communications Commission
FFT	Fast Fourier Transform

FIR	Finite Impulse Response
FMCW	Frequency Modulated Continuous Wave
FN	False Negative
FP	False Positive
FPS	Frames per Second
HHT	Hilbert-Huang Transform
HR	Heart Rate
HSA	Hilbert Spectral Analysis
I/Q	In-phase and Quadrature
ICNIRP	International Commission on Non-Ionizing Radiation Protection
IF	Intermediated Frequency
IoT	Internet of Things
IPI	Inter-Pulse Interval
IR	Infrared
IR-UWB	Impulse-Radio Ultra Wideband
LED	Light-emitting diode
LTS	Linear Trend Subtraction
MAE	Mean Absolute Error
MCU	Micro Controller Unit
MHOC	Multiple High Order Cumulant
MIMO	Multiple-In Multiple-Out
MTI	Motion Target Indicator
PCA	Principal Component Analysis
PD	Photodetector
PPG	Photoplethysmography
PRF	Pulse Repetition Frequency
RADAR	Radio Detection and Ranging
RF	Radio Frequency
RPM	Respiration per Minute
RR	Respiratory Rate
RX	Receiver

SD	Standard Deviation
SFCW	Step Frequency Continuous Wave
SNCR	Signal-to-Noise Clutter Ratio
SNR	Signal-to-Noise Ratio
SoC	System on Chip
SPI	Serial Peripheral Interface
SRR	Short Radar Range
SSAC	Selective Short-Term Autocorrelation
SSM	State-Space Method
ST	Swept Threshold
STFT	Short-Time Fourier Transform
SVD	Singular Value Decomposition
TI	Texas Instruments
ToF	Time-of-Flight
TP	True Positive
TX	Transmitter
UART	Universal Asynchronous Receiver-Transmitter
USB	Universal Serial Bus
UWB	Ultra Wideband
VMD	Variational Mode Decomposition
Wi-Fi	Wireless Fidelity
XEP	XeThru Embedded Platform

Chapter 1

Introduction

1.1 Motivation

Vital signs can be considered a universal language used to tell a history of the patient's health status, crucial in the evaluation of several conditions in the medical context [1]. These measurements aid physicians in diagnostic decisions, surgical interventions assessment, and proffering options concerning the response of patients to therapies. Moreover, consistent vital signs monitoring is crucial for the early detection of patient's clinical deterioration in hospital settings [2].

Out of all, Respiratory Rate (RR) and Heart Rate (HR) are classified as the most important vital signs indicators [3, 4]. Subtle changes in those physiological signals are related to responses in physical or physiological stress that can be associated with critical conditions. Therefore, the continuous monitorization of respiratory and heart related parameters is of paramount importance in the prediction of acute illnesses, helping the medical teams to act in the reversion of potential adverse events [5]. In fact, cardiovascular diseases are the number one cause of death in the world [6]. Most of these deaths could be avoided through the continuous monitorization of vital signs since manifestation in heart and respiratory signals start to be detected up to 8 hours before an acute health episode [7].

Over the years, several techniques for cardiorespiratory signals monitoring have been emerging, being increasingly adapted to small and wearable solutions to provide better comfort-quality signals ratio during patient's recordings [8]. However, most of the current and high-accurate systems in medical backgrounds are large, non-portable and require the use of many wires and skin-contact elements. In spite of being essential in routine medical exams, contact vital signs measurement techniques can bring a lot of discomfort in life quality of long-term admitted patients and may even make some necessary

Figure 1.1: Motivations for the use of contactless vital signs monitoring techniques.

procedures impossible for patient's recovery in clinical practice. One of the most clear example is related to patients with extensive burn injuries, in which the lack of natural skin and application of protective ointments inhibit the adherence of the electrocardiogram disks [9]. Other common related problems are skin irritations and redness due to the electrode material in contact with the body surface, so usually used in ambulatory exams and wearables devices for long-term monitorization [10]. Lastly, some medical exams as polysomnographys [11] may have their results compromised because of the numerous cables that can affect the sleep quality of the monitored subject.

The reasons mentioned above are just a few examples that call for new non-contact vital signs monitoring solutions. Radio Detection and Ranging (RADAR) technology, used for tracking objects, is pointed out as one of the most promising technologies solutions which have been suggested in most recent years. Moreover, radar technology applied as remote vital signs monitoring technique can bring not only benefits for the medical field but also in daily life applications such as automotive driving safety [12], newborn babies activity monitoring [13] and in-home monitoring [14].

Nevertheless, despite the clear advantages that radar technology could give in the continuous vital signs monitoring field, efforts need to be made in human radar application for better quality signals, mainly when applied to real world environments. External noise and motion artefacts continue to be reported as one of the major obstacles in the use of radar sensors as a continuous vital signs monitoring tool. Notwithstanding, promising algorithms together with more robust radar architectures can be the solution for higher precision radar vital signs extraction. Therefore, this technology continues to call for more studies that could bring new answers and solutions for precise applications.

More recently, the COVID-19 pandemic has increasingly intensified the need for non-contact vital signs monitoring techniques to reduce contagion hypothesis. In a health crisis as the current one that the world is facing, the subject's data is a strong indicator of health that can also be used to prevent some potential focus of infections. Moreover, while tests and clinical accesses are limited to avoid potential contact forms, remote vital signs tracking will enable doctors to assess the likelihood of viral infection in a patient's vital signs status.

1.2 Thesis Goals

The development of a complete wireless physiological monitoring system using radar technology was proposed by PLUX - Wireless Biosignals S.A [15]. PLUX is an innovative company recognized for the creation of advanced biosignal monitoring platforms that integrates wearable body sensors such as Electrocardiography (ECG), Electromyography (EMG), respiratory bands, and accelerometers combined with wireless connectivity and software applications.

The addition of a new radar sensor module from which biosignals could be measured at a distance, and without the need of a contact with the human body is well-aligned with PLUX mission. Moreover, this new product will contribute to advances in contactless biosignals monitoring studies since it would be integrated into PLUX software environment: a user-friendly and auxiliary tool for physiological signals extraction developed for researchers and physiotherapists.

Thus, this dissertation aims to study, develop and evaluate radars and signal processing techniques, to test the following hypothesis:

Radar technology is sufficiently accurate to be used in a future Wireless Bio-Radar product for non-contact respiratory rate and heart rate monitoring.

The development of this novel product can open doors for more research in this area and bring new opportunities to non-contact remote vital signs sensing applications. All the methods in this dissertation were developed considering all the rules of security and costs that a commercial product must guarantee. Hence, in order to achieve the main goal outlined above, the following objectives were distinguished:

1. Investigation of the use of radar technology in physiological signals acquisition.
2. Selection and configuration of an off-the-shelf radar sensor suitable to be used in this context.
3. Development of algorithms for radar signals processing and vital signs extraction.
4. Development and implementation of a protocol for radar data acquisition.
5. Assessment of the developed methods and collected bio-radar signals.
6. Idealization of a small product prototype based on results achievement and commercial assessment.

1.3 Thesis Outlines

This thesis is structured in seven chapters summarized below:

Chapter 1: Motivation, context and main objectives of this dissertation are described.

Chapter 2: State-of-the-art, where the current techniques used in vital signs monitoring, including radar techniques, are described.

Chapter 3: Theoretical concepts of radar technology based on cardiorespiratory sensing. The fundamentals of the radar type used in this study are presented as well as the vital signs mathematical models associated with each one of them. The cardiorespiratory system is also reviewed.

Chapter 4: The multi-purpose radar sensors used are presented as well as all the configuration performed in these sensors to optimize them for vital signs sensing acquisition and the data acquisition.

Chapter 5: A small proof of concept with previously configured sensors is performed. Signals processing algorithms and statistical tools used to evaluate radar data are here described.

Chapter 6: Results and discussion, concerns about the differences between the acquired sensors are given. Then, respiratory and heartbeat signals, as well as RR and HR parameters extracted from the developed signals processing methods are assessed.

Chapter 7: It is the concluding chapter where all the proposed goals are reviewed and answered. A general conclusion about the commercial viability of the future Bio-Radar product is also given.

In addition, four Appendices are presented at the end of this document with some relevant information and applications resulted from the developed work:

Appendix A: Detailed tables with metrics obtained from results.
Appendix B: General flow-chart designed to guide and help readers throughout the reading of implemented methodology.
Appendix C: Short report with some considerations about which studied radar should be used in a future wireless product, considering diverse commercial factors.
Appendix D: Presentation of a small prototype developed to show the concept of Wireless Bio-Radar sensor, using the methods and results obtained in this dissertation.

Chapter 2

State of the Art

Nowadays solutions for cardiorespiratory vital signs detection have been applied in several contexts, from clinical and diagnosis to healthcare and self-tracking activity applications. A brief summary of the current techniques for acquiring vital signs with a particular focus on novel radar techniques will be given in this chapter. The most common devices, signal processing methods and applications using radar sensors for physiological sensing are here explored.

2.1 Vital Signs Monitoring Systems

Among the five common vital signs - body temperature, blood pressure, pulse oximetry, respiratory rate (RR) and heart rate (HR) - RR and HR are the two most important vital signs used in the prediction of severe illnesses. Hence, several techniques for monitorization of these parameters have been studied, applied and improved over the last decades. These techniques can be divided into two principal groups: **contact-based methods** and **contactless methods**. Throughout this dissertation, vital signs terminology will be exclusively used to refer only RR and HR physiological parameters.

2.1.1 Contact-based Methods

The electrocardiography (ECG) is a simple and standard clinical test that records the electrical activity of the heart, attaching a varied quantity of electrodes on a subject's skin [16]. It is one of the most common and useful tools available to monitor the heart's health in a clinical context to diagnose Cardiovascular Diseases (CVD) [17]. In clinical and practical terms, the traditional 12-lead clinical ECG and the portable ambulatory ECG systems are the most common ECG acquisition techniques - Figure 2.1. An ECG lead

is obtained according to the localization of electrodes, representing the differences in electrical potentials measured in two points in space. In the 12-lead ECG, ten electrodes are affixed to the limbs and chest producing up to 12 groups of ECG signals derivation [18]. These robust measurements are usually practised in a medical environment, where data is collected through cables and posterior connected to a direct signal processing unit.

In contrast, ambulatory ECG monitoring systems are developed to be smaller and portable to render a view of ECG data over an extended interval of time [19]. These systems are more sensitive to detect CVD condition as they offer the possibility to review the recorded ECG data during the routine activity of the subjects and outside the clinical setting [20]. On the other hand, ambulatory ECG devices provide less information since they normally have only three leads, and signals are significantly contaminated by motion artefacts. Notwithstanding, new approaches to design devices for ambulatory, system-on-chip and commercial ECG systems have been proposed with the technology improvement, allowing better quality signals. More flexible and dry capacitive electrodes for long term monitorings, wireless raw data transmission between electrodes and main computer based on Bluetooth (BLE) or ZigBee technology, and real time-monitoring software processors, are some of the upgrades that have been made to wearable ECG devices [21].

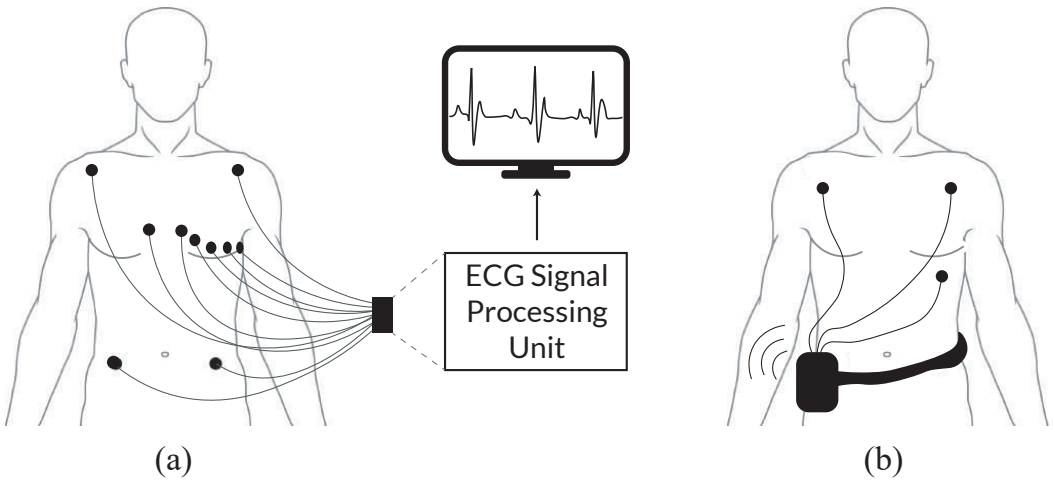

Figure 2.1: Representation of two popular Electrocardiography (ECG) systems based on a (a) 12-lead clinical ECG setting and (b) 3-lead ECG ambulatory device.

The Photoplethysmography (PPG) is an optical technique used to detect blood volume variations in human tissues [22]. It is a straightforward, non-invasive and low-cost method employed to measure cardiovascular signals at the skin surface. This technology is present in a widespread health monitoring applications such as pulse oximeters, vascular examination, digital blood pressures and others [23]. A basic PPG system requires two principal optic components: a light source (one or multiple) to irradiate the tissues and a photodetector to detect the small variations in light intensity resulted from blood volume changes [24]. The light sources often works at red and/or at near-infrared

wavelength for blood oxygen monitoring. However, the green light is the best option for HR measures [25]. The most distinguished waveform characteristic is the peripheral pulse synchronised with heartbeats (see Figure 2.2 (b)). On the other hand, heart information is not the only information comprised in these signals. Respiration, sympathetic nervous system activity and thermoregulation are some of the lower frequency signals modulated into PPG signals that can be extracted and processed as an additional health parameter [26].

Figure 2.2: Illustration of a Photoplethysmography (PPG) finger technique and resulted waveform signal. In (a) the typical Light-emitting diode (LED) and Photodetector (PD) used for transmission and reflectance of light; In (b) a comparison between a electrical ECG signal and a pulse PPG signal. Adapted from [23] and [24]

Beyond the previous methods that can measure respiration modulated on cardiac signals, RR can also be measured with alternative and more accurate techniques. These devices can be classified in different types, depending on their operation mode and how they are used [27]. Additional sensors can be used for volume and/or velocity of inhaled and exhaled air during breathing through respiratory airflow measurements. The temporal trend of volume or velocity allows estimate RR and could be collected from flowmeters, anemometers, and fibre optic sensors [28]. The human breath can also be measured through the characteristics of the inhaled and exhaled air such as carbon dioxide (CO_2), humidity and temperature. These parameters are often collected with sensors attached to airways in direct contact with one of the nasals via external sensor devices (Figure 2.3). Acoustic sensors as microphones can also be used to detect respiration activity [29].

In contrast to traditional airflow devices that usually have inconvenient facemasks, which adds extra and unnecessary airway resistance, small microphones on patients are capable of recording air pressure changes caused by the sound waves coming from the nose or trachea. Breath leads to successive contractions and relaxation of the diaphragm resulting in the displacement of the chest that expands circumferentially. Hence, instruments for the physical movement detection of the chest wall have also been used to acquire respiration signals based on strain, impedance, and thorax movements measurements, extracted from chest bands and accelerometers sensors [30]. Lastly, despite the techniques above mentioned, the most used method in clinical practice is still the subjective manual counting of patient respiratory using auscultation or observation skills.

The fast paced technological revolution has led to a worldwide changing in health

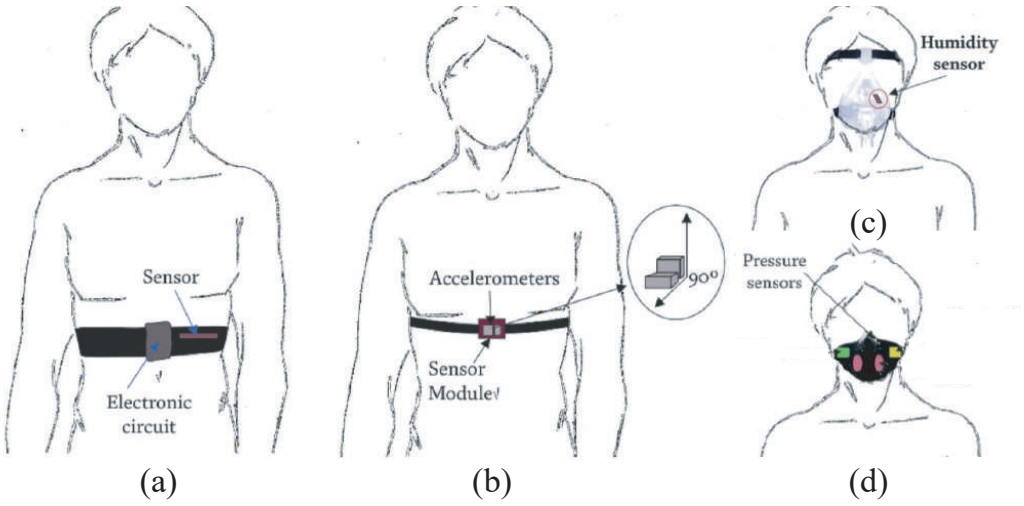

Figure 2.3: Methods used for respiration monitoring based on: (a) piezoresistive sensor; (b) accelerometer measures; (c) humidity sensor facemask; (d) impedance facemask based on forced oscillation technique. Adapted from [30].

monitoring access. The miniaturization of the electronic devices has enabled new stable, comfortable and flexible wearables designs encouraging people to monitor and manage their health status in daily life routines [31]. Some of the previous techniques here presented, have been recently adopted into smaller wearables such as smartwatches and smartphone health applications [32]. These standard devices contain a wide variety of sensors that can be used for smart health applications. For example, pulse rate applications via camera and LED have already demonstrated their accuracy in the measurement of this parameter [33]. Pressure applications attached to mobile phones were already used to perform spirometry tests, which have an essential role in respiratory diseases detection [34]. These new technologies and their inclusion in wearable devices pave the way for the future of remote medical monitoring solutions.

2.1.2 Contactless Methods

Contactless vital signs monitoring methods can be divided into three categories depending on the technique used: ballistocardiography, optical or radar.

Ballistocardiography (BCG) is a non-intrusive technique used in the assessment of the body's vibrations due to its cardiac and respiratory physiological signatures [35]. This method measures mass movements, where, in case of the circulatory system, is related to the repetitive movements of the human body, occurring due to the acceleration of blood as it is ejected and moved into large vessels (Figure 2.4). Contrarily to other generalized and well-established cardiological examination employed routinely in medical practice, BCG failed in proving its usefulness in the past. Economic reasons and its difficult implementation in clinical applications are some of the causes cited for the break of initial enthusiasm on BCG [36, 37]. However, after being disregarded in the last years,

BCG technique is being studied again. According to [38], a novel bed-embedded heart and respiration contactless device was studied with particular focus on the beat-to-beat heart rate monitoring task with a maximum overall detection of 83.9%, with the employment of machine learning algorithms to the signals. With application in other fields, BCG was also successfully applied in sleep apnea syndrome detection in [39].

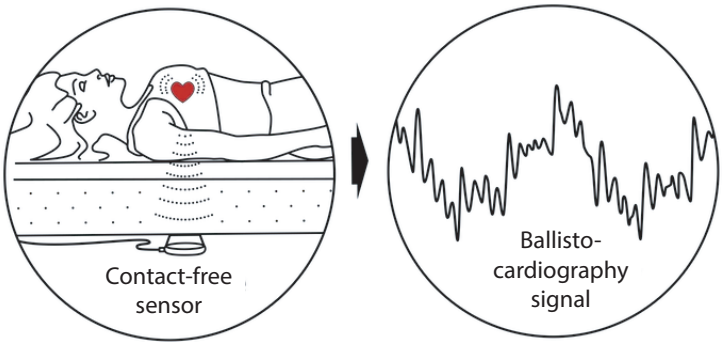

Figure 2.4: Ballistocardiography system installed under the bed for physhiological contactless signals monitoring [40].

Another field in contactless vital signs monitoring methods is imaging techniques, more concretely, video-based techniques and Infrared (IR) thermal approaches. Eulerian Video Magnification is one of emerging practices that use video frames sequences to magnify motions caused by respiration and variations in skin colour due to blood perfusion [41]. Small changes that are too difficult to see to the naked eye can be quantitatively analyzed by this technique to visualize small colour and motion changes in ordinary videos. Moreover, this technique could be applied, having only a good quality smartphone camera for vitals signs recording [42]. Besides Eulerian Video Magnification, other standard video techniques have already demonstrated their potential in cardiorespiratory signal monitoring using simple laptop RGB cameras [43]. Notwithstanding, cameras-based methods are dependent on good illumination environment conditions to work. Thereby, they cannot cover all the situations, especially at night during sleep where normally, there is no light available. Thus, IR techniques could be an excellent alternative to video-based camera approaches. In [44], respiratory rate of newborn babies was measured through this thermal imaging techniques. This method relies on the detection of temperature variations that occur in areas nearest to nose and mouth during inspiration and expiration moments. These methods usually need high computational image signal processing techniques for respiratory extraction; however, novel algorithms could be employed to simplify this process. For example, an only pixel-based approach in [45] was used to record breath from the human nose without recurring to image segmentation or nostril tracking. Exhalation and inhalation times result in lighter pixels and darker pixels at the intranasal surface, respectively (Figure 2.5).

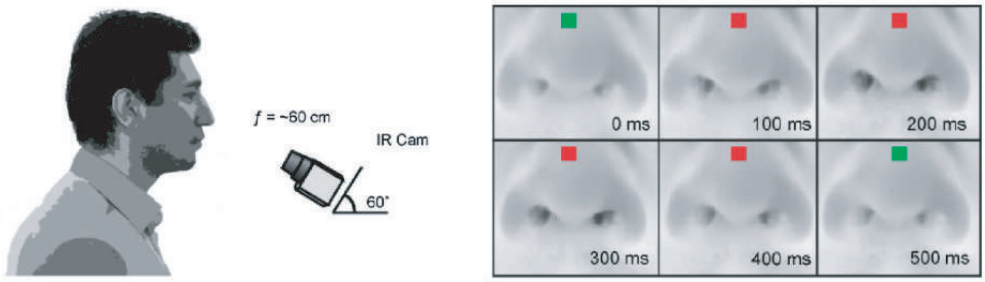

Figure 2.5: Thermography setup developed for contactless respiratory monitoring applications. Inspiration and expiration are marked by red and green squares, respectively [45].

Lastly, radar techniques have been considered as one promising technique in vital signs measurements. Vital signs detection with radar sensors relies on the modulation effect of the transmitted radar signal when it crosses the human body. This modulation is derived from chest displacement of the human target due to both mechanical respiratory and heart activity signal, along with common external noises from electronic sources and background medium conditions. As this dissertation focus is based on the radar technology usage as a mean to detect vital signs, a more in-depth description of hardware and signals processing issues will be explored in the next state of the art subsection.

2.2 Radar Systems for Vital Signs Sensing

Since the beginning of the XX century, and motivated by war, several efforts were allocated in the development of radar technology. The first radar systems were secretly used by military forces for target tracking at long distances. Afterwards, the radar technology started to gain other areas of interest in order to be applied, and in 1970, the first radar usage in healthcare was presented [46]. Although the idea of measuring physiological signal without direct contact was very attractive back then, the old radar devices were larger, more expensive and the amount of radiation released was far beyond the safety margin for human usage. For these reasons, the research on bio-radar technology was almost abandoned. Later on, with the technological improvements and the development of smaller and more compact devices, new techniques for remote vital signs sensing had been developed with the expectation of implementing non-invasive measurements tool in medicine.

Currently, the Continuous Wave (CW) [47], the Frequency Modulated Continuous Wave (FMCW) [48] and Impulse-Radio Ultra Wideband (IR-UWB) [49] are the most frequent radar types to apply in remote measurement of vital signs. These devices are distinguished by the type of transmitted signal which could differ in waveform, frequency, and power of the modulated Radio Frequency (RF) wave (Figure 2.6).

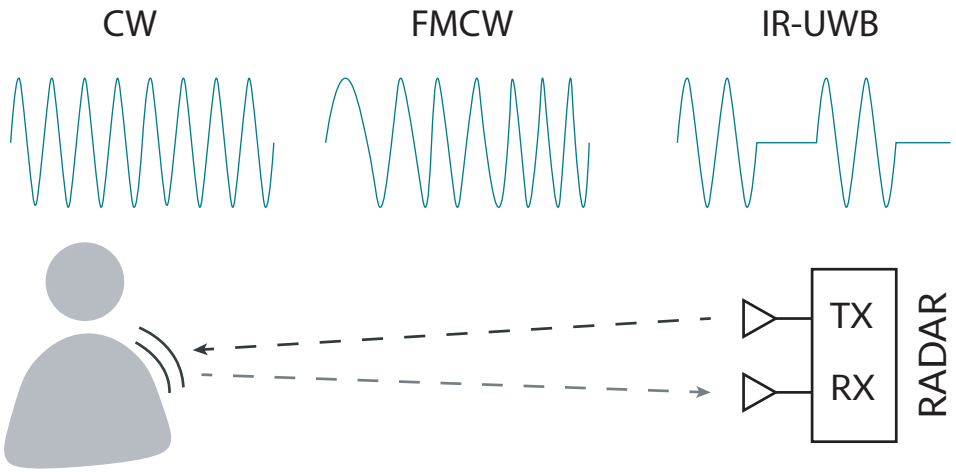

Figure 2.6: Usual radar operation modes used in vital signs sensing applications: CW, FMCW and IR-UWB.

The CW radars are the most common and simpler radar type. Several studies have already demonstrated the capacity of these radar systems in the measurement of respiratory and heartbeat signals in the microwave frequency band [50, 51]. The CW working principle is based on the doppler effect [52], where the target's velocity is obtained through the difference of frequency between emitted and reflected RF signals. For this reason, they are also known as Doppler Radar. Since the velocity of the chest during the successive expansion and contraction is insignificant towards the variation of RF frequency signals, the tracking of fine chest wall motion is acquired by phase shift measuring of the reflected waves over time. Thereby, the frequency of the signal is an important parameter to consider when using CW radar for vital signs sensing applications since the millimetric target chest displacement is measured over the total wavelength. In addition, higher frequencies of the carrier wave signal lead not only to higher sensitivity signals but also significant energy losses during their travel in the medium, which may guide into a detailed loss of cardiovascular signals. These concepts are explored in more detail in Chapter 3.

On the other hand, the simplicity of CW also brings some problems that must be considered in the implementation of a CW device for vital signs applications. First, these devices suffer from null-point problems, when targets cannot be detected in a specific range points [53]. Secondly, In-phase and Quadrature (I/Q) imbalance and phase noises should be considered in order to avoid misleading data [54]. These last two points could be solved by adding extra hardware mixer components or just adjusting the distance of the target from the radar. However, the major CW resides in the inability of detecting the target's position. Since this architecture radar is only able to track relative motions, the CW cannot detect the target position and can only access one single human, simultaneously. In order to provide CW radar with range information, the modulated continuous

radar wave has risen as an upgraded version of CW [55].

The FMCW is a popular radar that has been used for vital signs sensing applications, in which waves frequency are linearly modulated with time [56–58]. This property gives to these devices both Doppler and range information that allows a considerable number of radar applications as the multi-target vital signs detection [59]. Although it is not usually compared to CW and FMCW, the Step Frequency Continuous Wave (SFCW) radar can also be used for vital signs sensing [60, 61]. Notwithstanding, the same frequency concerns about produced waves should be accomplished in these modulated systems for correct phase variations measurements. Moreover, continuous-wave modulated devices have significantly more complex hardware architecture than the simple CW radars, consuming more energy from the power supply and requiring more complex signal radar processing methods.

Lastly, the IR-UWB radar has been recently introduced as a high-resolution radar system capable of vital signs measurements through pulse-timing techniques [62, 63]. Like the FMCW devices, the IR-UWB is a short-range radar capable of providing range information along with high-speed measurements. In 2002, the Federal Communications Commission (FCC) issued the first Ultra Wideband (UWB) radiation restriction, allocating an unlicensed band for commercial purposes [64]. The new regulation together with the clear advantages in the use of IR-UWB applied to medicine, has promoted a bump on research in remote monitoring systems based on this type of radar. Even within the restricted power FCC mask, these systems have been demonstrating their potential in medical areas from their imaging to their obstacles penetrating capabilities [65].

Table 2.1: General radar summarized features based on [66] study. Power consumption may vary from device to device according to the radar architecture arrangement used.

Sensor	**Millimetric Detection**	**Range Estimation**	**Power Comsuption**
CW	Yes	No	Low
FMCW	Yes	Yes	High
IR-UWB	Yes	Yes	Medium

Although the previously described radar have both capacities in the measurement of respiration and heartbeat signal derived from the monitored human targets, the radar characteristics should be balanced according to the desired application, considering the consumption, autonomy, and price of the devices. Table 2.1 summarizes the key characteristics of the three presented radar. Comparative power consumption between radar architectures was based on [66] study. Notwithstanding, regarding the type of radar used, additional signal processing techniques must be applied to extract and remove undesirable components from output radar signals. General techniques of signal processing employed into radar signals for cardiorespiratory extraction information will be following reviewed.

2.3 Radar Signal Processing Techniques

Several signal processing techniques for vital signs extraction from radar signals have been proposed in the last years. Radar signals extracted from human targets are a sum of respiratory and cardiac mechanical displacement along with environmental noise. Thereby, most of the studies are focused on the separation of respiratory, heartbeat and noise components, for further respiratory rate (RR) and heart rate (HR) extraction. This section reviews the principal and successful algorithms used in the extraction of vital signs from radar signals. All the radar hardware used in the subsequent studies are in compliance with the mandatory radiation rules.

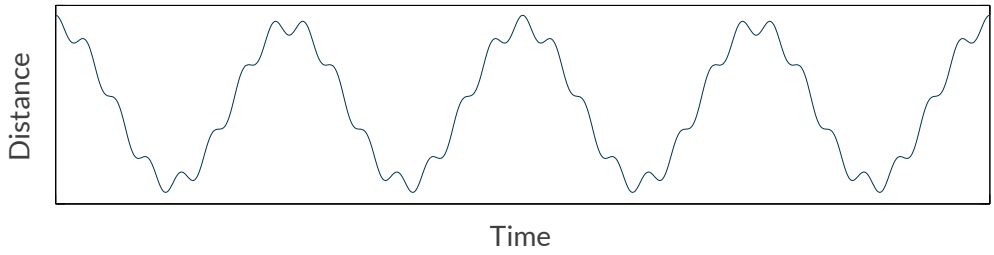

Figure 2.7: Simulated respiratory and heart waveform movement obtained from a radar device. In real applications an extra noise component is presented. Cardiorespiratory signals radar algorithms are typically applied with the aim of separate the different source components. Adapted from [55]

2.3.1 Frequency Techniques

Frequency techniques are the most basic methods that can be used in radar signal processing for the extraction of RR and HR values through direct examination of frequency components in the spectrum.

In [62] vital signs of a static human target located at one meter away from an IR-UWB radar were obtained through direct spectrum inspection, computed by a Fast Fourier Transform (FFT). However, the authors reported that heart peaks were much less evident than respiratory peaks in the spectrum. This is the major problem in detecting HR in radar signals. In fact, as breath displacement is much larger than heartbeat displacement, the main problem of the following studies is focused on the detection and separation of multiple signals, since heart expression is often masked by the stronger respiratory signals. Also, as breathing and heart movements consist of more than one frequency, it will result in the appearance of harmonics on the spectrum that can easily mask heart expression.

The vital signs of a subject after moderate physical exercise were measured in [63]. In the frequency domain, obtained via Chirp Z-Transform (CZT), it was not identified any peak related to heartbeat activity. Using a mathematical model and experimental observations, the authors reported that the main causes for the heartbeat signal attenuation in

the spectrum were the presence of respiratory harmonics and the intermodulation products between breath and heart signal sources, when those are close to heart frequency. The research group also reported that magnitude intensity of the signals differs with the physiological differences of each person and external environmental noise. For the reason described above, many studies have been concentrated on the development of methods for respiratory harmonics removal. In order to suppress the harmonics and recover the heart information, a Motion Target Indicator (MTI) was successfully used in the previous study. In [67], a novel technique called Multiple High Order Cumulant (MHOC) was developed to enhance Signal-to-Noise Ratio (SNR) and to reduce the higher harmonics of the signals.

2.3.2 Time-Domain Techniques

Time-frequency analysis shows the evolution of the vital signs along time. In [68] the Hilbert-Huang Transform (HHT) based on the combination of empirical Empirical Mode Decomposition (EMD) and Hilbert Spectral Analysis (HSA) was proposed to deal with low SNR conditions and non-stationary IR-UWB data.

In [69], the authors applied the HHT method to acquire the vital signs of two subjects at the same time in a simulation of an earthquake disaster. Short-Time Fourier Transform (STFT) could also be used for non-stationary signals analysis, but sometimes do not have a sufficient resolution. It was proposed the application of the Continuous Wavelet Transformation (CWT) in [70]. The CWT was also applied for heartbeat and respiration signal separation in [71]. In this study, the signal was previously denoised through the application of an Ensemble Empirical Mode Decomposition (EEMD). The results showed an increase in the SNR compared with traditional Finite Impulse Response (FIR) filtering method.

The signal processing motion signals originated by breath were extracted by the autocorrelation method in [72]. The autocorrelation coefficients were calculated recurring to the product of the fast-time row signals, resulting in the waveform formed by the periodical vital signs. In [73], the heartbeat signals over time domain were extracted using a Principal Component Analysis (PCA). Variational Mode Decomposition (VMD) methods are also commonly used to separate the different components of the signals. In [74], the VMD method was applied after clutter removing by a background noise removal MTI Filter. In [75] and [76] similar approaches were taken to measure vital signs of animals.

Phase-based methods are usually applied to continuous wave radar sensors [57]. However, these methods were also shown to have an application on IR-UWB systems with improved SNR signals results. In [77], two algorithms based on Complex Signal Demodulation (CSD) and Arctangent Demodulation (AD) were extended to IR-UWB radar processing. Instead of the typical FFT application along the slow-time direction, in these methods, the signals were processed along the fast-time direction to get phase variation of each reflected pulse (slow-time and fast-time terminology are common radar concepts

and are reviewed further in Subsection 3.2.4). To enhance the accuracy of heart rate estimation, a State-Space Method (SSM) resulted from the combination of CSD and AD methods were implemented in [78]. Finally, a logarithm method was proposed in [79] for direct phase variations monitoring of multiple targets.

2.3.3 Complex Environments

Until now, only studies into restrictive conditions were presented, where the target is static and situated in a few centimetres from radar devices. However, in real-life applications, the subjects are always moving along with the natural environment around them, and consequently, these external motions are reflected in radar signals as external noise. Using a simpler hardware architecture as CW radar, the external noise can easily mask the small displacement of chest since there are no other reference signals to compare. On the opposite side, short-range radar as FMCW and IR-UWB provides spatial information about all the environment that can be very useful in the detection and removal of external noise.

In complex environments, most of the algorithms need to be focused on the clutter removal for previous target detection. A detection algorithm for the periodic respiratory motion of trapped victims in a simulated rescue mission with low Signal-to-Noise Clutter Ratio (SNCR) conditions was proposed in [80]. The scattering of rabbles is reflected as Direct Current (DC) component in the slow time dimension. A Linear Trend Subtraction (LTS) method was employed to reduce the amplitude instability of the signals. To improve SNCR, a FIR filter and a frequency-domain windowing were applied in fast and slow time, respectively.

Lastly, Singular Value Decomposition (SVD) was applied to separate respiration signal from nonstationary clutter and reduce the effect of clutter in [81]. After the signal preprocessing, the authors used a STFT to estimate the subject location in a range up to 12 meters. As expected, more accurate results for range information were obtained in short distances and indoor environments. The proposed method was compared with typical algorithms employed on radar applications, such as Constant False Alarm Rate (CFAR), amplitude modulation Amplitude Modulation (AM) and MHOC. A significant SNR improvement over the other methods in tested conditions was observed.

Multitargets vital signs detection is another of the possibilities with short-range radar using FMCW and IR-UWB. An experiment with two subjects was conducted in [79], demonstrating the capability of the IR-UWB radar systems to distinguish the vital signs of multiple subjects in an indoor environment. In [56] simulations also showed that FMCW radars could handle multiple patients situated at different ranges by typical doppler shift measurements.

Finally, the biggest challenge is to acquire cardiorespiratory signals in a moving target during a daily life situation. Some approaches have already started to be studied in order

to try to overcome these obstacles. External human motion was cancelled by the manipulation of complex signal and arctangent demodulation in [82]. These techniques can be used to eliminate the false alarm caused by random body movement in, for example, sleep apnea monitors, lie detectors, and baby monitoring sensors. However, large body movements as gait, continue to have a high predominance in the noise of the signal, leading to the need of bolder approaches, as it was done in [83], where a heartbeat estimation and recovery approach to extract instantaneous heartbeat signals using an IR-UWB radar was developed.

2.3.4 General Flow Chart Diagram

Despite a large number of algorithms developed, there is a commonality on their signal processing structure. After the reception of the backscattered signals, all the undesirable noise elements should be removed. Next, the target distance in the radar range is obtained, and the physiological signals are extracted, see Figure 2.8. A detailed summary of the principal related stages is given below.

Figure 2.8: General flow-chart of usual signal processing steps applied to extract vital signs from radar-range signals.

The output of echo signals depends on the hardware radar device used. The backscattered signals can be represented in the form of RF signals sampled by fast Analog-to-Digital Converter (ADC) modules, or in complex baseband signals resulting from I/Q channels transformers. Complex I/Q representation is commonly used due to its signals processing advantages.

The clutter removal stage includes all the techniques applied to remove the undesirable noise from the IR-UWB signals, that is all the non-human activity presented in these signals. This undesirable noise comprehends common noise sources from static and non-static reflections of the objects in the background, crosstalk of antennas, and thermal noise as well as other types of external noise.

The target detection comprise all the methods that correctly distinguish human echo signals from other high energetic sources. In case the distance of the human target is known, this step can be manually programmed. Otherwise, methods for localizaton of the target could be employed to automatic target range bin detection. In general, a human target can be identified due to the presence of the cardiorespiratory cycles.

The vital signs extraction step is dependent on the aim of the study. The collected signals from the target location over time contains the periodical breath and heart motion. Therefore, the separation of the signals should be performed in order to obtain individual

information. As it has been seen, this separation can be done in the frequency or time-domain. Due to the magnitude difference of both signals, the breath signal can be easily obtained when compared to heart signals. Thus, more complex techniques may be needed for the recovery of weak heart information.

2.4 Applications

Since the appearance of typical frequency and time-domain methods to more complex and sophisticated mixed algorithms, a great number of signal processing techniques have been developed for the extraction of the physiological signals. However, most of the studies with promising results have been performed in selective situations, where the subjects are monitored in noiseless surrounding environments. Thus, further research in radar signal processing is required to obtain more general and more robust algorithms for real life applications. Notwithstanding, these systems also have some applications in real life.

One of the more simple applications concerning radar sensors could be the monitorization at elderly people's homes. However, noise and undesirable activities must be removed from the signals obtained. For example, Wang *et al.* investigated [76] ways to differentiate domestic pets from human beings in order to precent false alarms in domestic radar sensors. This research group concluded that despite pets have similar respiratory frequencies to humans, their physiological movements amplitude was lower due to anatomical differences. Therefore, it was possible to distinguish these two living beings thanks to a parameter that is based in cardiac and respiratory signals ratio.

In the hospital environment, Kim *et al.* studied RR of 42 babies [84]. This studied had as its primary goal to understand if it would be possible to obtain precise RR measurements recurring to radar sensors. However, they reported that the artefacts arrived from babies movements can limitate the use of the device.

On the other hand, Lee *et al.* compared cardiac signals derived from healthy volunteers and volunteers with atrial fibrillation, obtained by radar sensors. These signals were compared with ECG ground truth, and both techniques enable the clear identification of the chronically ill patients [85].

As already stated, radar sensors can be used to monitor sleeping disorders due to the low subject's mobility. More recently, Lee *et al.* implemented a neural network with the purpose to classify patterns in respiratory signals, acquired with an IR-UWB radar sensor, during sleeping. The algorithm classified, with a 93,9% of accuracy, euphnea, braquipnea, tachypnea, apnea and motion patterns [86].

One of the most interesting characteristics of IR-UWB sensors are the high material penetrability and consequently, their ability to measure through the wall. This feature was several times used in rescue missions simulations, where the urgency requires quick methods for life detection [69].

The radar technology can also be used as an additional tool for the improvement of existing systems. In [87], a IR-UWB radar was combined with a mobile ECG as additional information to support the arrhythmia classification of ECG recordings, especially in situations of patient slight motion. The proposed system has improved the heart analysis combining features from ECG signals and radar into a Convolutional Neural Network (CNN) used for classification of heart events.

Finally, another recent applicability is the use of radar sensors in automotive applications. The passenger detection in cars is essential to ensure maximum safety, especially in autonomous driving. Driver vital signs detection, such as RR and HR, can emit alert messages when the drowsiness of the driver increases, compromising the safety of people inside the car [88].

Chapter 3

Theoretical Concepts

Theoretical concepts in radar technology for cardiorespiratory sensing are presented in this chapter. These are divided into two main topics based on cardiorespiratory physiology and radar technology. The cardiorespiratory system is firstly reviewed with a focus on working principles of the respiratory and cardiac systems. Then, a general overview of radar technology principles is given, followed by a more in-depth review in the fundamentals of both radar systems architectures used in this work: the IR-UWB and FMCW. At last, merging radar and biological topics, a vision about the interaction of RF radar waves with the human body, as well as the vitals signs models of radar-human body interaction for each one of the radars described, are explored.

3.1 Physiology of Cardiorespiratory System

The cardiorespiratory system comprises the respiratory system (lungs and airways) and the cardiovascular system (heart, blood, and vessels). The respiratory system allows the oxygen through-flow from the air into the venous blood and the removal of carbon dioxide. These exchanges of gases between air and blood occur by simple diffusion across the alveolar-capillary membrane [89]. The following subsections give the basic concepts of respiratory and cardiovascular systems physiology.

3.1.1 Cardiovascular System

In the cardiovascular system, the heart is a muscle that acts as a pump. Venous blood is pumped to the lungs, whereas arterial blood is pumped to the body parts, having the blood vessels as a mean of transportation. The heart is composed of four muscular chambers: two atriums and two ventricles. Whereas the atriums help the blood to move into the ventricles, the ventricles then supply the blood either through the lungs or through

the peripheral organs [90, p. 103]. Two atrioventricular valves (tricuspid and mitral) and two semilunar valves (aortic and pulmonary) are also present in the heart, preventing backflow of the blood from the ventricles to the atria during systole and, from the aorta and pulmonary arteries into the ventricles during diastole, respectively. The opening and closing of these valves occur due to pressure gradients, where they open when a pressure gradient forces the blood move in the forward direction, and they close when the same gradient pushes blood backward [90, p. 108-109].

On the other hand, the comprehension of the relationship between the heart's electrical activity and its mechanical muscle behaviour is of extreme importance. The electrical activity measured by the electrocardiogram, and recorded from the surface of the body, is generated by the muscles of the heart and surrounding during a beat. So, in order to generate electrical impulses, which in turn causes the contraction of the cardiac muscle, the heart is endowed with specialized excitatory muscles and conductive fibres. Figure 3.1 shows the excitatory and conductive system of the heart.

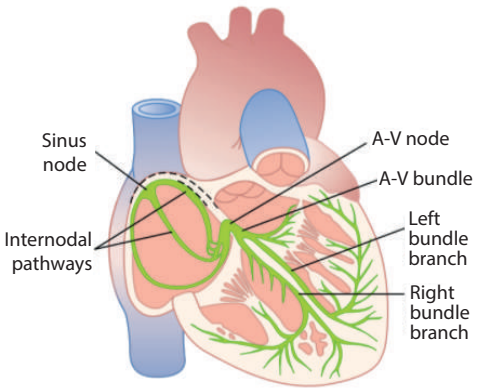

Figure 3.1: Conductive system of the heart that controls cardiac contractions [90].

The rhythmical impulse is initialized in the sinoatrial (sinus) node that is directly connected with the atrial muscle fibres. This impulse travel throughout the heart, and the internodal pathways ensure that the impulse reaches the atrioventricular (A-V) node. Once it reaches the atrioventricular node (where the impulse is delayed), the A-V bundle conducts the impulse to the right and left bundle branches of Purkinje fibres, is then spread to all parts of the ventricles [90, p. 108-109].

A normal electrocardiogram is comprised of three major deflections: a P wave, a QRS complex, and a T wave. Figure 3.2 depicts the electrical activity and its relation to the behaviour of the cardiac muscle. The P wave is representative of the depolarization of the atria. The time interval between this wave and QRS complex (P-Q interval), corresponds to the time that comprehends the beginning of electrical excitation of the atria until the beginning of excitation of the ventricles. Then, ventricular depolarization causes the emergence of QRS complex. Finally, T waves surge as a result of ventricles repolarization, recovering from the depolarized state [90, p. 123-125].

With the function of pumping blood by the ventricles, occurs the propagation of

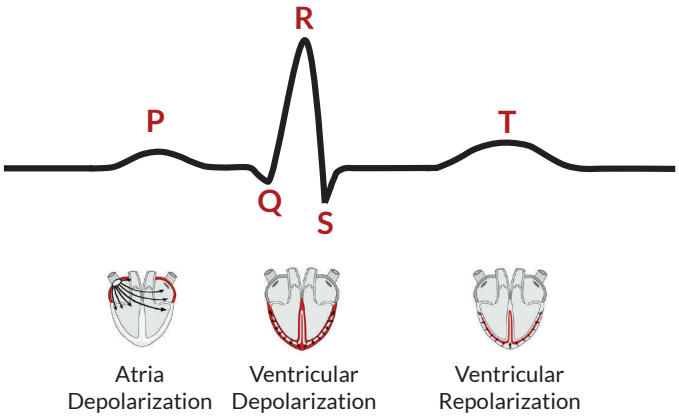

Figure 3.2: ECG wave representation and corresponding atrial and ventricular mechanical activity stages.

pressure waves throughout arteries walls that increase during systole and decrease during diastole. The stiffness of these walls has an impact on the pressure waves pace, where a greater hardness of arteries walls leads to a quicker transmission of the wave. When it is transmitted to peripheral blood vessels, it is noted that the volume of the pulses changes, according to each cardiac cycle. The propagating pressure pulse inside the arteries generates a combination of wave modes inside the tissue and on the skin surface, that results in small skin displacements over time [91].

3.1.2 Respiratory System

The respiratory system includes the lungs and the airways. The mechanics behind pulmonary ventilation has two origins. The first is done by downward and upward movements of the diaphragm that causes the lengthening or shortening of the chest cavity. The second method concerns the elevation and depression of the ribs to increase or decrease the anteroposterior diameter of the chest cavity [90, p. 471]. These two methods are shown in Figure 3.3.

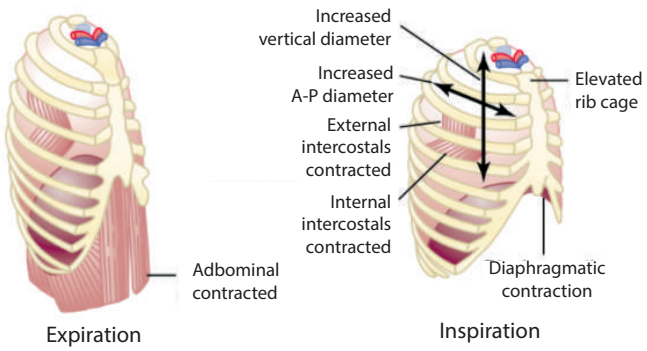

Figure 3.3: Contraction and expansion of the rib cage during expiration and inspiration [90].

Respiration is divided into pulmonary ventilation, which is the inflow and outflow of air, diffusion of O_2 and CO_2 between blood and alveoli, transportation of the gases and regulation of ventilation [90, p. 471]. Each respiration cycle consists of an inhalation phase followed by an exhalation phase as can be seen in Figure 3.4. During inspiration, the diaphragm contracts and pulls the lower surfaces of the lungs downward [90, p. 472]. This contraction of the diaphragm creates an increase in intrathoracic volume, which in turn, lowers intrathoracic pressure, initiating the air flow into the lungs [92, p. 192].

Concerning the expiration, the diaphragm relaxes, and the elastic recoil of the chest-wall, lungs, and abdominal structures compresses the lungs where the air is expelled [90, p. 472]. The expiration is a passive process where the outflow of the air occurs by the reverse pressure gradient between the lungs and the atmosphere [92, p. 192]. As the expiration is a passive process and inspiration is an active one, the time of inhalation is shorter than exhalation.

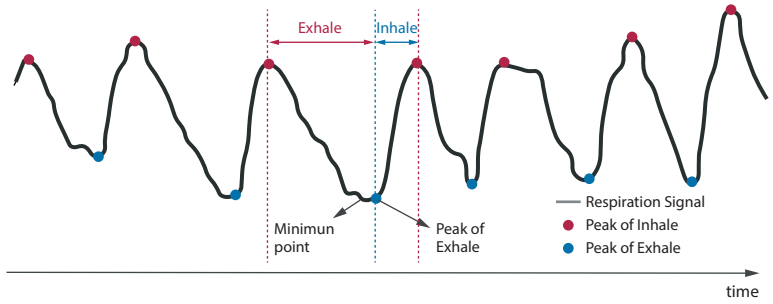

Figure 3.4: Typical respiratory waveform and respective inhalation and exhalation phases [93].

3.1.3 Vital Signs Reference Values

The measurement of vital signs helps to assess the general health status of a person. As mentioned before, only the respiratory rate (RR) and the heart rate (HR) are analysed in this work. Normal RR and HR ranges differ with age, gender, weight, exercise, emotions and other factors in populations. Table 3.1 shows the reference values of frequency and tissue's displacement for a healthy adult at rest [94, 95]. These values take into account the vital signs parameters reference used in practical clinical contained in the range of 12 to 20 Respiration per Minute (RPM) for RR and 60 to 100 Beat per Minute (BPM) for HR [94].

Table 3.1: Vital signs reference parameters for an healthy adult in a rest condition.

Vital Signs	Rate per Minute	Frequency (Hz)	Displacement (mm)
Respiratory Rate	12 to 20 (RPM)	0.2 to 0.4	4.0 to 12
Heart Rate	60 to 100 (BPM)	1.0 to 1.7	0.1 to 0.6

3.2 Radar Principles

RADAR, an original acronym for Radio Detection and Ranging, is an electromagnetic sensor that uses radio frequency (RF) waves for the detection and location of reflecting objects. Nowadays, radar devices are everywhere and play a crucial role in several areas such as navigation, military fields, air traffic control, biological research, weather observations and most recently, in human tracking. Thereby, depending on the desired radar application, these systems can operate in a frequency range between the 3 MHz and the 300 GHz. All the information presented in this section were based mainly in two references [96] and [97].

3.2.1 General Characteristics

The general principle of a radar system is very simple and is based on the emission of RF signals, that are later reflected in the medium and detected again by the radar for posterior analysis. Nonetheless, the implementation of these systems is complex and requires a wide range of expertise from different engineering fields, from mechanical and electrical engineering to data signal processing and microwave experiments. Over the years, several types of radar have been developed to satisfy the different needs of customers. However, despite the different existing radar architectures, all the devices can be divided into five principal elements: a Transmitter (TX), a Receiver (RX), the antennas, a signal processor, a waveform generator, and the main controller block (see Figure 3.5).

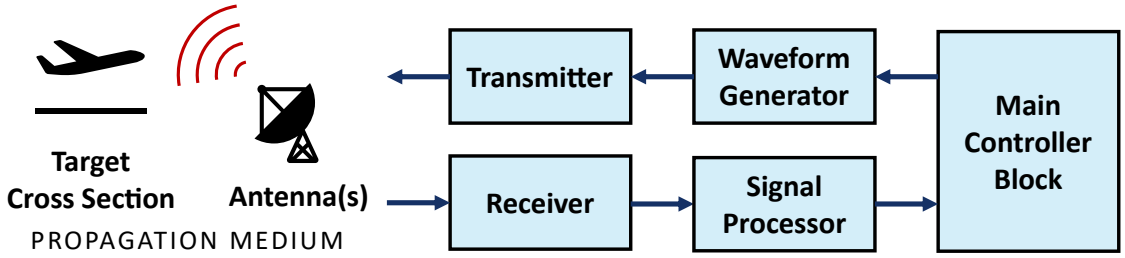

Figure 3.5: Principal components of a general radar system. Schema based on [97] illustrations.

The transmitter TX is the module responsible for the emission and generation of RF signals with suitable waveform and power values for radar application. However, the transmitter and waveform generator are not only the elements accountable for signal modulation but also share this job with the antenna's devices. The antenna is the structure that allows the transmission of energy into the space and posterior collection of echo signals on the receiver. In most devices, each transmitter and receiver contain at least one TX antenna and one RX antenna incorporated. The design of antennas is a crucial step in radar manufacture since it has a significant impact on the gain, filter, and direction of emitted signals. After the reflection of signals, the echo signals are detected at the receiver RX and processed in the signal processing module. In this module, the received

RF signals are transformed into readable data from where range[1], direction, velocity, and other information of the targets can be extracted. Usually, this is a customizable module in which elements arrangement is dependent on diverse factors as waveform, the type of signal and the own radar application. Lastly, the central controller corresponds, as the name indicates, to elements used for radar hardware manipulation and data displaying for users.

3.2.2 Radar Equation

The reflected signals quality is dependent on parameters such as the transmitted signals, the gain of antennas, the radar cross-section related to the target area, the environment and the distance between the target and the detector. All these parameters are presented in the Radar Equation 3.1, used to evaluate radar performance and from it, the the maximum radar range can be estimated.

$$P_r = \frac{P_t G_t A_e \sigma}{(4\pi)^2 R^4} \tag{3.1}$$

Where,
P_r = Receiver Signal Power,
P_t = Transmitter Signal Power,
G_t = Transmitting Gain of Antenna,
σ = Target Radar Cross Section,
R = Distance between the transmitter and the target,
A_e = Effective Area (or Aperture) of the receiving antenna expressed as:

$$A_e = \frac{G_r \lambda^2}{4\pi} \tag{3.2}$$

where G_r is the gain of receiving antenna and λ is the transmitted RF wavelenght.

Equation 3.2 has the a biggest importance in the final size and design of radar final production size, since these depend mainly on the size of antennas related to A_e. The smaller the aperture, the smaller the size of the antenna which in turn is related with the wavelenght of RF transmitted wave. That is, higher radar frequencies allow smaller and ergonomic devices.

The Radar Equation is a quite useful reference when studying radar systems since it can describe all the essential characteristics that should be considered when designing a radar model for a specific application. However, this equation does not specify the nature of emitted and received signals and, for a better representation of real systems, other parameters factors should be added to Radar Equation in order to obtain more reliable radar systems representations.

[1] In radar principles, the word range refers to the distance measured between the radar and the target.

3.2.3 Waveform Classification

Radar sensors can be distinguished by different features, from the radar waveform to its system components layout, and consequently, characterizing a radar depends on many factors. Thereby, for a simple understanding and overview of the principal radar groups, in Figure 3.6 these were divided using their time-domain waveform characteristics into two big radar groups: the continuous wave radar and the pulse radar.

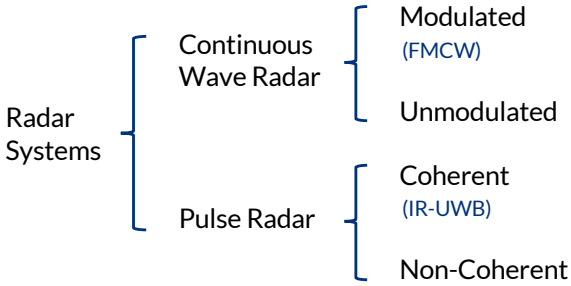

Figure 3.6: Radar Classification by time-domain waveform of transmitted RF wave. IR-UWB and FMCW used in this work are a type of modulated continuous wave radar and coherent pulse radar, respectively.

The continuous wave radar systems are known for employing continuous sine waves. These systems use the doppler effect for the detection and tracking of targets and can detect their target range through frequency wave modulations. On the other hand, the pulse radar uses a repetitive strain of short-duration pulses for target range detection on time-domain data. The pulse radar can also be divided into coherent and non-coherent pulses describing the relationship of between phase variations on emitted and reflected pulses. Pulses emitted with random phases are classified as non-coherent systems while radar sensors that emit their signals always with the same phase shift are classified as coherent pulse radar. The two radars used in this work fall in the following categories: IR-UWB and FMCW. A more detailed explanation about these radar systems is given in Sections 3.3 and 3.4, respectively.

3.2.4 Short-Range Radar Concepts

Short Radar Range (SRR) are, as the name indicates, radar sensors with the ability to detect objects very close up to a few meters. Modulated continuous wave and pulse radar sensors are the two most common architectures used in the design of SRR devices. SRRs are often characterized by their small size and low power radiation emission systems, offering the ideal features to be introduced in human tracking radar systems applications. Radar sensors explored in this dissertation can be considered as SRR due to their short-range capacity. Therefore, some radar and SRR terminology that will be used throughout this dissertation will be here clarified, namely, the data structure of output data commonly used in any SRR, regardless the type of radar used.

A convenient and straightforward way of present SRR digital data is a range-time matrix form expressing space and time information. Figure 3.7 illustrates a typically Range-Time Radar Matrix with a conceptual [mxn] size.

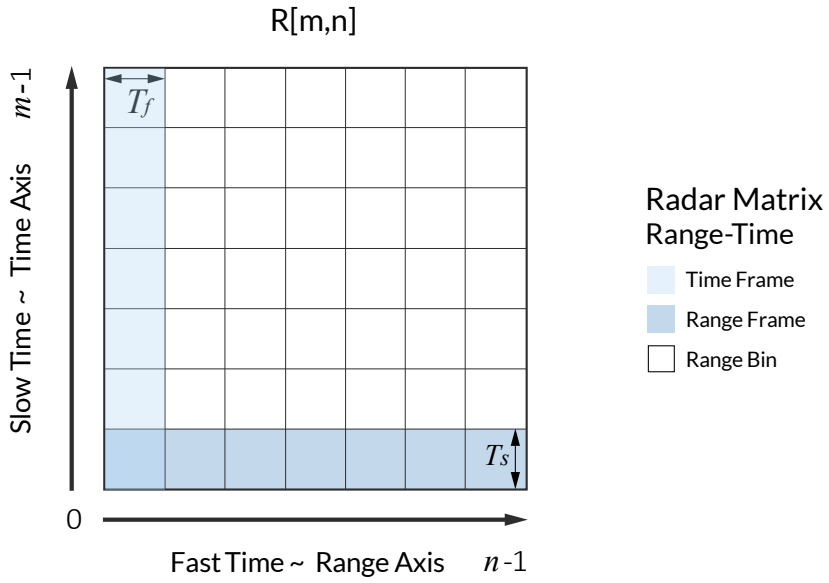

Figure 3.7: Range-time radar matrix representation.

Range-Time Matrix R[m,n] arranges all the radar collected sample points in stacks of range frames in a two-dimensional array of size M-by-N. M defines the length of the first dimension, usually called **slow-time**, and N defines the length of the second dimension called **fast-time**. Slow-Time and Fast-Time samples result from the sampling rate of data in specific periods, and therefore, both have time units.

Fast-Time Axis: corresponds to the frame formed by the highest sampling rate of the system F_s and to the sampling interval T_s given by $\frac{1}{F_s}$. Fast-Time axis is also referred to as the range axis since its values are equivalent to a given distance within the radar range interval. This conversion differs from device to device and should be analysed case by case. Each sample in a range frame is called a range bin. In this work, fast time is assigned to the rows of matrix R with dimension N.

Slow-Time Axis: corresponds to the frame formed by the sampling rate f_s in which each range frame is streamed. Naturally, f_s should always be less than F_s with a given period of T_s. In radar real applications context, this axis represents the evolution of targets identified and located at a certain range bin. Each sample in a slow time axis is directly associated to a time bin. In this work, slow time is assigned to columns of matrix R and dimension M.

Similarly and practically, fast-time contains the amount of signal reflected at each distance, where each square (range-bin) along the fast-time axis on Figure 3.7 corresponds to a certain distance, whereas slow-time corresponds to the temporal evolution of these events at each distance (or range-bin). In addition, Nyquist frequency should be considered on both F_s and f_s, depending on the desired radar application.

3.3 IR-UWB Radar

IR-UWB is a type of pulse radar that uses Ultra-WideBand technology to achieve greater range spatial resolutions. These sensors are also capable of tracking small chest movements for physiological signals caption when configured with appropriately features. General concepts about these sensors characteristics and working principles are presented next. The vital signs mathematical model used in this type of radar is also presented at the end of this subsection.

3.3.1 UWB Technology

Ultra-Wideband UWB technology is based on the transmission of very short pulses that result in large spectrum signals. These systems have traditional applications in radar imaging, wireless communications and are very popular for low power consumptions applications. According to the FCC, a signal is classified as Ultra-WideBand if it has a fractional bandwidth B_f greater than 0.25, or an absolute minimum bandwidth of 500 MHz [98]. The fractional bandwidth B_f is given by Equation 3.3

$$B_f = \frac{f_H - f_L}{f_c} \tag{3.3}$$

where f_H and f_L are the higher and lower points in the spectrum, respectively, and f_c is the center frequency, or carrier signal frequency.

Due to the use of a very wide spectrum range, UWB systems may lead to interferences with other important and well-established operating radio services, and therefore, UWB systems are only permitted to operate in restricted frequency bands defined by regulatory bodies in different regions of the world. In 2002, the FCC issued the first UWB radiation restriction, allocating an unlicensed band frequency between 3.1 and 10.6 GHz for commercial purposes [64]. Currently, this is the largest unlicensed UWB band authorized in the world. However, because of possible interference problems with other big and well-established technologies operating in narrowband frequencies, only a maximum radiated power of 41.3 dBm/MHz is currently approved for indoor applications. This power makes UWB devices within the unlicensed band, to only operate over short distances because of the imposed power restrictions. In fact, the low spectral power density characteristics over a wide frequency band of the UWB signals, are only interpreted as noise by the other narrowband technologies as can be perceived in Figure 3.8.

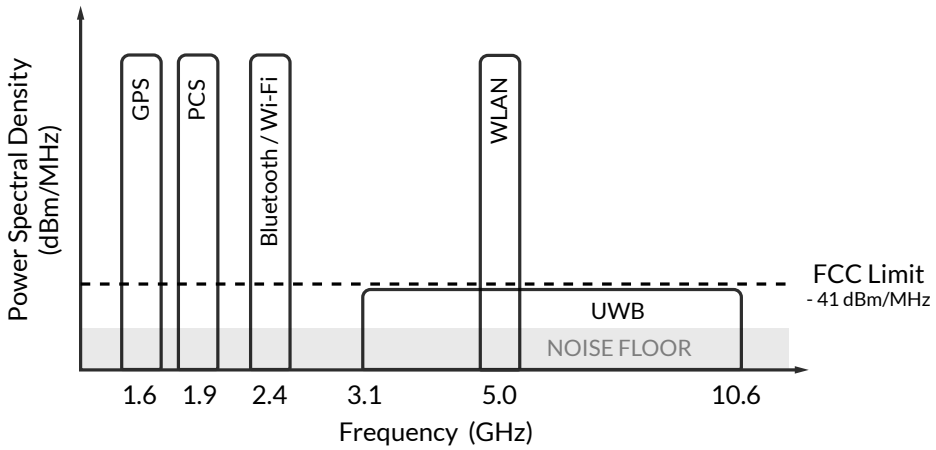

Figure 3.8: Regulated UWB spectrum: conventional narrowband systems versus ultra-wideband systems operating within the unlicensed band. Adapted from [99].

3.3.2 IR-UWB Fundamentals

IR-UWB radar systems, are based on the pulse radar architecture in which target distance is achieved with pulse-timing technique [100]. The typical IR-UWB signal is a gaussian waveform of pulse-width τ_p modulated by a carrier wave of frequency f_c. These pulses are periodically emitted at a pulse Pulse Repetition Frequency (PRF). The Inter-Pulse Interval (IPI) is inversional proportional to PRF and defines the time occurred between two pulses emission. A IR-UWB signal is represented below in Figure 3.9.

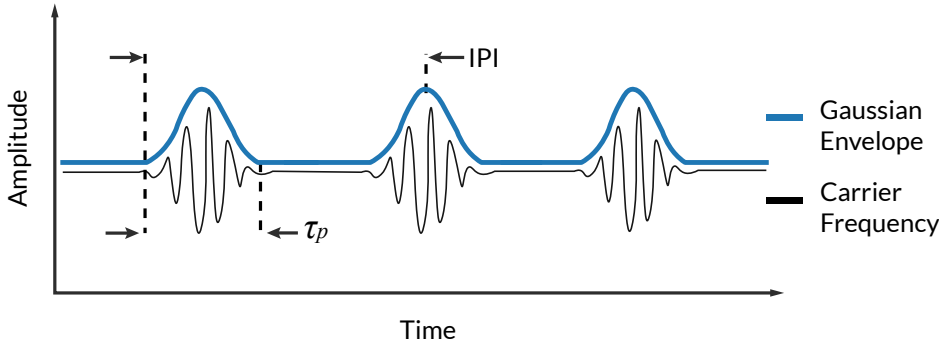

Figure 3.9: Typical IR-UWB signal representation: a short pulse train of RF signal modulated by a gaussian function.

Contrarily to CW systems, the transmitter and receiver in pulse radar devices are never working on simultaneous. IR-UWB systems are always swapping between two states: the transmission time T_t when the receiver is OFF, and pulses are emitted by transmitter (ON), and the listening time T_l when the transmitter is OFF, and receiver (ON) is ready to detect the backscattered signals. This process is illustrated in Figure 3.10.

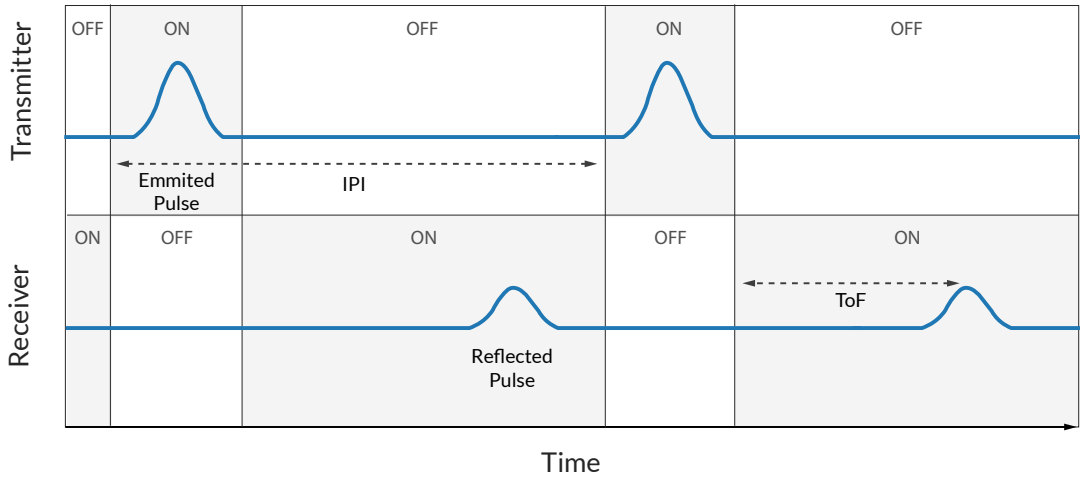

Figure 3.10: Working principle of IR-UWB transmitter and receiver. A pulse emmited during the transmission time T_t is detected after a time ToF during the listening time T_l.

The time τ occurred between the transmission, reflection and detection of a pulse is called Time-of-Flight (ToF), and can be translated to a range R measure by the Equation 3.4

$$R = \frac{c}{2\tau} \tag{3.4}$$

where c is the speed of light at which radio waves travel in the medium. Then, by applying Equation 3.4 to listening time T_l frame, the set of pulses sampled in a different time τ, are related to different distances and T_l can be translated to the respective range frame.

During the transmission time T_t, reflected pulses cannot be sensed by receivers, and for this reason, pulse radar suffers from a blind range where targets cannot be detected. That is, for a target situated at a distance equivalent to τ within an interval T_t, its reflection will fall into the blind range (when the receiver is OFF) and the target will not be detected. Thus, in IR-UWB systems, there is a minimum distance R_{min} from which the target should be situated to be detected. R_{min} can be obtained by Equation 3.5 below:

$$R_{min} = \frac{cT_t}{2} \tag{3.5}$$

On the other hand, as the pulses are expected to be received in a specific time windowing T_l before the next pulse be emitted, the targets should be located within a maximum range in order to avoid data ambiguities. When targets are situated beyond the maximum range limit, their echo signals can be detected in the next frames after another pulse be emitted. This can result in phantom targets effects over range matrix. Hence, targets should be situated in a maximum range R_{max} given by Equation 3.6:

$$R_{max} = \frac{c}{2PRF} \tag{3.6}$$

The range resolution of the radar is its capacity to discriminate between targets that are relatively close in either range or frame. In the case of pulse radar, range resolution depends on the width τ_p of the transmitted pulse. Hence, pulse radar range resolution can be expressed by ΔR in Equation 3.7 where,

$$\Delta R = \frac{c\tau_p}{2} \tag{3.7}$$

Finally, IR-UWB devices are often provided by coherent pulse radar architectures. In this type of systems, pulses are always transmitted with the same phase what allow the integration of pulses for an increase of the SNR of the received signals. The sum a sequence of received pulses tends to cancel random noise and reduces the noise power variance while the power of the signal of interest is improved. This is a very important feature due to the low power restrictions of these sensors in the unlicensed band. Figure 3.11 shows a reflected echo pulse signal after integration of 16, 64 and 512 pulses.

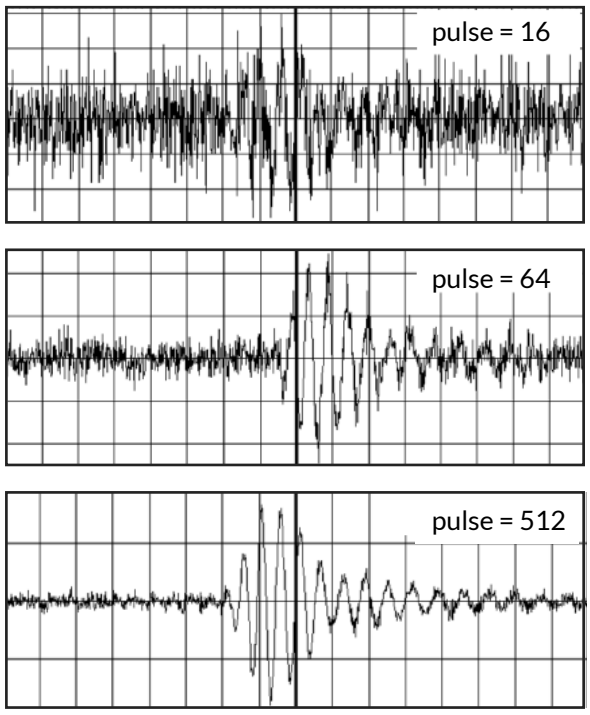

Figure 3.11: Exemplification of the pulse integration technique used in coherent IR-UWB radars. The greater the number of pulses used in the integration process, the larger the SNR of the sampled echo signal. Adapted from [101].

3.3.3 Vital Signs Sensing: Mathematical Model

The principle of vital signs remote sensing using a IR-UWB radar is based on the measurement of the human body distance to the radar. A schematic model that was described for the first time in [63] is illustrated on Figure 3.12. In this model, a subject is located at a nominal distance d_0, from the radar.

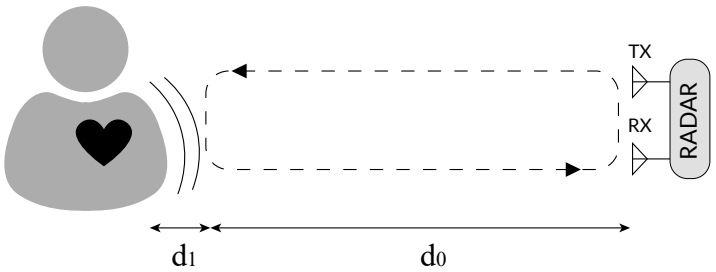

Figure 3.12: IR-UWB vital signs model radar schema. Representation of the mathematical vital signs model presented in [63]

The chest displacement caused by respiratory and cardiac events, cause a d_1 variation on target distance over time, and therefore, the cardiorespiratory cycle can be extracted from the time-of-flight and amplitude of the reflected pulses. Vital signs activity can be described as a sinusoid function of distance d over time t represented in expression 3.8:

$$d(t) = d_0 + d_1(t) = d_0 + m_b \sin(2\pi f_b t) + m_h \sin(2\pi f_h t) \tag{3.8}$$

where f_b and f_h are the respiratory and heartbeat frequencies, and m_b and m_h are the amplitudes displacements caused by respiratory and heartbeat motion, respectively. Therefore, for a typical multi-channel radar system, the echo signals can be described as the sum of the cardiorespiratory and noise components as following:

$$r(t,\tau) = \sum A_i p(\tau - \tau_i) + Ap(\tau - \tau_d(t)) \tag{3.9}$$

where $p(t)$ is a normalized received pulse, A_i is the amplitude of multipath components, τ_i is the pulse delay, and A is the amplitude of the pulse reflected on the body. As seen in the previous section, the Time-of-Flight, τ, of a pulse is related to distance d (or range R) as described in Formula 3.4. Thus, applying Equation 3.4 to 3.8, chest movement caused by respiration and heartbeat can also be obtained as a sum of τ_0 from nominal distance d_0 and τ_b, τ_h from respiratory and heartbeat displacements, where:

$$\tau_d(t) = \tau_0 + \tau_b \sin(2\pi f_b t) + \tau_h \sin(2\pi f_h t) \tag{3.10}$$

with $\tau_d(t)$ as the time delay variable related to vital signs chest modelling. Lastly, echo signals $r(t,\tau)$ described by the equations above, are stored in a matrix $R[m,n]$ after the sampling of detected signals. Range frames of size n are sampled at a sampling period T_f in fast-time, and stored in m discrete-time sequences in a slow-time period T_s. Therefore, $r(t,\tau)$ is presented in sampled instant forms by **R** in Equation 3.11:

$$R[m,n] = r(t = mT_s, \tau = nT_f) \tag{3.11}$$

Figure 3.13 illustrates a visual example of the equation above. Pulses being reflected by a displacement d_1 around d_0 over time t, result in a sinusoid that contain cardiorespiratory information of the monitored target.

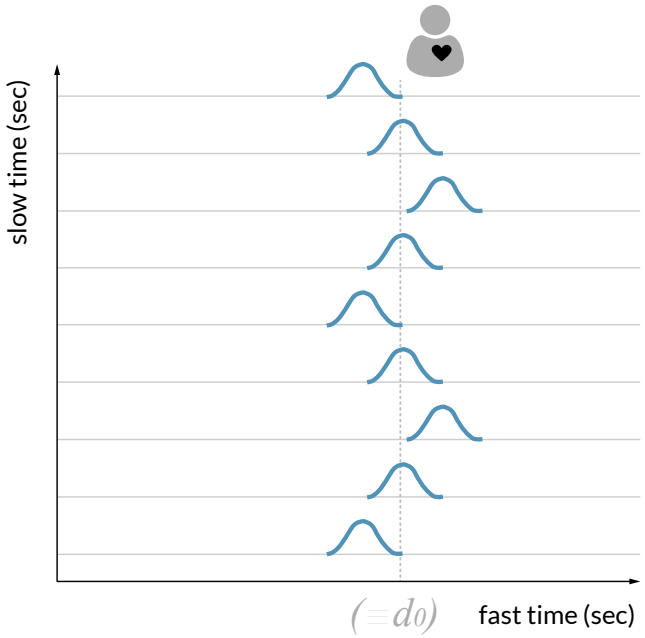

Figure 3.13: IR-UWB vital signs mathematical model representation in a matrix R.

3.4 FMCW Radar

The FMCW radar is a type of continuous-wave radar characterized by the emission of frequency-modulated signals called chirps [102]. Contrarily to the traditional CW radar, the FMCW is capable of providing speed measurements along with distance and angle measurements. Next, fundamentals about FMCW technology and how this technology can be used to acquire vital signs according to phase measurements are going to be described.

3.4.1 FMCW Fundamentals

FMCW operates by emitting, receiving and processing chirps. A chirp, represented in time and frequency domain in Figure 3.14, is a sinusoid signal which frequency increases linearly with time. It is defined by a start frequency f_C, a duration T_c, a Bandwidth B and a Slope S which translate the frequency rate of the chirp. Chirp parameters should be configured according to the radar application requirements.

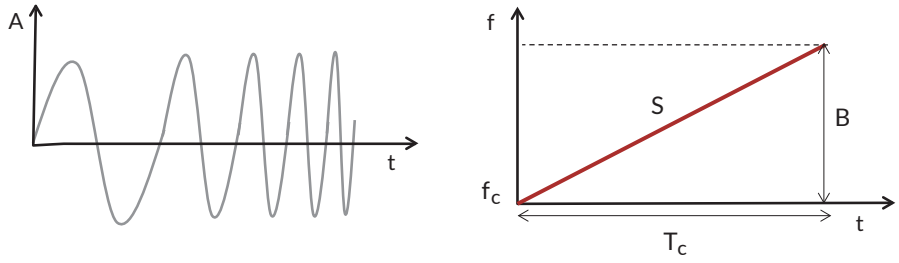

Figure 3.14: Chirp Representation in (a) time domain and (b) frequency-time domain [102].

The operating principle of FMCW radar is based on the comparison of both received and transmitted signals from where a new Intermediated Frequency (IF) signal is generated from which it is possible to extract range information. For a better comprehension, this process is simplified for a single target in figure 3.15 and described below.

For a static object at a certain range R, the reflected RX chirp in only a delayed version of the reflected TX chirp by a time delta τ. Thus, the distance at which the chirp was reflected, that is the object range, can be obtained through the measurement of time displacement between the emitted and reflected chirp. As the RX and TX are just the same signal shifted by a time delay τ with the same frequency characteristics, their subtraction results in a sinusoidal signal, the IF signal, with a constant frequency f. Thus, depending on the chirp displacement, their subtraction will result in signals with different frequencies. Each frequency will be then related with a unique time τ associated with a unique distance, or range R. Since time τ is a typical small fraction of time in the total time of T_c chirp, this value is usually negligible.

Hence, for a single object at a range R from the radar, an IF signal with a constant frequency is generated, being its value given by:

$$f = 2\frac{SR}{c} = 2\frac{BR}{T_c c} \tag{3.12}$$

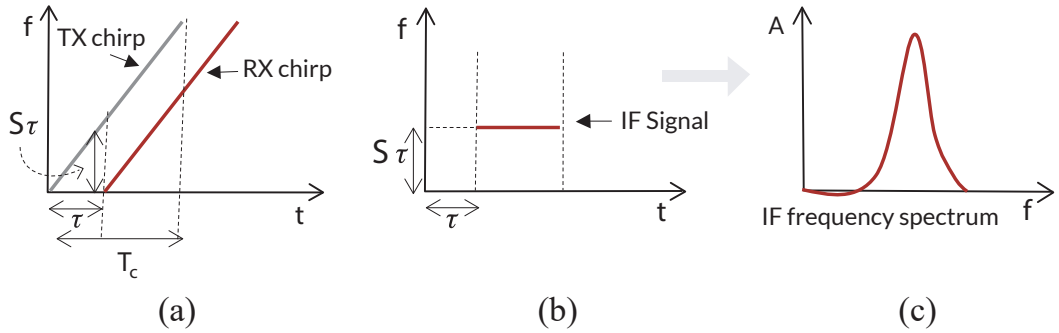

Figure 3.15: Working principle of an FMCW using chirp mixing: (a) Representation of a TX and RX chirp in frequency-time domain, (b) IF signal in frequency-time domain after TX and RX chirp mixing process, and (c) IF signal in frequency domain.

On the other hand, in real environments TX chirps are reflected at diverse range points with different magnitudes. Thus, IF signals are actually comprised of all the frequencies resulted from the mixing of different chirps that were reflected at different ranges, where each frequency will be associated to a different delay, τ. Therefore, and similarly to the reasoning applied to one single target, with the spectrum computation of multi-frequency IF signal is possible to recover the range frame from the environment, associating each frequency to the respective distance given by equation 3.12. Moreover, considering all the previously described process, some concerns about chirp parameters values should be taken. In the case of FMCW, the range resolution will be dependent on the spectrum resolution, which in turn is dependent on the chirp Bandwith B, according to equation 3.13:

$$\Delta R = \frac{c}{2B} \tag{3.13}$$

Another parameter to take into account is the maximum range R_{max} achieved by the configured radar. This parameter will be dependent on frequency sampling F_s of ADC module in the FMCW:

$$R_{max} = \frac{F_s c}{2S} \tag{3.14}$$

3.4.2 Vital Signs Sensing: Mathematical Model

Following the FMCW model described in [103], the transmitted chirp of a FMCW radar can be expressed by as:

$$x_T(t) = A_T \cos(2\pi f_c t + \pi \frac{B}{T_c} t^2) \tag{3.15}$$

where A_T is the transmitted power transmitter and the other variables are related to chirp parameters already described in the previous page. Due to the range-correlation effect, residual phase noise can be neglected in short-range radar and will not be taken into account for this rationale. Considering equivalent conditions given in the UWB schema, it is assumed that for one target located at a nominal distance d_0 from the radar, the motion displacement of the chest resulted from cardiorespiratory activity is given by d_1 (see Figure 3.12). Assuming that the distance from the chest to the radar is equal to $d(t) = d_0 + d_1(t)$, and the delay t_d of the reflected chirp is given by $\frac{2d}{c}$, where c is the light speed. The received RX chirp, reflected from a distance d, can be described as:

$$x_R(t) = A_R(\cos(2\pi f_c(t - t_d)) + \pi \frac{B}{T_c}(t - t_d)^2)) \tag{3.16}$$

Furthermore, after the mix of the received signal with a replica of the transmitted signal, and taking into account approximations that will not be here detailed, IF signal can be described by Equation 3.17 from where frequency f and phase θ terms, resulting from the difference between transmitted and received chirps, can be found:

$$x_{IF}(t) = A_T A_R \exp(j(2\pi \frac{2Bd_0}{cT_c} t + \frac{4\pi(d_0 + d_1(t))}{\lambda})) \tag{3.17}$$

From equation 3.12, $\frac{2Bd_0}{cT_c}$ term can be reduced to f, whereas $\frac{4\pi(d_0+d_1(t)}{\lambda}$ term is nothing more than the phase shift $\theta(t)$ associated to each beat frequency f. Thus, IF signal can be simplified as:

$$x_{IF}(t) = A_T A_R \exp(j(2\pi f t + \theta(t))) \tag{3.18}$$

where equation 3.18 is a simplified expression of IF signal which translate the frequency f and phase θ of a chirp reflected at a certain distance d. As chest displacement d_1 is given in a millimetric range, this small scale vibration can only be sensing along phase changings over time t at a target in d_0 related to a fixed frequency f. Hence, in order to obtain the change in chest displacement, multiple chirps should be transmitted in sequence to notice the chest displacement. The variation of phase over slow-time, used to extract small vibration movements from objects, can be defined by Equation 3.19 where:

$$\Delta\theta = \frac{4\pi\Delta d}{\lambda} \tag{3.19}$$

Furthermore, assuming R[m,n] notation and after the sampling of IF signal, Equation 3.18 can be expressed in slow-time and fast-time notation for the n-th ADC sample and the m-th chirp as:

$$R[m,n] = A_T A_R \exp(j(2\pi f nT_f + \frac{4\pi}{\lambda} d(nT_f + mT_s) \tag{3.20}$$

where T_s is the period at each IF signal is output or chirp is emitted in slow-time, and T_f is the sampling frequency of radar ADC represented in fast-time range. As referred before, the small vibration of chest displacement have not enough expression to be sensed at fast-time frame, and therefore the next approximation is made for a fixed target:

$$d(nT_f + mT_s) \approx d + d(mT_s) \tag{3.21}$$

Finally, the variation of phase over slow-time, in matrix R, can be extracted fixing a frequency-range bin n-th by measuring the phase at time indices mT_s:

$$x(n, mT_s) = \frac{4\pi}{\lambda} \theta(n, mT_s) \tag{3.22}$$

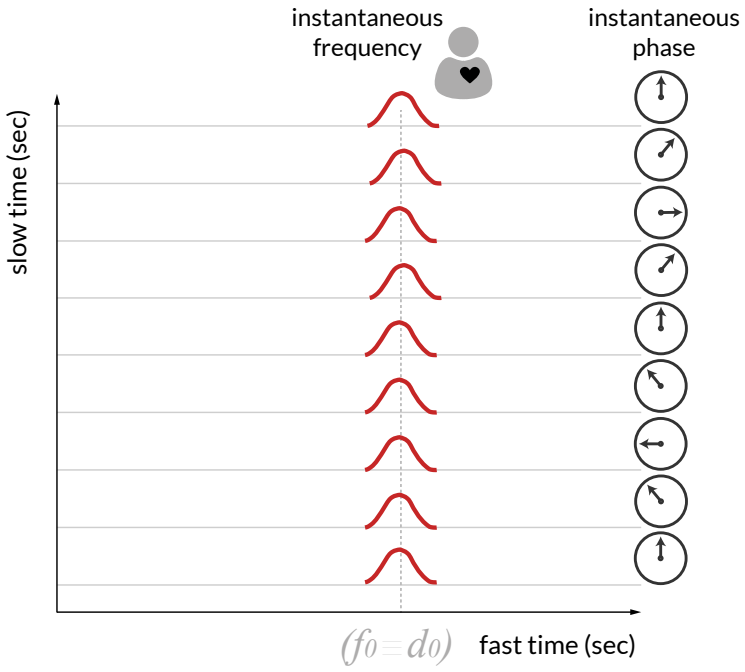

Figure 3.16: FMCW vital signs mathematical model representation in a matrix R.

3.5 Interaction of RF Waves with Human Body

Electromagnetic waves suffer from multiple phenomenon effects of reflection, transmission, and absorption when crossing mediums with distinct physical characteristics. Hence, analysis of physical effects beyond the interaction of radio waves with human targets is very important for a better comprehension of cardiovascular radar data information.

In a first approximation, the human body can be compared to a multi-layer model, in which each layer corresponds to a particular tissue with specific thickness, density, permittivity and conductivity [104]. The permittivity ϵ of each layer can be derived from Cole-Cole Model [105] showing that for higher RF incident frequencies, the permittivity of the human tissues is severely diminished [106, 107]. Figure 3.17 shows a multilayered model with permittivity ϵ calculated for different tissue's layers.

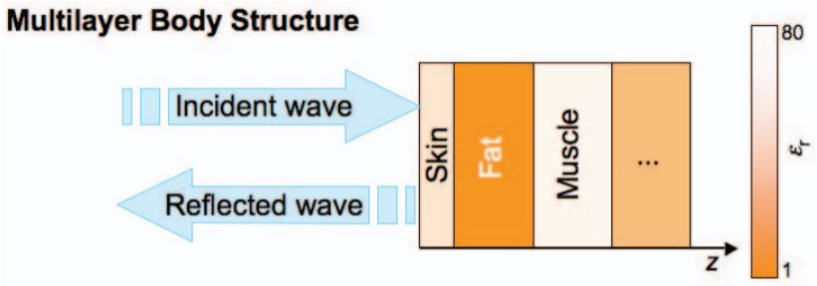

Figure 3.17: Multilayered model structure and different permittivity ϵ of each layer tissue [107].

Despite RF waves in low frequency conditions being able to penetrate the human tissue, the major quantity of detected energy on the radar is coming from the reflection of radiation in air/ skin boundary surface [108]. When an electromagnetic wave hits in a boundary surface between two different dielectric mediums, part of the wave is reflected while the other is transmitted for the second medium. The reflection coefficient, $R_{1/2}$, between two different dielectric mediums is defined as the ratio of the intensities of the reflected and incident waves, and could be given by respective dielectric constants, ϵ_1 and ϵ_2 of the different mediums:

$$R_{1/2} = \frac{\epsilon_1 - \epsilon_2}{\epsilon_1 + \epsilon_2} \tag{3.23}$$

where n is dependent on dielectric proprieties of tissues. According to the last equation, it is estimated that approximately 70% of the radar wave energy is reflected in the surface air/skin [108]. The remaining energy is then propagated into the human body being continuously absorbed and echoed into the deeper tissue's layers. These numbers suggest that the majority of respiratory and heartbeat signals detected by radar devices are coming from direct measurements of body surface displacement over time, whereas a minor part is directly reflected from heart surface – Figure 3.18. Nevertheless, the origin of

cardiovascular signals as well as their appearance on radar signals is not always the same and differ from several factors such as the frequency, the angle of beam incidence on body surface, the corporal position and tissues composition.

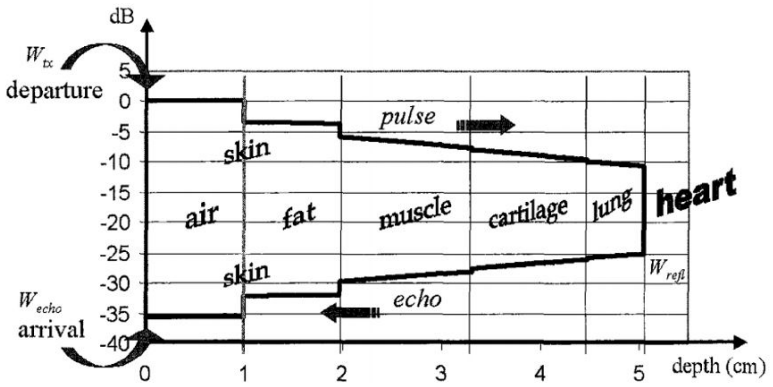

Figure 3.18: Staderini model showing how RF signals are reflected between tissues boundaries and move on through layers inside the human body. [109]. This model assumes the emission of a 1.5 GHz RF pulse used in an IR-UWB architecture.

Chapter 4

Radar Configuration and Data Process Pipeline

This section focus on the IR-UWB and FMCW radar sensors selected to be used in this study. The main objective of this chapter is to briefly present sensors capabilities as well as the configuration performed in each sensor, here adapted to be exclusively used as vital signs sensing sensors. The working principle of sensors is described together with the rationale behind the configuration performed. In the end, a final section summarizes all the embedded configuration performed in both radar sensors to clarify its importance in offline signals processing algorithms developed in the next chapter.

4.1 Context

Subsequently to the previous research performed and presented in Chapter 2, a new search was initiated to find a commercial radar that could be integrated into a future remote vital sign monitoring product. Four criteria were established for the radar sensor selection:

1. The radar must be able to detect small displacements in the millimetric scale for chest movements monitoring;
2. The radar should distinguish different targets located in the same area to enable, in a foreseeable future, multi person monitoring;
3. The individual radar chip price should be considered in a final product for sale;
4. The radar sensor must comply with the worldwide regulation of radiation emission, easing up making the certification process.

According to the prior requirements, the XeThru X4 [110] by Novelda AS and the mmWave IWR1843 [111] by Texas Instruments were chosen as the best sensors options in the prevailing market. The X4 is an ultra-wideband impulse radar combining a 7.29 and 8.75 GHz transmitter, whereas the TI IWR1843 is a single-chip radar based on FMCW technology operating in the band range of 76 GHz to 81 GHz. The fundamentals of IR-UWB and FMCW radar technology were described in Section 3.3 and Section 3.4, respectively.

As multi-purpose industrial radars, the X4 and the IWR1843 have to be configurated depending on the desired application. **The hardware architecture, capabilities and limitations of both sensors need to be first understood in order to find their ideal settings for vital signs detection**. As mentioned before, while IR-UWB uses very short and periodical pulses for target detection, the FMCW uses a modulated frequency continuous wave. Naturally, this is translated into different radar data types, and different methods are required for vital signs acquisition by each one of the sensors. **In this study, the configuration performed in these radars was also designed to provide an equivalent output radar raw data**. Thus, regardless of the radar technology used by the devices, both were programmed to produce the same kind of structured data with analogous information. Data coming from both sensors can be further treated and processed by a unique general algorithm for vital sign monitoring in offline mode, without distinctions between radar sensors. The main purpose of doing these equivalence between the raw data was to allow an easier performance comparison evaluation of signals extracted from the different sensors in Chapter 5, making both radars agnostic. The results of this comparison will be considered to conclude about which radar should be used in a future PLUX remote vital signs module. Finally, Figure 4.1 summarizes all the steps required and used to configure both IR-UWB and FMCW sensors. In the next sections, each topic is described for each one of the mentioned radar models.

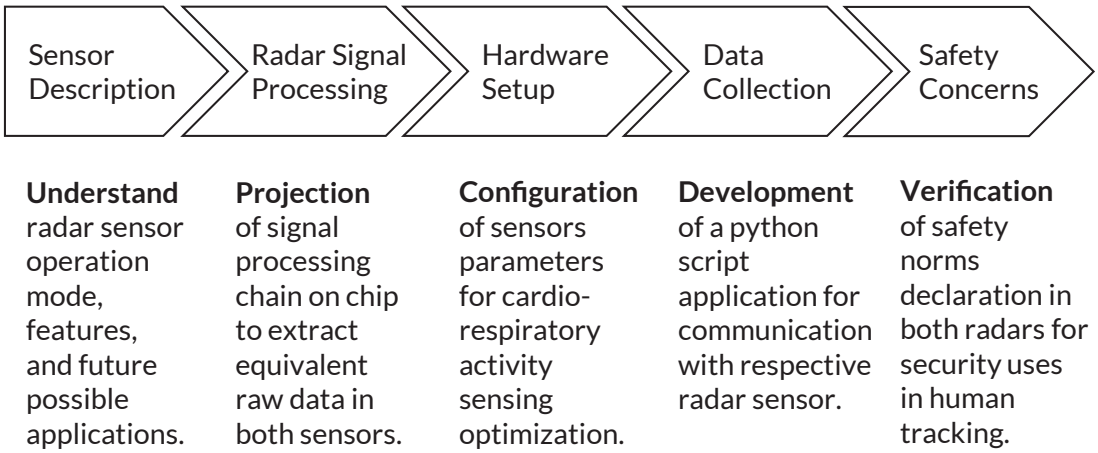

Figure 4.1: Methods employed to configure IR-UWB and FMCW sensors in order to maximize their potential in vital signs sensing and make their raw data output equivalent.

4.2 IR-UWB Radar

The XeThru X4 is an impulse Radar Transceiver System on Chip (SoC) featured by a 7.29/8.75GHz transmitter, a direct RF-sampling receiver and other related controller circuits. It is a fully programable sensor where configuration and communication can be done through a Serial Peripheral Interface (SPI) connected to an external Micro Controller Unit (MCU) host. The X4M03, used in this study, was developed as an easily X4 integration tool for investigational and commercial purposes. X4M03 and the general X4 diagram block are illustrated in Figure 4.2.

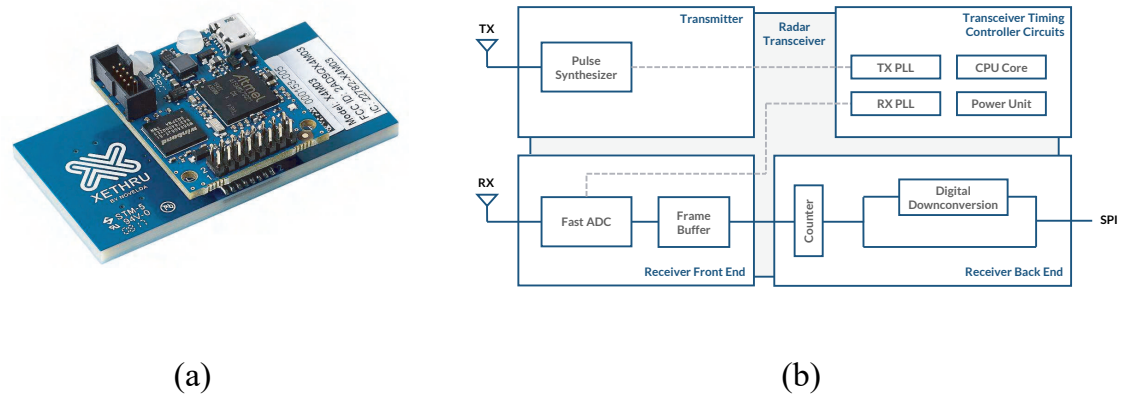

Figure 4.2: IR-UWB radar system used in this study: (a) X4M03 IR-UWB radar development kit and (b) X4 sensor general block diagram.

As an IR-UWB system, X4 consists of a transmitter, receiver and a back-end receiver controller where received echo signals data are processed. Beyond X4, the X4M03 includes an XTMCU module which contains an Atmel MCU linked to X4 that enable the development of Digital Signal Processing (DSP) algorithms for custom user applications. This MCU role is to extract and configure the X4 module.

Different antennas designs lead to different output signals, and therefore, the antenna used should be considered. The X4A02 is a differential directional patch antenna exclusively designed and certificated for the X4M03 product. This antenna contains an integrated filter optimized for frequencies between the 6.0 and 8.5 GHz, which is very useful for Wireless Fidelity (Wi-Fi) noise signals prevention.

At last, a Power Management Unit is also available and can be arranged for low power consumption applications. This is a very useful feature since it can be used to increase radar autonomy. In the presented work, energy consumption was not considered, and therefore this module was not configured.

4.2.1 Radar Signal Processing

The signal chain processing implemented on X4 radar is illustrated in Figure 4.3.

Figure 4.3: Embedded radar signal chain processing from the reception of RF echo pulses to the emmission of the digital complex range frame (or raw data).

4.2.1.1 Coherent Integration

As a coherent pulse-radar, the X4 uses an integration technique to improve the SNR of the reflected pulses. This integration is performed along with the sampling of the reflected signals in a process called Swept Threshold (ST) [112, 113]. In ST method, the backscattered RF signals $P(t)$ are compared with a sweep threshold $V(t)$, which increases over time during a configurable time-windowing T. Then, for each comparison that occurs between two pulses emissions, all the P values above V in an instant t are added to a range frame counter that is filled during that interval. After this time T, all the radar echo frames summed in that time-windowing will generate a unique RF echo frame data in which SNR gain will be dependent on the sweep time integration. Overall, ST method sums the pulses echo signals for signal-quality enhancement (see Figure 4.4).

Since X4 is only allowed to operate in very restricted power conditions of the unlicensed band, this ability to increase SNR is especially important to track the chest movements of a human target. However, signal integration is limited by the speed requirements of the application. That is, greater signals integration requires more time to compute RF digital frames.

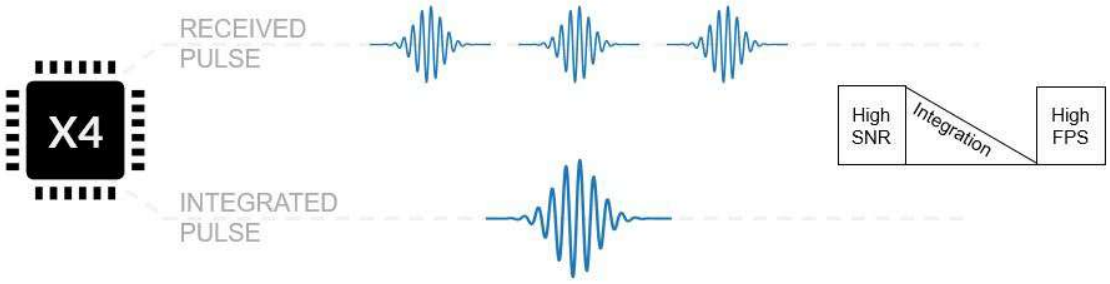

Figure 4.4: Integration signal processing step configured in X4 to improve SNR of the received pulses. High pulse integration allows the detection of millimetric expression over time that allows vital signs sensing.

According to the previous statements, and considering that vital signs are extracted over slow-time direction (concept covered in Subsection 3.3.3) the X4 was configured to perform a maximum signal integration required to make the correct sampling of the

cardiorespiratory signals. According to Nyquist Theorem [114], the minimum number of Frames per Second (FPS) should be at least twice the highest frequency of expected signals. For an adult in a rest situation, the maximum physiological frequency signal expected is 1.7 Hz due to heartbeat (based on reference values of Table 3.1). Hence, a short and empirical test was performed in order to find the best trade-off between integration values and FPS value. A value of 20 FPS was decided to be used. Integration values are obtained from ST parameters and could be found in more detail in a general equation, further presented on Section 4.2.2, used to configure all the X4 parameters.

4.2.1.2 RF Downconversion

The I/Q demodulator is an optional digital processor module on the X4 which allows, the conversion of sampled and integrated RF echo signals into an equivalent complex number structure represented by means of Quadrature (Q) and In-phase (I) signals.

I/Q data [115] grant a much more precise mean of representing the amplitude and phase of a time-domain signal. Instead of looking at the signal as a flat curve in a time-amplitude representation, the I/Q data allows a "3-D"representation signal, avoiding all the related problems of 2-D signals analysis such as negative frequency concepts, or null point problems in case of radar applications. In mathematical terms, the In-Phase (I) signal corresponds to the original 2-D signal, whereas Q component is a result of the original signal shifted by 90 degrees. As a result, every single point of the 3-D signal can be represented as a phasor in the complex plane - Figure 4.5. Hence, these two components can be easily used to recover amplitude (A) and Phase (P) values of the original time-domain signal, taking into account their representation as shifted sinusoids in the real and imaginary plan.

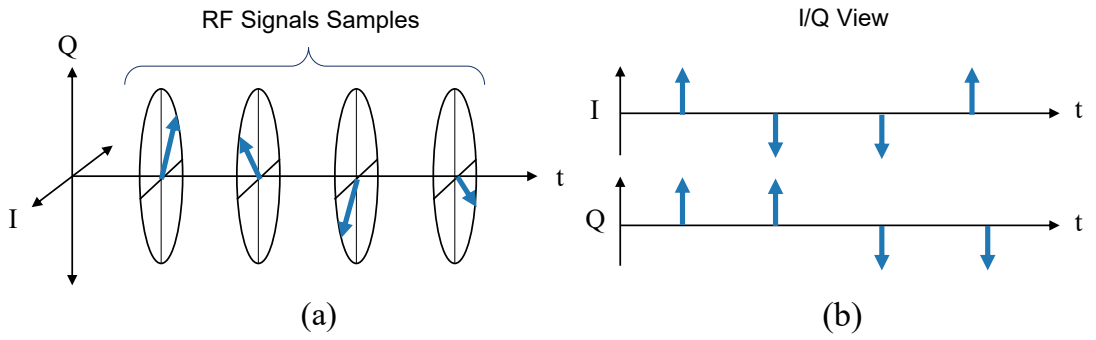

Figure 4.5: I/Q representation of a time-domain signal: (a) 3D representation, each sample have a phasor representation over time and (b) 2D representation where each signal are the projections of 3D signal in I and Q axes.

In coherent pulse radar sensors, the signals are always transmitted with the same phase. This allows the X4 system the capabilities to sense phase variations in the carrier wave of received echo pulses over time and consequently, detect very tiny movements

with high resolution. Although it is possible the use of the high spatial resolution of an IR-UWB radar for chest movement tracking over time, a phased-based method was used due to radars equivalence purpose. This phase tracking signal is very similar to the concept used in CW radars and consequently, phase variations that occurred in X4 RF signals could also be described by Equation 3.19. The I/Q data structure representation is then a much more practical in the extraction of RF phase over time, and therefore, the integrated module in the X4 was activated to directly transform the RF range echo data into I/Q complex range data, outputting a complex number comprised by real and imaginary part, corresponding to I and Q signal, respectively.

For an easier visualization of this process, Figure 4.6 represents at the top a typical RF range echo signal sampled by the X4 after coherent integration and at the bottom their own representation as I/Q and Amplitude/Phase data (A/P). **Note that, in our study, only I and Q channels are sent by the X4**, and therefore the RF signal is a reconstruction of original signal by inverse I/Q data manipulation. Similarly, A/P data is also a representation of amplitude and phase of original RF signal, originated from I/Q data. The amplitude component is often called as baseband signal since it is only an envelope representation of the RF frame.

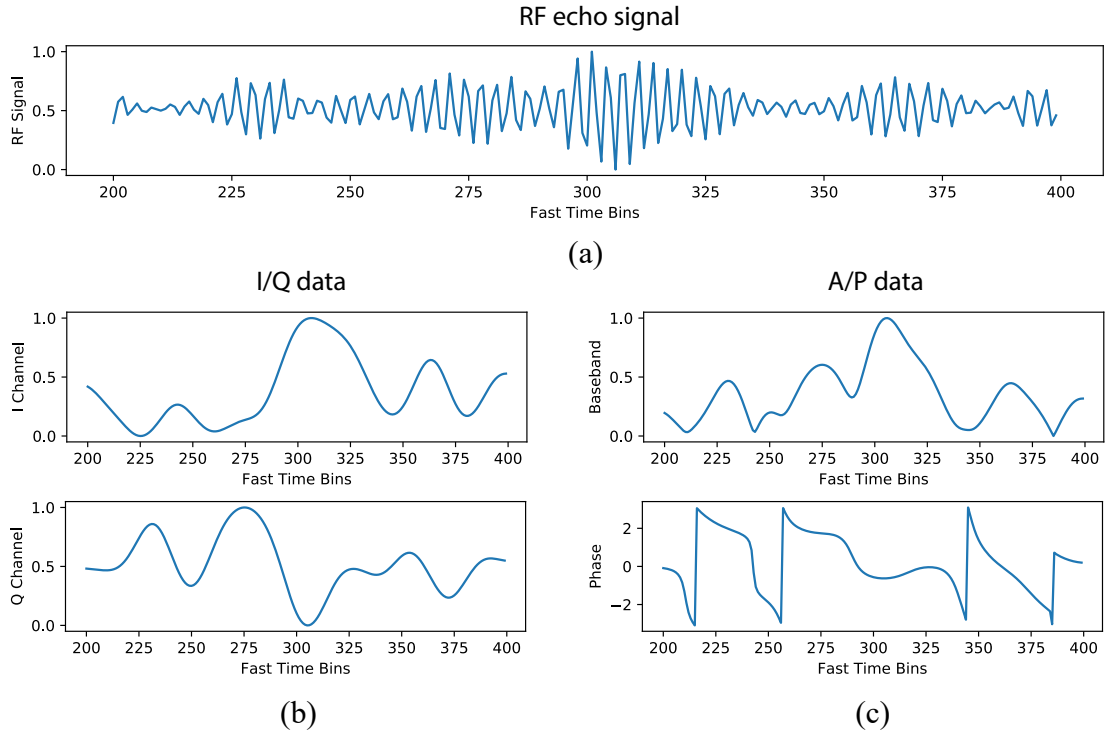

Figure 4.6: X4 output radar data examples: (a) RF echo signal after integration process, (b) I/Q data representing the real and imaginary part of the raw data signal sent by X4 and (c) A/P data representing the baseband and phase signal of RF echo signal obtained through I/Q manipulation. All signals are normalized excepting phase frame that is contained in a $-\pi$ to $+\pi$ interval.

4.2.2 Hardware Setup

Configuration in the X4 is about finding the best trade-offs between the frame size, speed, and SNR of the collected RF range frames through the adjustment of 7 transceiver parameters presented and described below. These parameters should be set according to Condition 4.1:

$$FPS \geq \frac{PRF}{Iterations \times PulsesPerStep \times (DAC_{max} - DAC_{min} + 1)} \times D \tag{4.1}$$

where FPS is the maximum number of frames per second that is possible to emit without data ambiguities, PRF (Pulse Repetition Frequency) is the frame size related to maximum radar range and D is a duty variable. The denominator values are parameters of Swept Threshold (ST) sampling technique related to integration level. Indeed, Equation 4.1 mathematical describes the concept of integration *versus* speed already mentioned before. The parameters chosen to achieve 20 FPS and key characteristics used in this work are presented on Table 4.1.

Beyond integration and speed, other related IR-UWB radar conditions mentioned in IR-UWB theoretical concepts (Subsection 3.3) have to be considered. First, the frame length was defined to be shorter than $1/PRF$ condition. Second, and related to power emission regulation, TX center frequency was defined according to European Telecommunications Standards Institute (ETSI) rules. Global RF power and FPS value were also evaluated together, confirming that both did not break the regulatory agreement.

For this configuration, the standard XeThru Embedded Platform (XEP) firmware was uploaded into the XTMCU module. XEP is an open source project developed for an easy configuration between the X4 hardware with the host system.

Table 4.1: Parameters used in X4 IR-UWB radar configuration.

Parameter	Value	Unit
TX Center Frequency	7.29	GHz
Pulse Width	0.6	ns
Pulse Repetition Frequency (PRF)	15.18	MHz
Sampling Rate	23.33	GS/s
Frame Length	1536/9.9	bins/m
Frame Per Second (FPS)	20	Hz
Frame Resolution	0.64	cm
Iterations	64	-
Pulses Per Step	56	-
DAC max	950	-
DAC min	1150	-
Duty Cycle	95	%

4.2.3 Data Collection

For configuration and communication with X4 module, three python functions were created using XEP Application Programming Interface (API). XEP allows two types of communications interfaces for data transferring: Universal Asynchronous Receiver-Transmitter (UART) and Universal Serial Bus (USB). USB was the interface used in this first experimental test. XEP firmware asks for the confguration parameters before starting an acquisition, thus three principal functions were created to log data:

- **Start Acquisition:** The X4 chip is activated and configuration parameters (presented on Table 4.1) are uploaded to chip, and radar frames start to be sent via USB from the device.
  Function call: start_uwb()
- **Acquisition:** During an acquisition (at every 50 milliseconds or 20 FPS) a new complex radar range frame is received and stored into a row of a predefined data matrix.
  Function call: log_uwb()
- **Stop Acquisition:** When data acquisition is interrupted the matrix with collected radar data and acquisition parameters are saved into a *.txt* file.
  Function call: stop_uwb()

Developed code and practical examples could be found in **X4 folder** at:
https://github.com/alexandrasdl/RADAR-WORLD.

4.2.4 Safety Concerns

The X4 SoC complies with the international transmission power standards for UWB systems concerning the maximum total transmitted power, regulated by FCC and ETSI. International Commission on Non-Ionizing Radiation Protection (ICNIRP) guidelines were used by NOVELDA AS, to evaluate the electromagnetic safety of the XeThru technology [116]. The X4 transmitter power is below ICNIRP reference levels and other familiar technologies such as 5 GHz Wi-Fi, 3G mobile phone and Bluetooth, not representing any hazard to human's health when operating within the announced power limits. The X4M03 parameters used (Table 4.1) are in accordance with the mentioned standards.

4.3 FMCW Radar

The IWR1843 is an integrated single-chip radar based on FMCW technology which offers a frequency range of 76 GHz to 81 GHz, with up to 4 GHz continuous chirp. It is a high performance sensor from the mmWave series developed by Texas Instrumentals. The mmWave series is a class of intelligent radar sensors that use very short-wavelength in the electromagnetic spectrum for high accuracy measurements in millimetric ranges. These sensors were designed to be used in the next generation of Internet of Things (IoT) devices, and for this reason, they can perform robust digital processing signal on-chip. In this work, the IWR1843 Radar BOOST development board was used - Figure 4.7 (a). The block diagram of IWR1843 is illustrated in Figure 4.7 (b).

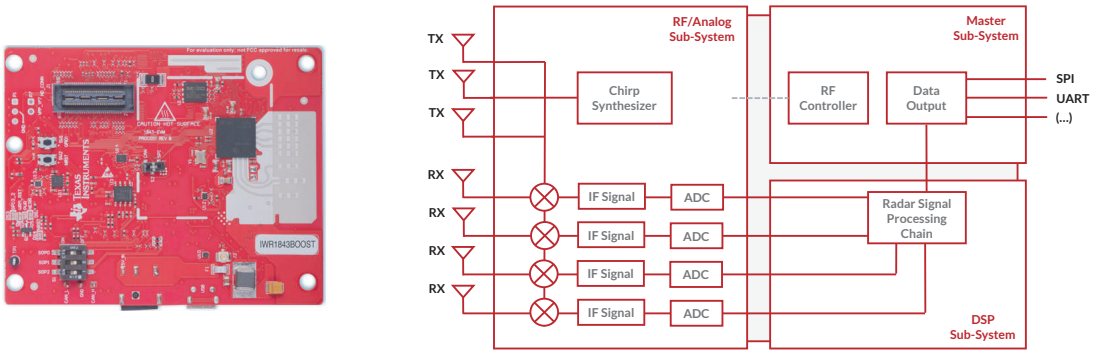

(a) (b)

Figure 4.7: FMCW radar system used in this study: (a) IWR1843 BOOST development board and (b) IWR1843 sensor general block diagram.

The IWR1843 features 3 principal blocks which have including two processors: the C674x DSP used to run high-level signal algorithms processing and an hardware accelerator (HWA) unity to perform more common digital signal processing methods as FFT computations. In fact, this FMCW radar is able to make all the vital signs processing on chip however, the algorithms developed in this work for cardiorespiratory information extraction were applied (off-chip) after raw data acquisition.

With respect to the antennas, IWR1843 is provided with a set of Multiple-In Multiple-Out (MIMO) antennas with 3 transmitters (TX) and 4 receivers (RX). MIMO antennas provide extra sensing capabilities sensor that a mono antenna, giving it for example a better angle resolution, a feature that mono antennas cannot perceive. Despite the manipulation of the signals received from different antennas could give better vital sensing capabilities to FMCW, only a pair of TX/RX antennas was activated in this study.

4.3.1 Radar Signal Processing

For equivalence purpose between radars, the output of this FMCW radar should be in complex range frame format as it was previously set in the X4 IR-UWB radar. Therefore the in-chip processing capabilities of the IWR were used to convert the reflected chirps into this format. The radar chain processing used in this FMCW sensor is illustrated on Figure 4.8.

Figure 4.8: Embedded radar signal chain processing from the reception and mixing of chirps signals to the return of the digital complex range frame (or raw data).

4.3.1.1 Chirp Mixing

As seen in the previous chapter, the FMCW radar working principle is based on the comparison of transmitted and received chirps. In the IWR1843, this process takes place at the a RF/Analog subsystem with a mixer structure (see Figure 4.7 (a)). Here, the TX and RX chirps are multiplied together in an analog process resulting in a new IF analogous signal. This IF signal contains all the information needed about frequency and phase differences between transmitted and received chirps. Thereafter, the IF signal is sampled by a high-speed ADC, with a sample rate in accordance with the maximum range defined by Equation 3.14. The FMCW concepts mentioned above can be reviewed in Subsection 3.4 of the theoretical concepts chapter.

4.3.1.2 Complex FFT Computation

Following the model described in Subsection 3.4.2, in FMCW radar, millimetric chest movements can be extracted from phase analysis over slow-time direction. Using IF signals sequences, phase variations can be obtained in a specified frequency (related with target position) using Equation 3.12. Hence, to easily recover the phase frames, FFT was applied to each IF signal. The FFT transformation converts the IF signals from its original time-domain to a complex representation in the frequency-domain. Two-side spectrum in complex form of real and imaginary parts are returned by FFT, and therefore, complex radar range frames can be recovered, in the fast time direction, from the direct FFT application to IF signals. These complex values can be then offline converted to a polar referential in order to obtain magnitude and phase values of the IF spectrums.

For FFT computation, the embedded signal processing capabilities of the IWR1843 were used, and FFT computed inside the chip after IF signal sampling. The choice of a FFT computation inside the chip was made for two main reasons: First, there was a hardware resource limitation in IF signal transferring. Since IF signal was expected to

be sampling at 2 MHz, UART communication, which is a serial protocol widely used in embedded application, does not have enough throughput to transfer all the data. Second, and as mentioned several times before, to achieve complex output, equivalent with X4 sensors.

Figure 4.9 (a) reports an example of the complex radar raw data emitted by the IWR1843 radar. The real and imaginary range frames directly obtained from the sensor are represented in (a), whereas the recovered amplitude and phase of complex IF spectrum are illustrated in (b).

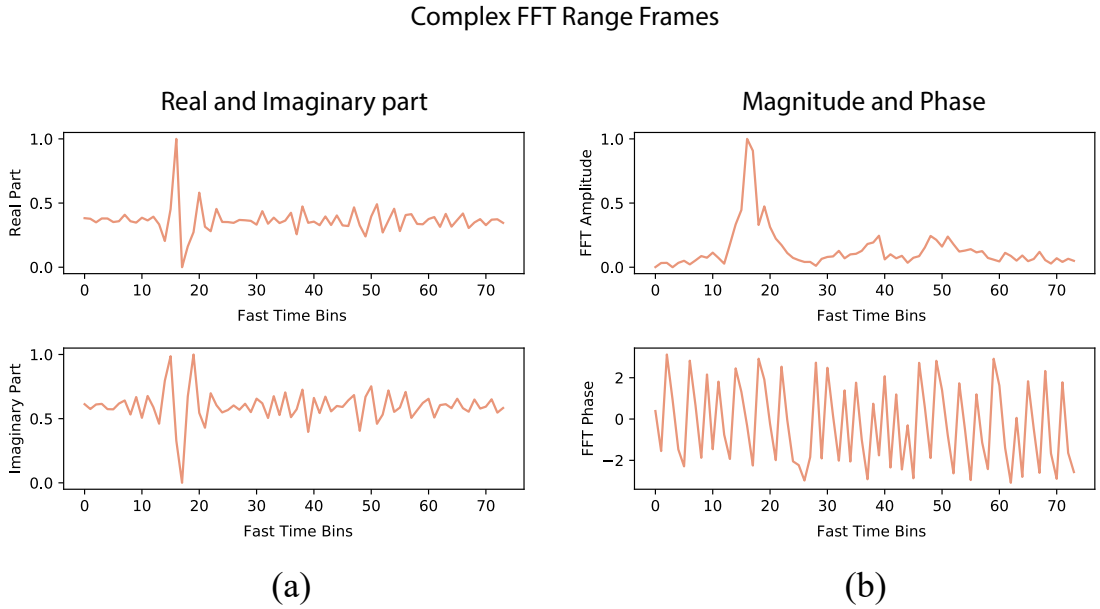

Figure 4.9: FMCW output radar data examples. (a) Real and imaginary part components of complex FFT computed on IWR1843 chip (raw data) and (b) the amplitude and phase representation of FFT computed from extracted data. All signals are normalized excepting phase frame that is contained in a $-\pi$ to $+\pi$ interval.

4.3.2 Hardware Setup

For the IWR1843 configuration, the mmWave SDK Out-of-Box Demo for XWR18xx firmware code was adapted only to emit FFT complex data and was flashed into the IWR1843 board. The mmWave Demo visualizer tool was also used for a first parameters adjustment. This is a Texas Instruments (TI) tool, where chirp parameters and other sensor specification can be tested before being implemented in a final product.

As a FMCW system, the radar capabilities are dependent on chirp parameters, which were defined according to range problem conditions. As we are interested in acquiring at a sampling rate equal to X4, for equivalence purposes, a unique chirp was configured to be emitted at 20 Hz. ADC sampling rate was set to 2 MHz, allowing the detection of targets up to 3.75 meters (see Equation 3.22). Table 4.9 summarizes the chirp and IRW1843 parameters used in this study.

Table 4.2: Key parameters used in mmWave IWR1843 FMCW radar configuration.

Parameter	Value	Unit
Bandwidth (B)	4	GHz
Starting Frequency (Fc)	77	GHz
Chirp Duration (Tc)	50	μs
Slope (S)	0.8	GHz/μs
ADC Sampling Rate (Fs)	2	MHz
Frame Length	100/3.75	bins/m
Frame Per Second (FPS)	20	Hz
FFT Frame Resolution	3.75	cm

4.3.3 Data Collection

Configuration and communication of IWR1843 with a master computer were performed via UART. The uploaded firmware requires that, before starting a new acquisition, a chirp profile file is sent with the configuration. Only after that, the IWR1843 is able to streaming data where complex range profiles are computed and send out to a host at 20 FPS. Similar to the X4, three python script functions were created for the initialization, reception and storage of the data. *PySerial* was used for the access of the two serial ports used by this sensor. One port is used for chirp configuration while the other is used for faster data transferring from radar. The python functions are briefly described below:

- **Start Acquisition:** Serial ports are open, IWR1843 is activated, and configuration parameters (presented on Table 4.2) are uploaded to chip.
  Function call: start_fmcw()

- **Acquisition:** During an acquisition, at every 50 milliseconds, a radar output packet frame is received via a serial port. This packet needs to be converted from their byte structure to integer complex data range frames. Only after, complex data is stored as a row in a predefined matrix.
  Function call: log_fmcw()

- **Stop Acquisition:** When data acquisition is interrupted, the matrix data and acquisition parameters are saved into a *.txt* file. The serial ports are closed.
  Function call: stop_fmcw()

Developed code and practical examples could be found in **IWR1843 folder** at:
https://github.com/alexandrasdl/RADAR-WORLD.

4.3.4 Safety Concerns

The IWR1843 BOOST Board is declared to be in conformity with the European radio equipment legislation [117], not representing any danger to human or animal health.

4.4 Raw Data Equivalence

In the last sections, it was shown how both radar sensors were configured to 1) be optimized to detect small motions with maximum SNR possible while respecting Nyquist Frequency, and 2) to perfom an initial internal radar signal processing in order to output data that is equivalent between both IR-UWB and FMCW radar sensors.

Regarding the X4, the previously integrated and sampled RF echo signals frames are internally converted into complex I/Q frames data. Hence, the X4 output is characterized by the return of complex frames, where real and imaginary parts of each point are the I and Q signals, respectively.

Regarding the IWR1843, the TX and RX chirps are mixed, creating the IF signal which is transformed internally into a frequency spectrum using a FFT, originating, in an analogous form to the X4, complex ranges frame data. The output of the IWR1843 radar is then also characterized by the emission of complex frames, where real and imaginary components of each point correspond to the real and imaginary parts of an FFT spectrum, respectively.

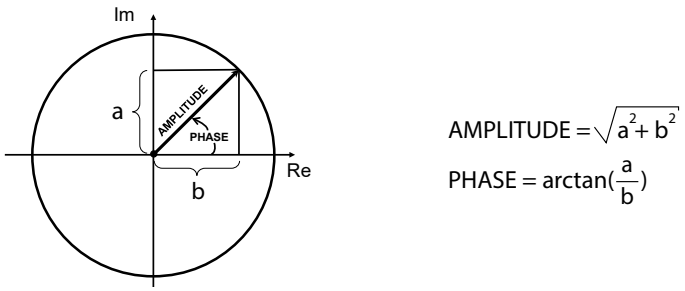

Figure 4.10: Phasor Representation. Regarding the use of a IR-UWB or FMCW radar in our collected radar data, output samples were programmed to be represented as phasors, where amplitude and phase with the same physical meaning can be obtained.

Despite the different nature of the output complex data in both radar, this equivalence process permits a similar data processing chain for both. That is, assuming that each point could be represented by a phasor (see Figure 4.10), the amplitude and phase of signals could be recovered by applying the same functions to signals. These amplitude and phase have the same physical meaning regarding the complex data nature, and therefore, data collected from FMCW and IR-UWB radars can be further processed, taking into account only their physical meaning. The resulting amplitude frames correspond to range profiles, where the relative signal amplitudes are dependent on the distance from the radar of the

object that reflect it, and phase frames, corresponding to the phase shift of the reflected wave when impacted the object.

In summary, the collected amplitude matrix should be used to detect the range bin where the target is situated, whereas phase matrix should be used to collect the millimetric chest displacement over slow time direction in the selected range bin target position. Hence, due to the equivalent radar process, the same signal processing algorithms could be posteriorly applied in offline mode for the extraction of heart and respiratory components. This fact will allow a better comparison performance between the quality of signals emitted by both sensors.

Finally, Figure 4.11 summarizes the modifications performed in each radar, and respective chain processings, to create the output radar raw data equivalent. Note that, only complex range matrix maps $R[m,n]$, or raw data, is effectively collected from each radar sensor and amplitude and phase maps computed afterwards.

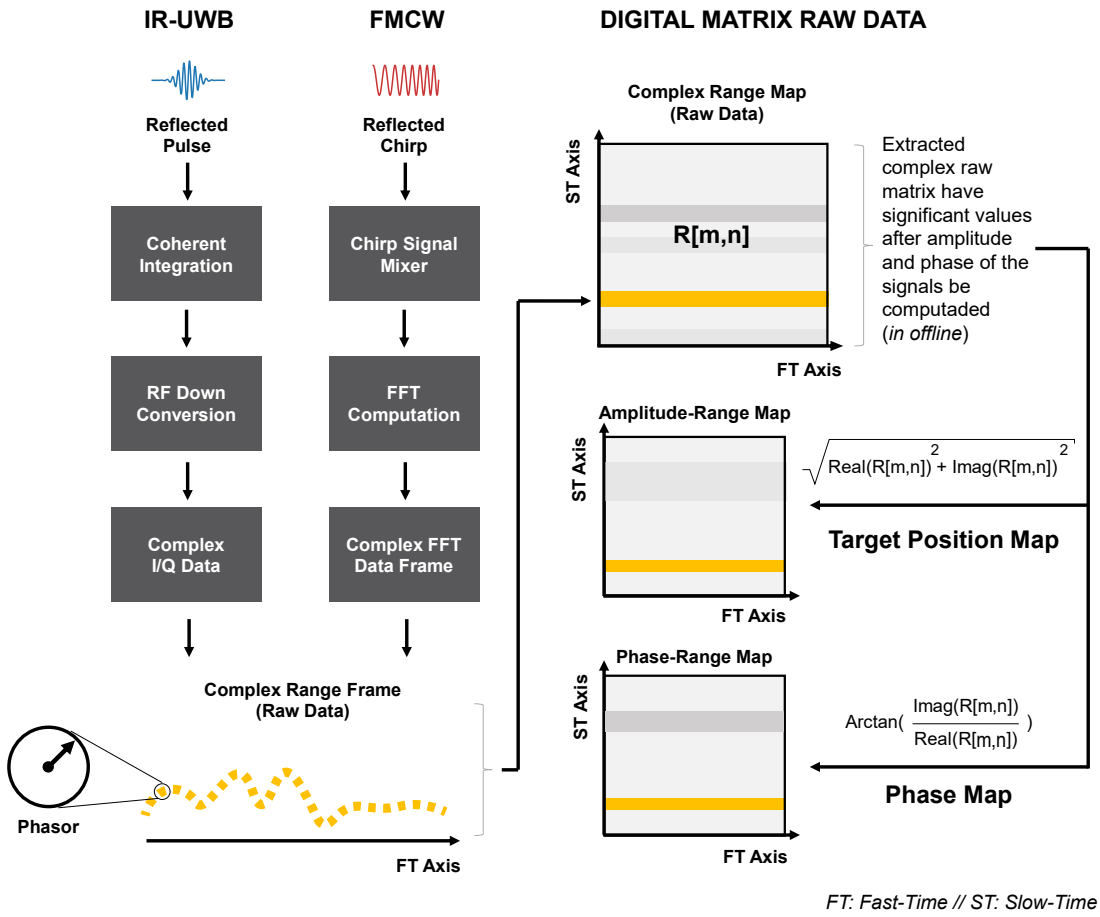

Figure 4.11: General diagram of raw data equivalence process resulted from the configuration and embedded signal processing of IR-UWB and FMCW radars.

Chapter 5

Data Acquisition and Signal Processing

This chapter intends to evaluate the practical viability in the use of radars for cardiorespiratory sensing. Experimental data collection, employed signal processing techniques and cardiorespiratory data assessment methods are presented.

5.1 Context

To validate the reliability in the use of the previously configured radar sensors in vital signs sensing, an experience with 10 healthy subjects was performed. As we are interested in making a first assessment of the ability of radar sensors in measuring millimetric chest movements in real environments, all the employed methods, described in this chapter, were developed to be simple and to give us preliminary results about their potential.

Due to the radar raw data equivalence process performed in the previous chapter, the same signals processing algorithms are applied with no distinctions between the type of radar used. It is very useful since it allows us to compare the results obtained between signals collected from different radar and conclude which one presents better performance.

Finally, different methods were chosen to separate and assess respiratory and cardiac components. As our primary interest is the development of algorithms that can be further employed in a Bio-Radar system, the presented algorithms for vital signs extraction were designed to be further implemented in real-time or batch processing applications.

All the methods were developed using the coding platform *Python* [118]. A general flow chart of the signal processing methods used and analysed in this work is given in Figure B.1 of Appendix B. It is recommended the visualization of this diagram to get a general overview of the developed work, from the detection of an echo RF signal to the extraction of respiratory and heart rate parameters.

5.2 Data Acquisition

This section describes the materials and methods used for radar data acquisition.

5.2.1 Population

The study protocol was applied to a population of 6 females and 4 males with ages comprised in the interval of 18 and 24 years old. As the cardiac and respiratory frequencies are age-dependent, a restriction interval of ages was imposed as a criterion of subjects to eliminate a variability factor of RR and HR in the studied population [119, 120]. All the participants were informed about the safety conditions of the materials used in the study. Any special outfits or some extra accessory were not requested to the participants. It was asked if the individuals suffered from any cardiorespiratory disease that could be reflected in the collected signals. Table 5.1 details the studied population characteristics.

Table 5.1: Characteristics of the studied population.

Subject	**Gender**	**Age**	**Reported Diseases**
Subject 1 (S1)	F	18	
Subject 2 (S2)	M	23	Occasional Dyspnea
Subject 3 (S3)	F	23	
Subject 4 (S4)	F	21	
Subject 5 (S5)	F	24	
Subject 6 (S6)	M	23	
Subject 7 (S7)	M	24	
Subject 8 (S8)	M	23	
Subject 9 (S9)	F	21	
Subject 10 (S10)	F	19	Asthma

5.2.2 Experimental Setup

To simulate a complex daily life environment, the experiments were performed in a small living room. During the experiments, both radar systems were placed side by side on a table, while the subject was seated in a chair at a distance d from the radars. The sensors were positioned at a distance of 1 meter from the floor to be aligned with the subject chest.

The experimental local represented in Figure 5.1, two different zones could be distinguishable: a control unit zone and a radar range zone. The radar range zone is all the area covered by the radar system, that is all the area where the radar systems can detect objects and the zone where the subject is positioned. The control unit zone is all the area where radar systems cannot detect any target and where the computers for receiving data are located.

In this experience, the X4M03 and the IWR1843 radar sensors were used with the same arrangement described in the last Chapter 4. Both were connected to a master

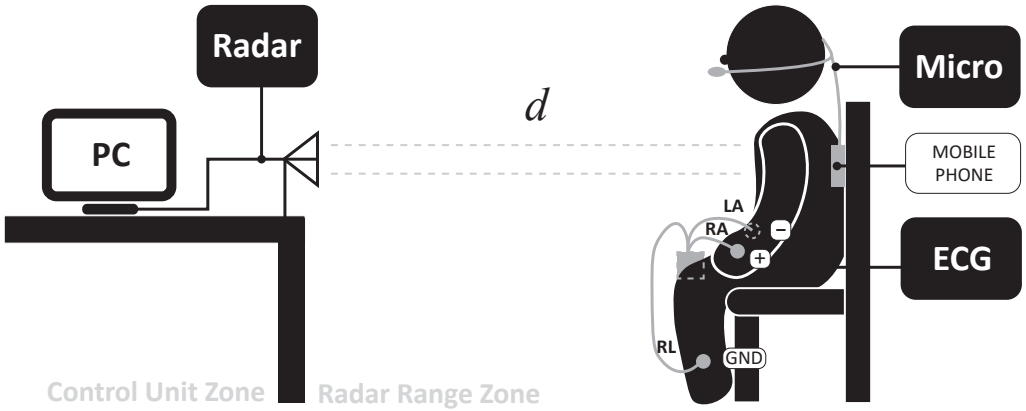

Figure 5.1: Experimental setup schema.

computer for configuration and data transference. For each radar, a python script was developed for data storage using the respective radar's functions described in Subsection 4.2.3 and 4.3.3. These scripts were programmed to record 60 seconds of radar data automatically, together with a "beep" sound of 250 Hz (from now on called BIP) set up to be played for 5 seconds, before and after, signalling the interval of data recording. These sounds were used with two main goals: first, to understand when a recording was initiated and finished within the acquisition protocol, and second to synchronize radar data with reference data, which will be described further in this chapter.

Concerning radar data acquisition parameters, the sampling rate for data frames was set to 20 FPS. Furthermore, only frame bins corresponding to a distance between the interval of 0.3 and the 3 meters were stored. This distance range interval meets test specs and still prevents antenna crosstalk effects of IR-UWB signal [121]. Henceforward, X4M03 and IWR1843 will be referred to as Radar 1 (R1) and Radar 2 (R2), respectively.

To check is the values recorded with the radars are good, breath sound and the ECG of the participants were also collected simultaneously during the radar time monitoring, to serve as ground truths. The ECG was recorded with a BITalino. The BITalino is a wearable device capable of recording biosignals which contains diverse modules for custom physiological signal measurement. In this study, an ECG BITalino module was used to record the electrical heart activity at a sampling rate of 1000 Hz. Similarly to the script developed for radar, another python script was created to receive and store the ECG data using the BITalino API. As a wearable, BITalino is capable to send data via Bluetooth (BLE), and therefore a second computer was used to run the python script to receive data via BLE. This script was programmed to play a sound of 2500 Hz (from now on called BOP) for 5 seconds before and after ECG data recording. ECG electrodes were attached to the participant's right arm (RA), left arm (LA) and right leg (RL) as it can be seen in Figure 5.2.

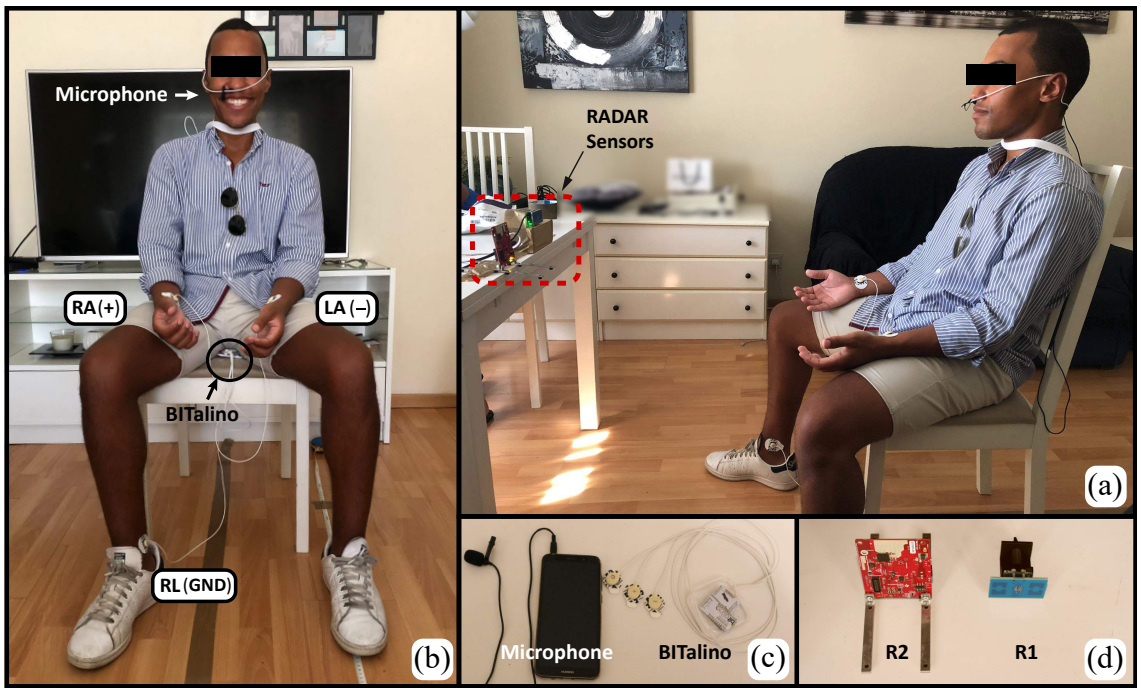

Figure 5.2: Experimental setup and materials used: (a) Frontal view of a participant placed with reference devices at 2.5 m from radar sensors; (b) Lateral view of a participant at 0.5 m from radar sensors; (c) Reference devices; (d) Radars used.

Lastly, for respiratory events reference, a small lavalier microphone placed under the participant's nose was used to detect their inspiratory and expiratory moments of breath. The microphone was connected through a cable to a mobile phone positioned in the backside of monitoring subject, and audio data captured by the microphone at 48 kHz was stored into *.wav* files using an app instaled on the mobile phone. Table 5.2 resumes the four devices and associated configurations used in this experience.

Table 5.2: Summary of materials used in the experimental test.

Sensor	Hardware	Software	FS	Timer
X4M03 - IR-UWB Radar	PC 2	Script 2	20 FPS	Automatic (60 s)
IWR1843 - FMCW Radar	PC 2	Script 3	20 FPS	Automatic (60 s)
ECG Bitalino	PC 1	Script 1	1000 Hz	Manual
Microphone	Mobile Phone	Audio Record App	48000 Hz	Manual
FS: Frequency Sampling	FPS: Frames Per Second		PC: Personal Computer	

5.2.3 Protocol Acquisition

The acquisition protocol has a duration of approximately 20 minutes, including the time spent in the microphone and electrodes placement as well as the time spent instructing the participants about the protocol acquisition. The acquisition protocol was repeated with the participant placed at 0.5, 1.5 and 2.5 meters from radar sensors. Scripts for the

ECG and radar acquisition were initiated and controlled on computers by a specialised person located at the radar range zone. Some notes were taken during the measurements related to the participant's stress status, subtle movements and some possible noises during radar acquisitions when these events were considered relevant for data analysis considerations. The acquisition protocol performed for one single distance is described below, and a timeline chart of it is shown in Figure 5.3.

Acquisition Protocol: Firstly, audio recording is manually started on the mobile phone. From that moment on, participants must remain in silence until the microphone is turned off again to avoid external audio sources overlapping the participant breath sound. In the PC 2 at the control unit zone, the scripts for ECG data collection are initiated, and the first BOP sound is played from the master computer. The sound emitted from the computer should be loud enough in order to be detected by the microphone placed on the participant. After a BOP sound of 5 seconds, BITalino starts, and ECG participant data is collected remotely. With the respiratory and cardiac activity instruments on radar monitorization starts. R1 should be first turned on and followed afterwards by R2 next. Both monitorizations were performed at different time intervals to avoid potential radio interferences. Thus, R1 is started by running Script 1 in the PC 1. Similarly to the ECG data collection, before R1 data began to be collected, a BIP sound is heard during 5 seconds. Afterwards, the R1 will be acquiring data for precisely 60 seconds. During the first 45 seconds of radar recording, the subject should breathe regularly without abrupt movements while sitting relaxed on a chair. Then, in the last 15 seconds, the subject is asked to hold his breath continuously until the second BIP sound is heard. This BIP sound is automatically played at the end of 60 seconds of radar recording when it stops to acquire data. Next, the same procedure is adopted to R2 radar. After the final R2 BIP sound, ECG is manually turned off, and a new 5-second BOP sound is heard signalling the end of heart activity recording. Lastly, audio capture is manually interrupted.

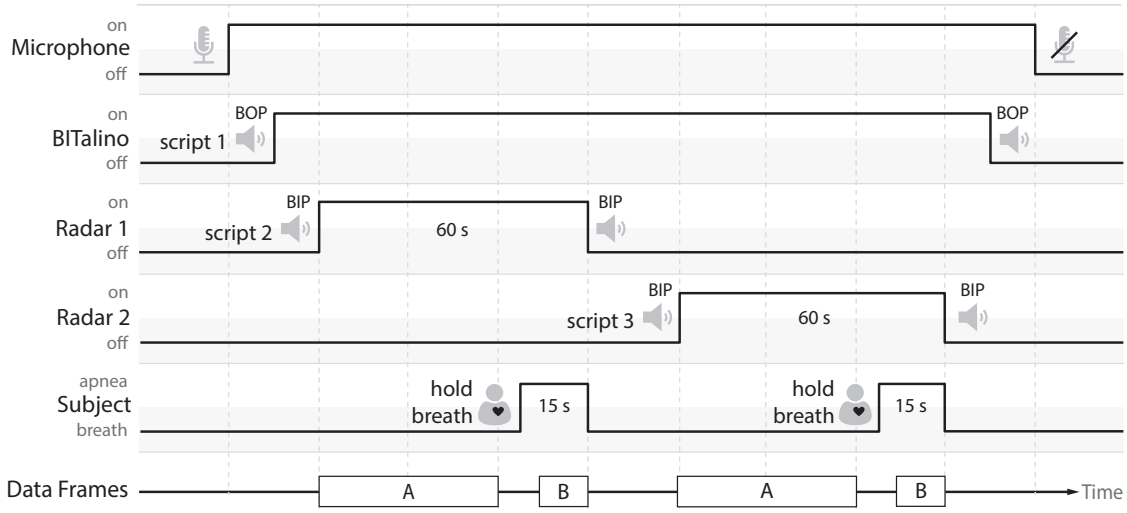

Figure 5.3: Timeline chart of the protocol acquisition applied to a single distance d.

5.3 Data Synchronization

After data collection, it was necessary to proceed with the synchronization of radar data with respective respiratory audio and ECG signals reference. As mentioned before, besides the microphone being used as a respiratory reference tool, it was also used for synchronization of data coming from the four sensors used, where BIP and BOP sounds were used to time alignment of the signals. Thus, knowing the frequency samples of the signals and the times where BIP and BOP sound occur, the reference and radar data could be time-aligned.

Therefore, BIP and BOP sound timings of ECG and radar records needed to be first annotated. For this, Audacity (an audio recording and analyzing application) was utilized for audio signal visualization and time annotation of BIP and BOP sounds. Since ECG and radar sounds were programmed to be played with different frequencies, the spectrogram mode option was used for easy identification of these mono frequency sounds (Figure 5.4).

The annotation of the first sound is sufficiently for data synchronization, however, the second BIP and BOP sounds were also annotated to verify the integrity of the recorded data. That is, in the scope of the acquisition protocol, for the correct data integrity, the time between annotated radar audio BIP sounds should be nearest 60 seconds, due to the automatic timer of radar data in the script. On the other hand, BITalino recorded data should also fit the time range between BOP sounds, to check is any ECG data was lost or if the segment is unsuccessfully aligned. As far as data integrity concerns, all the data was verified as correctly recorded and synchronized.

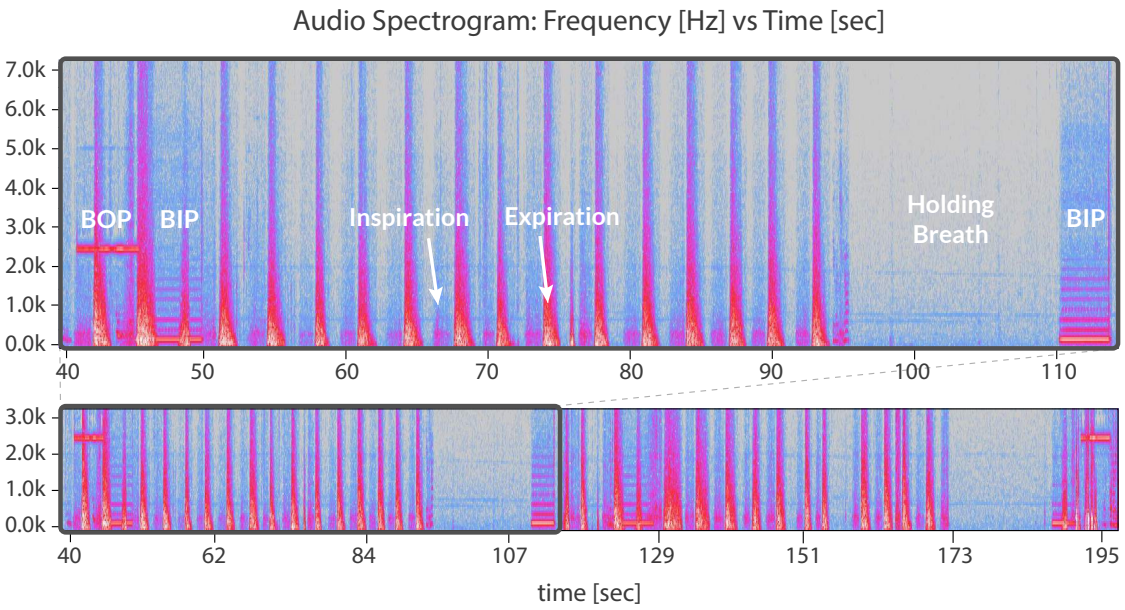

Figure 5.4: Audacity spectrogram used to annotate BIP and BOP sounds times for data synchronization.

5.4 Signal Processing: Reference Data

Respiratory Audio and ECG signals were collected to be used as reference data for cardiorespiratory radar signals evaluation. The respiratory rate (RR) and heart rate (HR) values of each subject were determined through the mean of distances of inter-peaks events. In this section, preprocessing signal methods employed to filter ground truth signals before RR and HR reference values computation are presented.

5.4.1 Audio

The respiratory audio signal is characterized by a sequence of inspiratory and expiratory moments produced by the airflow coming from the subject nose. In the audio signal, expiratory vibrations usually have a more prominent magnitude when compared with inspiration (see Figure 5.5, top subplot).

Before applying any filter to the signal, these were subsampled in order to reduce the computational complexity of the subsequently applied methods. Thus, the total number of samples in the audio frames were firstly reduced by a factor of 100. Next, and to better visualize the inspiratory and expiratory cycles, the reference audio envelope was extracted (see Figure 5.5, bottom subplot) by applying a moving average filter to the absolute of the original audio raw signal. The moving average filter was implemented with a time-window length of 1 second (or 480 data samples). At last, the processed audio signals were normalized.

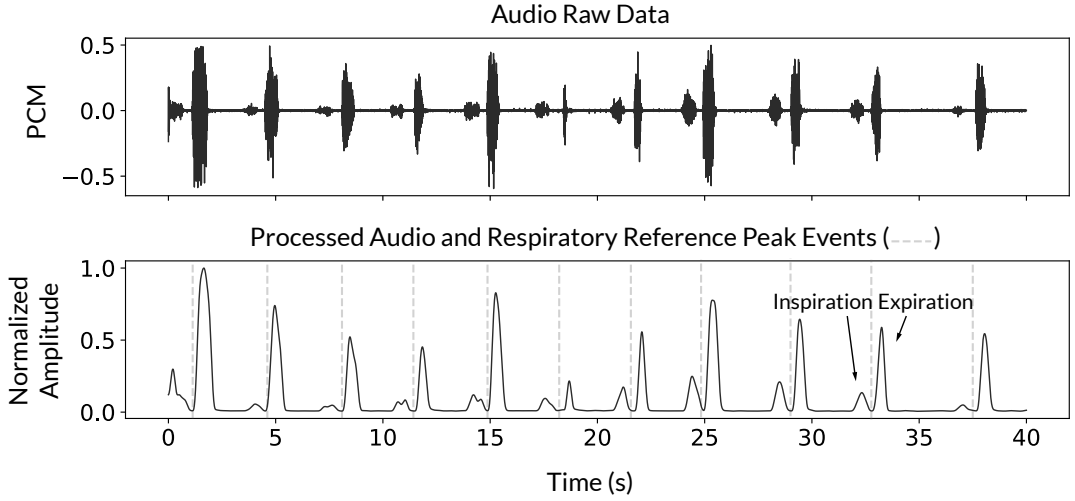

Figure 5.5: Respiratory reference signal before (top) and after (bottom) preprocessing methods applied for audio envelope extraction. Respiratory patterns are visible on signals.

Temporal peaks, used to compute reference RR value in each subject recording, were estimated based on a delayed temporal position of expiration peaks. In the first instance, expiratory peaks were detected by a peak finding method, applied along with a threshold

defined to automatically remove all the inspiratory peaks below 0.5 (one half of normalized signal). To confirm that the expiratory events were correctly detected, all the processed signals were checked, and peaks that were not detected by the imposed conditions were manually added. In case of doubts, audio frames were reproduced in *Audacity* to confirm their existence. In order to obtain reference values of maximum inspiration (or chest displacement) instants, detected expiratory peaks were delayed in 0.5 seconds or 240 data samples. These reference values correspond to dashed lines on Figure 5.5.

Finally, with N the number of segments created between two adjacent respiratory events, and pp_n the temporal distance of each segment, Equation 5.11 can then be used to compute reference RR value, in Respirations Per Minute unit (RPM), from a given audio reference signal:

$$RR_{REF} = 60 \times \left(\frac{1}{N} \sum_{n=1}^{N} pp_n \right)^{-1} \quad (RPM) \tag{5.1}$$

5.4.2 ECG

The mechanical heart activity is only possible due to the presence of a robust biological electrical system that works as a trigger for cardiac muscle contractions. ECG reflects this heart electrical activity and therefore, QRS events could be used as a data reference for a heartbeat event.

In this experiment, the R-peaks of QRS complexes were used as heart event references. In order to remove external noise manifestation on ECG signals, a digital Butterworth bandpass filter in a frequency range of 0.5 Hz to 20 Hz was applied. Subsequently, the R-peaks were easily identified through a find peaks method. An ECG acquired from Bitalino, and its post-processing signal is represented on Figure 5.6.

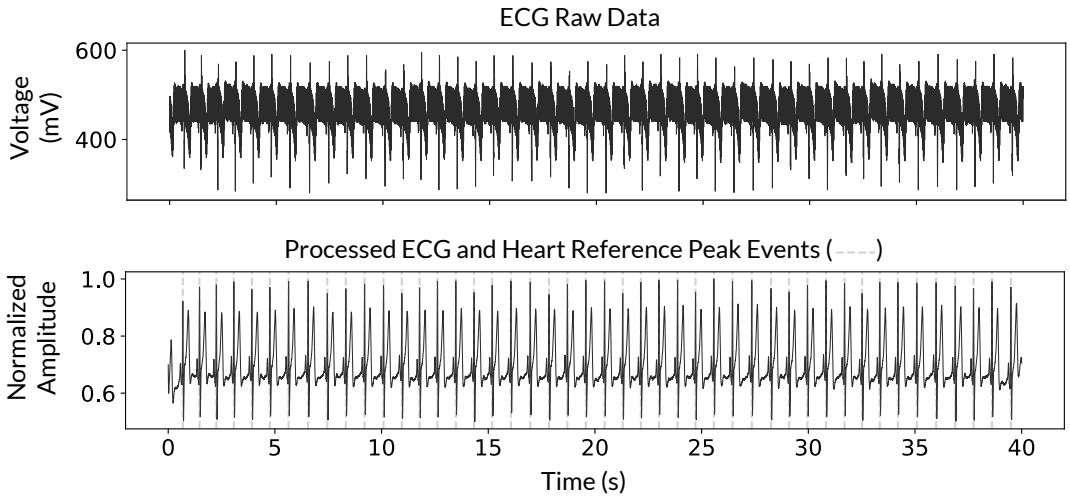

Figure 5.6: Heartbeat Reference Signal extracted from a BITalino before (top) and after (bottom) applied preprocessing methods. Dashed lines marks R peaks temporal positions, defined as reference heart events.

Hence, HR could be extracted from the mean of R-peaks segments intervals. With N being the number of R-R segments in a temporal frame, and rr_n the duration of each n-th R-R segment, HR reference value can be given, in Beats Per Minute (BPM) unit, by Equation 5.2 below:

$$HR_{REF} = 60 \times \left(\frac{1}{N} \sum_{n=1}^{N} rr_n \right)^{-1} \quad (BPM) \tag{5.2}$$

5.5 Signal Processing: Radar Data

Millimetric movements of the chest due to cardiovascular activity can be detected through phase variations of the backscattered radar signals over time. In the case of X4, the phase variations are detected in very short pulses, whereas in IWR1843, the phase changes are detected in frequency-modulated continuous waves. However, due to raw data equivalence process performed in Chapter 4, the raw radar data obtained from both radars are qualitatively similar, and therefore, the same signal processing algorithms can be applied to different radar data, regardless the radar sensor used. Figure 5.3 illustrate the steps applied to extract cardiorespiratory phase signals. Each step is described below:

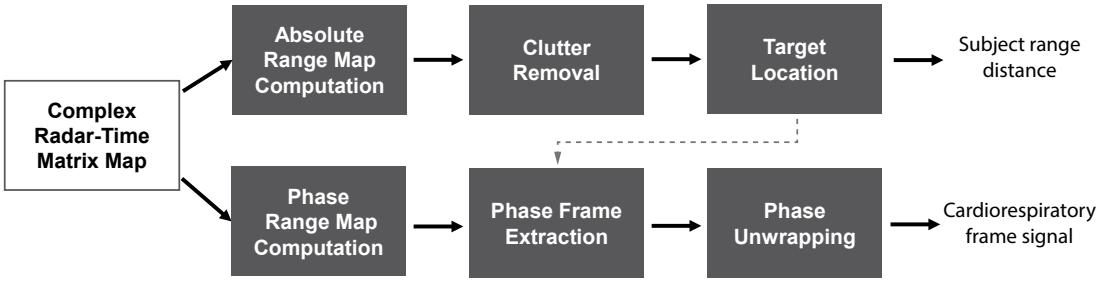

Figure 5.7: Flowchart Diagram of preprocessing methods used for cardiorespiratory phase extraction from radar raw data.

5.5.1 Amplitude-Range and Phase-Range Maps Computation

Radar raw matrix data R[m,n] is presented in the complex from where each data sample is represented by a phasor. Considering the rationale of Subsection 4.4, amplitude and phase maps needed to be demodulated from R[m,n] data. In this experiment, amplitude-range maps were used to automatically select the range bin from where cardiorespiratory phase signals should be extracted, over slow-time direction (axis m in Figure 3.7) in phase maps. Hence, amplitude-range matrix $R_{ABS}[m,n]$ were obtained computing the amplitude of each sampled phasor by Equation 5.3:

$$R_{ABS}[m,n] = \sqrt{\Re\mathfrak{e}(R[m,n])^2 + \Im\mathfrak{m}(R[m,n])^2} \tag{5.3}$$

where, $\mathfrak{Re}(R[m,n])$ and $\mathfrak{Im}(R[m,n])$ terms are the real and imaginary parts of the matrix R[m,n]. Similary, the phase-range matrix $R_{PHASE}[m,n]$ was obtained computing the phase of each sampled phasor by Equation 5.4:

$$R_{PHASE}[m,n] = \arctan\left(\frac{\mathfrak{Im}(R[m,n])}{\mathfrak{Re}(R[m,n])}\right) \tag{5.4}$$

Once this study only aims to assess the possibility of detecting targets and not to evaluate the signal's quality between radars, all amplitude-range maps were normalized.

5.5.2 Clutter Removal

In a complex indoor environment, RF signals are not only reflected by the desired targets but also reflected by all the objects present within the radar range. In a room as the one used in this experience, background clutter signals usually originate from the floor, walls, furniture, and other objects. Indeed, as these objects have a larger cross-area than a human target, they conquer a more significant power expression on radar data. On the other hand, all the clutter present in the room are static, and consequently, signals reflected from these objects could be considered as stationary. As a result, clutter signals from the background can be seen as DC components and subsequently removed. Therefore, to enhance the subject expression on radar amplitude map, clutter signals were removed by subtracting averaged amplitudes values over slow-time range bins to $R_{ABS}[m,n]$ matrix. This technique could be simplified by denoting $\hat{R}_{ABS}[m,n]$ as the R matrix after clutter removal, and $x_{m,n}$ the m-th slow time sample of the n-th range bin, in Equation 5.5:

$$\hat{R}_{ABS}[m,n] = R_{ABS}[m,n] - \frac{1}{M}\sum_{m=1}^{M} x_{m,n} \tag{5.5}$$

5.5.3 Target Localization

After clutter removal, only the manifestation of the non-static targets is expected to have a more significant variable amplitude expression on the radar maps $\hat{R}_{ABS}[m,n]$. Thus, for target distance location, the energy values of $\hat{R}_{ABS}[m,n]$ were computed and summed along the slow-time axis resulting in a new array of size N. The maximum value found in this N range-frame and the respective range bin n index were then obtained. Equation 5.6 describe this process:

$$n = \arg\max\left(\sum_{m=1}^{M}(\hat{R}_{ABS}[m,n])^2\right) \tag{5.6}$$

where n matches a range location r_{target}, given by Equation 5.7, that is dependent on range frame resolution f_{res}:

$$r_{target} = n f_{res} \tag{5.7}$$

f_{res} is dependent on radar used and can be found in Tables 4.1 and 4.2 of the previous chapter. Moreover, to Equation 5.7 should be added the range offset set in radar acquisition protocol. In this experience, this value is 0.3 meters since range maps were defined within the interval of 0.3 to 3.0 meters.

Despite the development of a robust target location algorithm is not the principal focus of this work, a correct selection of range bin n is essential to extract a high-quality cardiorespiratory phase signal. Therefore, r_{target} values obtained by the method described above were compared with the real target distances values (0.5, 1.5 and 2.5 meters).

Figure 5.8 summarize the process of human target localization until now described, where an overview of the amplitude-range map transformation along the employed methods is shown.

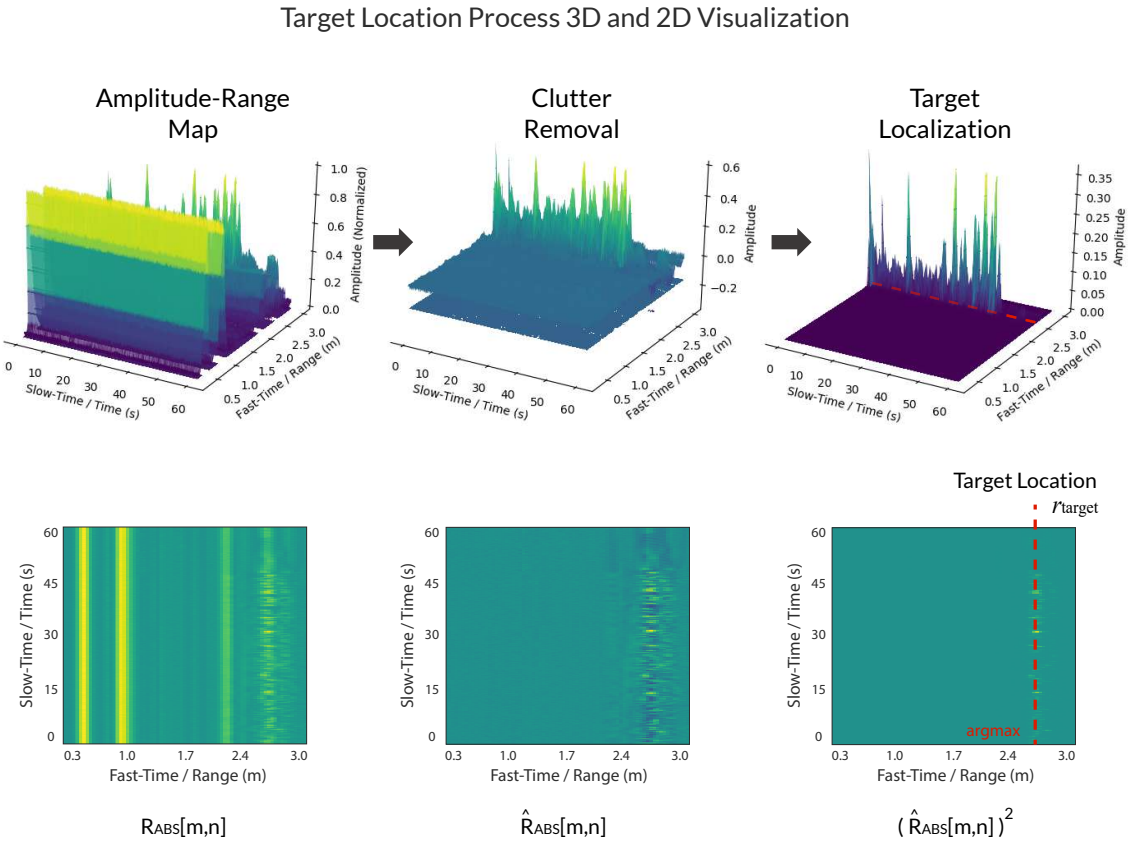

Figure 5.8: Evolution of a range-amplitude map during the three signal processing methods applied for automatic human target location estimation (red dashed line).

5.5.4 Frame Extraction and Phase Unwrapping

Slow-time phase signals from the range-bins n detected with the previous method (see red dashed line in Figure 5.8), were extracted from phase-range maps $R_{PHASE}[m,n]$. A typical phase signal is shown in Figure 5.9:

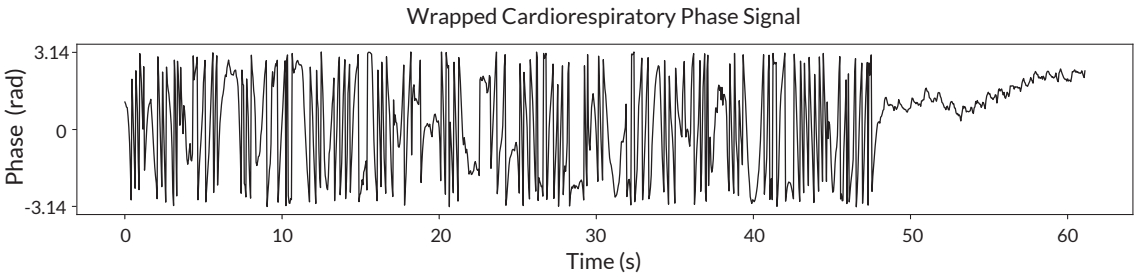

Figure 5.9: Example of a wrapped phase signal extracted over the slow-time direction from a phase-range map. This signal is obtained in the n-th bin where human position was estimated.

The extracted phase signal contains the millimetric motion variations that occured, at the target location range bin n, during the 60 seconds of data recording. As the phase maps $R_{PHASE}[m,n]$ were computed using an arctangent transformation (Equation 5.4), the output of these maps is contained in the restricted $-\pi$ to $+\pi$ interval. Since the amount of physical millimetric chest displacements is related to phase variation in radar signals, in some cases, this phase variations might exceed the π range limits - Figure 5.10 (a). Therefore, an unwrapping function was applied to the phase signals in order to recover their original cardiorespiratory shape - Figure 5.10 (b). In this study, the standard NumPy unwrapping phase function was used. There, phase unwrapping is performed by adding or subtracting a 2 π value to the phase values, where consecutive phase values are greater than $\pm\pi$.

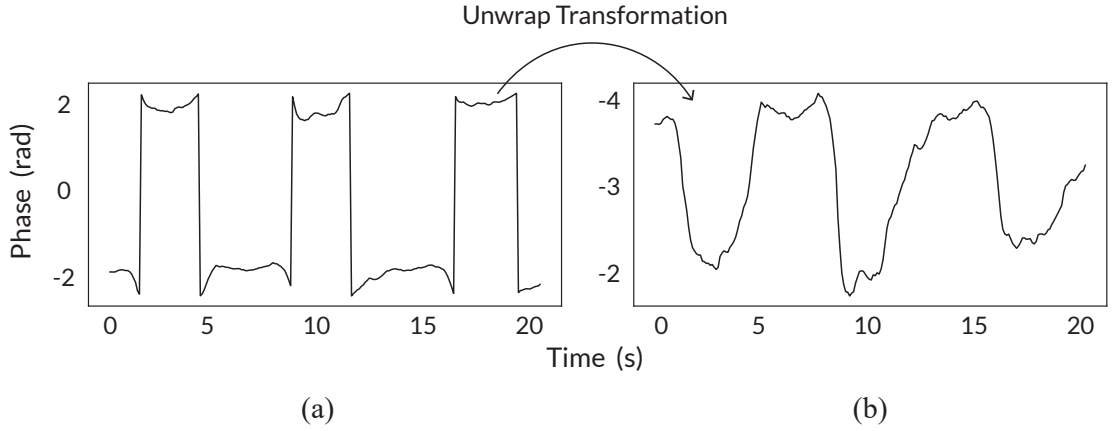

Figure 5.10: Unwrapping process. In (a) the signal exceeds the phase range $[-\pi, +\pi]$ limits. In (b), the recovered shape signal after an unwrapping function transformation.

5.6 Methods for Cardiorespiratory Frames Evaluation

For the evaluation of cardiorespiratory signals from radar frames, the unwrapped data was divided into two different moments: the first 40 seconds - **Frame A** - where subjects were relaxed and natural breathing and in the last 10 seconds - **Frame B** - where subjects were asked to hold their breath (see Figure 5.11). Frame A and B contents represent the different physiological situation with different radar signals expression and different analytic value. Data between 40 to 50 seconds was discarded since it corresponds to the transition moment where the subject goes from normal breathing to an apnea.

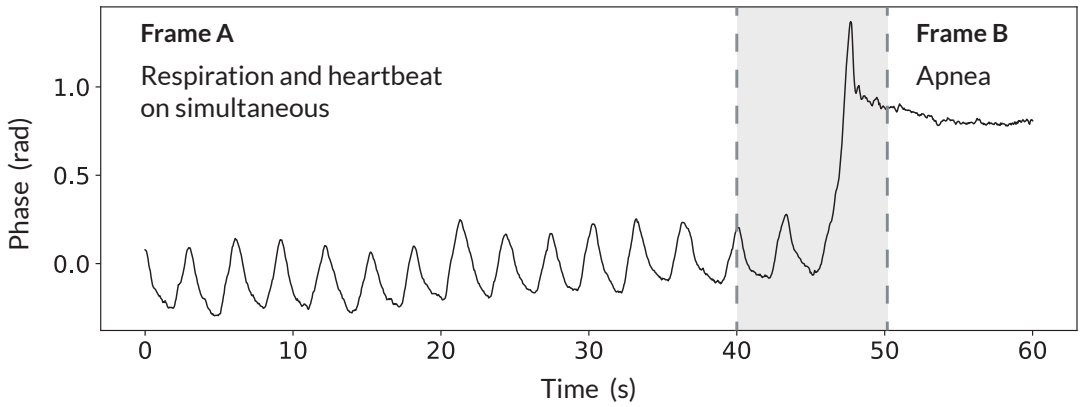

Figure 5.11: Representation of an 60-second unwrapped cardiorespiratory radar signal collected from experimental setup. In first 40-seconds (Frame A), subjects were naturally breathing and in the last 10-seconds (Frame B), subjects were in apnea.

In Frame A, respiration and heart activity were measured simultaneously. This frame represents the day-to-day conditions, with breath and heart movements being measured at the same time. In contrast, in frame B, only heart expression was measured in participants undergoing voluntary apnea. Thus, qualitative and quantitative methods were chosen to assess respiratory and heart signals based on each frame content. In a first qualitative analysis, **unwrapped cardiorespiratory signals** were reviewed by visual inspection in order to gain intuition about the real prominence of vital signs in the radar signals. Then, a quantitative analysis was performed to **isolated components of respiratory and heart signals**. Only frame A was used in qualitative analysis since apnea status does not represent a natural human condition. For a better understanding by the reader, Figure 5.12 summarises all the key points verified in both qualitative and quantitative analysis, further presented on Chapter 6. All the quantitative methods and algorithms used to extract vital signs from respiratory and isolated heartbeat components are described in the next two sections.

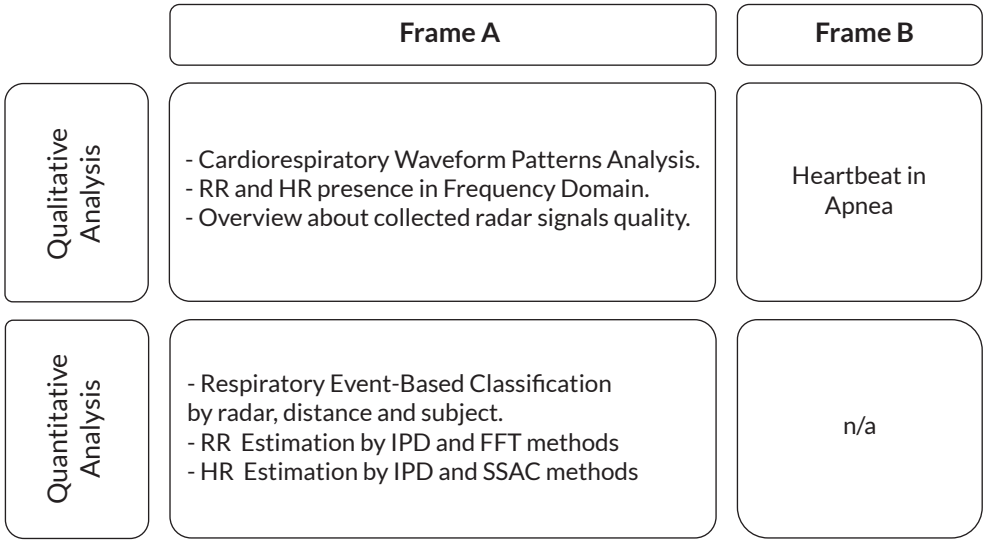

IPD: Inter-Peak Distance // FFT: Fast Fourier Transform // SSAC: Selective Short-Term Autocorrelation
RR: Respiratory Rate // HR: Heart Rate // n/a: non-applicable

Figure 5.12: Qualitative and quantitative analysis perfomed to assess respiration and heartbeat expression on cardiorespiratory radar signals.

5.7 Respiratory Signals Evaluation

This section describes the methods used to extract and quantitatively assess respiratory parameters from Frame A signals. Firstly, the respiratory components were extracted from radar signals. Then, the radar peaks from each recorded Frames A were detected and compared against their ground truth signals. Finally, two methods were applied for respiratory rate (RR) estimation. These methods as well as extracted metrics and statistical tools used to assess respiratory presence in radar signals are described below. **It is important to notice** that all respiratory parameters were extracted from respiratory component signals and not from the original unwrapped Frame A signals (from where the respiratory component is extracted as shall be seen below).

5.7.1 Respiratory Component Extraction

In order to separate the respiratory radar component from the residual noise of Frame A, a 2nd order Butterworth bandpass filter with between 0.1 to 0.4 Hz was applied. These values were chosen considering the reference respiratory values of Table 3.1.

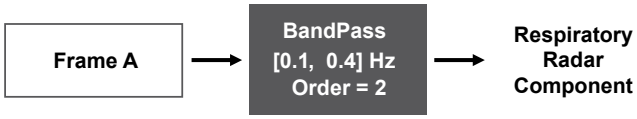

Figure 5.13: Schema of signals processing method used for respiratory component extraction from Frame A data.

5.7.2 Event-Based Classification

To assess the quality of radars in detecting respiratory events, the peaks of respiratory component frames were flagged as estimated breath events. Since radar data were recorded in static conditions, it is expected that the only activity present in respiratory component signals be respiration and/or common Gaussian noise. Consequently, a peak-to-peak comparison between the estimated breath events and reference audio events should show coherence in the time-domain axis. Otherwise, if the detected radar peaks do not be marked near a breath event in the reference signals, it could mean a low respiratory-to-noise ratio quality of radar signals or other problems that should be identified.

Hence, following the rationale above, a direct comparison between radar respiratory signals and ground truth events was performed based on a **event-based classification** [122, 123]. Event-based evaluation classifies the radar events as True Positive (TP), False Positive (FP), and False Negative (FN) concerning ground truth event instances where:

- **True Positive**: a radar event output that has a temporal position overlapping with the temporal position of a reference event in the ground truth signal.
- **False Positive**: an event in the radar output that has no correspondence in temporal position to a reference event in ground truth signal.
- **False Negative**: a reference event in ground truth signal that has no correspondence to an event with the same label in the radar output within a defined tolerance.

For the extraction of TP, FP, and FN metrics, two generated arrays extracted from reference audio signal and respiratory radar component are compared: the reference array and the estimation array. The next methodology was then applied in an algorithm build to extract the above metrics:

1. **Generation of Reference and Estimated Respiratory Event Arrays:** At each new frame, a new reference and estimated respiratory event arrays were created, based on reference and estimated temporal index positions of audio and radar signal, respectively. In reference array a tolerance window of 2 seconds, centered in each peak reference, was added.
2. **Calculation of distances between reference event and estimated event:** To remove duplicate events contained in the same tolerance window (false positives) and detect empty tolerance windows with no associated radar peaks (false negatives), a distance method was used. Therefore a new array was generated with all the distances values obtained between estimated and reference events.
3. **Removing of non-suitable distances:** For the selection of valid events, the pre-created distance array is processed in order to find TP, FP, and FN based on event

distances. Thus, the array is iterated over where for each ground truth respiratory event, an estimated event reference is associated. In the case of two or more reference events are located within the same time-window reference, only the radar event with the minimal distance to reference peak (centre of time-window) is associated with a reference event.

4. **Metric classification:** After the previous selection, all the events can be classified as the metrics purposed. All the events associated with a reference event are classified as true positives. All the estimated events that were not associated with any true event are considered as false positives. And at last, all the reference events which were not associated with any estimated event, that is, that does not have any occurrence inside their reference time-window, were classified as false negatives.

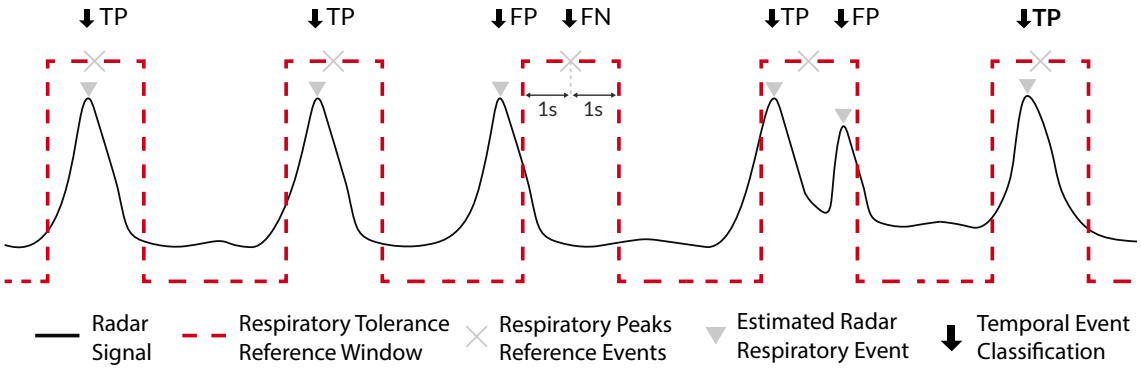

Figure 5.14: Estimated respiratory radar events were classified against a tolerance reference window according to TP, FP and FN metrics. TP: radar event inside a tolerance reference window; FP: radar event outside a tolerance reference window or double radar event inside a tolerance reference window; FN: no respiratory estimated event in an empty tolerance reference window.

The computed metrics were used to verify if the quality of respiration detection in radar signals varied with each one of the three monitoring conditions used: radar, distance or subject. Hence, the metrics were sorted and summed for each one of the three assessed groups. The quantity of associated error was measured with an Error Rate metric given by Equation 5.8:

$$Error(\%) = \frac{FP + FN}{REAL} \times 100 \tag{5.8}$$

where REAL corresponds to the total number of estimated respiratory events in an evaluated frame, given by the total of TP + FP events. Due to their minor impact in the results of this test, all the errors associated with the uncertainty of the synchronization process, time-window tolerance and others were neglected in this study.

5.7.3 Respiratory Rate Estimation

In order to estimate RR parameter from respiratory component signals, two standard peak techniques were applied in time and frequency domain. All the estimated RR_{RADAR} values were round to Respiration Per Minute (RPM) unit.

5.7.3.1 Method 1: Inter-Peak Distance

In the first method, estimated RR values were obtained by averaging the temporal distances between consequent peaks detected from the radar respiratory component. Hence, being N the number of segments created between two adjacent radar respiratory peaks events, and $\overline{pp}$ the temporal length of each segment, RR_{RADAR} was given by Equation 5.9 below:

$$RR_{RADAR} = 60 \times \left(\frac{1}{N} \sum_{n=1}^{N} \overline{pp} \right)^{-1} \quad (RPM) \tag{5.9}$$

5.7.3.2 Method 2: FFT

Another option to obtain the reference RR_{RADAR} parameter is the examination of the respiratory component radar in frequency-domain. Therefore, in this second method, the FFT function of $SciPy$ module was used to compute the spectrum of these signals. Then, RR_{RADAR} was estimated by the automatic detection of the most prominent spectral peak and associated index, or respiratory frequency value. Once again, a common peak finding function was used. The estimated frequency value (in Hz) was then converted to RPM unit.

5.7.3.3 Statistical Assessment

In order to compare the similarity between reference RR_{REF} and estimated RR_{RADAR} values, diverse metrics and assessment tools were used. Since one of the final objectives of this study is to conclude about the reliability of the signals processing algorithms and radars used for remote vital signs monitoring, the performance of each pair radar-method was assessed and compared: R1-M1, R1-M2, R2-M1 and R2-M2, where M1 and M2 are the methods 1 and 2, respectively, presented above.

The Mean Absolute Error (MAE) and Standard Deviation (SD) of the individual Absolute Error (AE) metrics were computed for a first analysis of the applied methods. Then, dispersion plots were used to visually assess the performance of each radar-method pair in RR estimations. Lastly, using the RR estimated values obtained from the method that presented a lower error, a Bland-Altman analysis was made to finalize a conclusion about the applicability of radars as respiratory monitoring tools, and to compare the performance between radars used (R1 and R2).

5.8 Heartbeat Signals Evaluation

Frame A and Frame B were used to analyse the heartbeat component presented in radar signals. All the methods here presented were developed based on a first qualitative signals assessment of these signals. Contrarily to respiratory analysis, the heart activity was not directly compared with ground truth due to their unstable and unpredictable presence on radar signals. Only the heartbeat components extracted from Frame A signals were used for Heart Rate (HR) estimations.

5.8.1 Heartbeat Component Extraction

Heartbeat was expected to be seen as small peaks appearing over the noisy respiratory signals in Frame A. Hence, to enhance and recover the small beat peaks, Frame A was processed using three steps summarized in Figure 5.15.

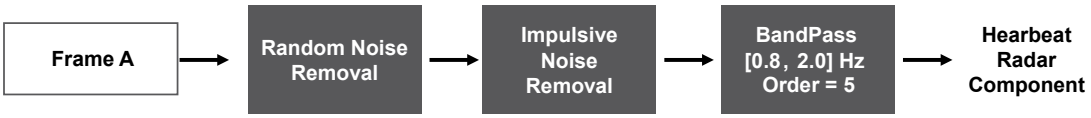

Figure 5.15: Schema of signals processing method used for heartbeat component extraction from Frame A data.

Random Noise Removal: Heartbeat peaks should have an approximate predominance between 0.1 and 0.6 mm on radar signals (consult Table 3.1). Hence, to eliminate random noise over the heartbeat peaks, a smoothing filter based on a Hanning window of 10 samples (or 0.5 seconds) was first applied. A short size window was used since this step aimed to increase SNR without distorting the heartbeat peaks.

Impulse Noise Removal: Respiration and random body movements are the first contamination sources of the heartbeat signals. Thus, in order to attenuate this amplitude contrast, a trending curve with impulsive respiratory expression was subtracted to signal. This curve was obtained by applying a new smooth filter to radar signals using a Hanning window of 50 samples (or 2.5 seconds).

Bandpass Filter: Finally, a 5th order Butterworth bandpass filter was applied to reject the remaining out-of-band noise on heartbeat radar expression, in the range of 0.8 to 2.0 Hz. These values were chosen considering the reference interval of 60 to 100 BPM for an adult at rest, according to the conditions of the experience (adult population monitored in relaxed situations).

5.8.2 Heart Rate Estimation

Two methods were used to estimate HR parameters from radar signals: a inter-peaks distance method and a novel **S**elective **S**hort-Term **A**uto**C**orrelation algorithm. All the estimated values were rounded to Beat per Minute (BPM) unit.

5.8.2.1 Method 1: Inter-Peak Distance

Similarly to method 1 previously used for RR estimation (subsection 5.7.3.1), an inter-peak distance method was also used to estimate the HR values from the heartbeat component signals. Hence, with N the number of segments created between two adjacent radar heart peaks events, and $\overline{pp}$ the temporal length of each segment, HR_{RADAR} is given by Equation 5.10 below:

$$HR_{RADAR} = 60 \times \left(\frac{1}{N} \sum_{n=1}^{N} \overline{pp} \right)^{-1} \quad (BPM) \tag{5.10}$$

5.8.2.2 Method 2: SSAC

A method called Selective Short-Term Autocorrelation (SSAC) was proposed, considering the qualitative analysis performed to Frame A signals. Assuming that heart expression could be null in some radar time series, this algorithm aimed to identify in which radar frames, the estimated HR could be a valid value or not. To this effect, SSAC first computes a set of sequential HR values extracted from the autocorrelation of short-time over processed frame A. Then, SSAC assigns an estimated HR value to the analysed radar frame, or, define the frame as a null cardiac sensing frame. For this classification, SSAC checks if in the collected set there are repeated estimated HR values in a distance inferior to a given time interval t. As within a 40-seconds interval is not expected that HR presents huge variations at rest, the existence of repeated frequencies around a certain interval threshold could reveal sporadic heart manifestation. SSAC is divided in three stages:

A. Short-Term Autocorrelation Instead of applying autocorrelation to the full data frame like in the traditional autocorrelation, the short-term autocorrelation is merely applied for a specific small data window of size N. Expressing x[n] as the n-th sample data in the selected window frame, short-time autocorrelation R_{xx} at lag k is given by Equation 5.11:

$$R_{xx}[k] = (\sum_{n=1}^{N} x[n]x^*[n-k]) \tag{5.11}$$

In the 40 seconds from Frame A, a sliding window of 200 samples (10 seconds) sliding at 5 seconds was used. In total, 7 R_{xx} short signals were computed. k was set as 1.

B. Short-Term Heart Rate Estimation A set S of 7 time sequential HR values were estimated from each R_{xx} signals. HR values were obtained, applying the inter-peak distance method to each one of the R_{xx} segments in the set. Values were rounded to BPM unit.

C. Heart Rate Estimation In this step, previous estimated HR values were removed from S, considering the next two order conditions:

1. Remove all the values that are not contained in the reference interval of 60 to 100 BPM, that is, outside the reference heart rate values for an adult at rest.
2. Remove all the non-double HR values in the sequence, that is, HR values that are not repeated more than once on time sequence S.

Therefore, in the case of the values in S that do not meet the aforementioned conditions, the analyzed frame is classified as "NULL", and none reliable HR value is obtained from a NULL frame. Otherwise, if in S are repetead HR values contained in the reference HR interval, a final estimated HR value is returned given by the mean of remaining HR values in S.

5.8.2.3 Statistical Assessment

The same statistical assessment methods described in Subsection 5.7.3.3 were also applied for HR estimated values.

Chapter 6

Results and Discussion

In the previous chapter, the process for acquisition and processing of radar signals, collected using an IR-UWB and a FMCW radar from 10 subjects, was described. Subsequently, in this chapter, results and discussion of this small proof of concept are presented to understand the viability for the use of these sensors and methods in acquiring vital signs accurately. Hence, a small discussion about the collected radar data and their difference is firstly performed, followed by the results for the target localization. Then, the results for the respiratory and heartbeat signals monitorization, which is the main topic of this discussion, are presented. The quality of the signals, offline processing algorithms and radar performance is also evaluated using quantitative and qualitative methods. The values presented in this section, which resulted from statistical computations, were round to 2 significant figures (excepting subsection 6.3.2.1 metrics).

6.1 Dataset Characterization

In this study, 6 radar maps per participant were obtained, adding to a total of 60 complex data radar maps. In order to verify radar data integrity and gain some intuition about radar maps trends, all datasets were manually reviewed, unfolded into their respective amplitude and phase range maps.

Figure 6.1 illustrates an example of amplitude and phase maps from a recorded complex data map for each sensor. These maps were acquired with a target (Subject 1) positioned at one meter from the radars. The different radar technology is clearly observed between these maps, even when acquiring data in the same room space. Using the Radar Equation presented in Section 3.2.2, these data differences can be explained by three radar parameters: the frequencies used by each radar, the power of each transmitted RF wave and the resolution of radar frames.

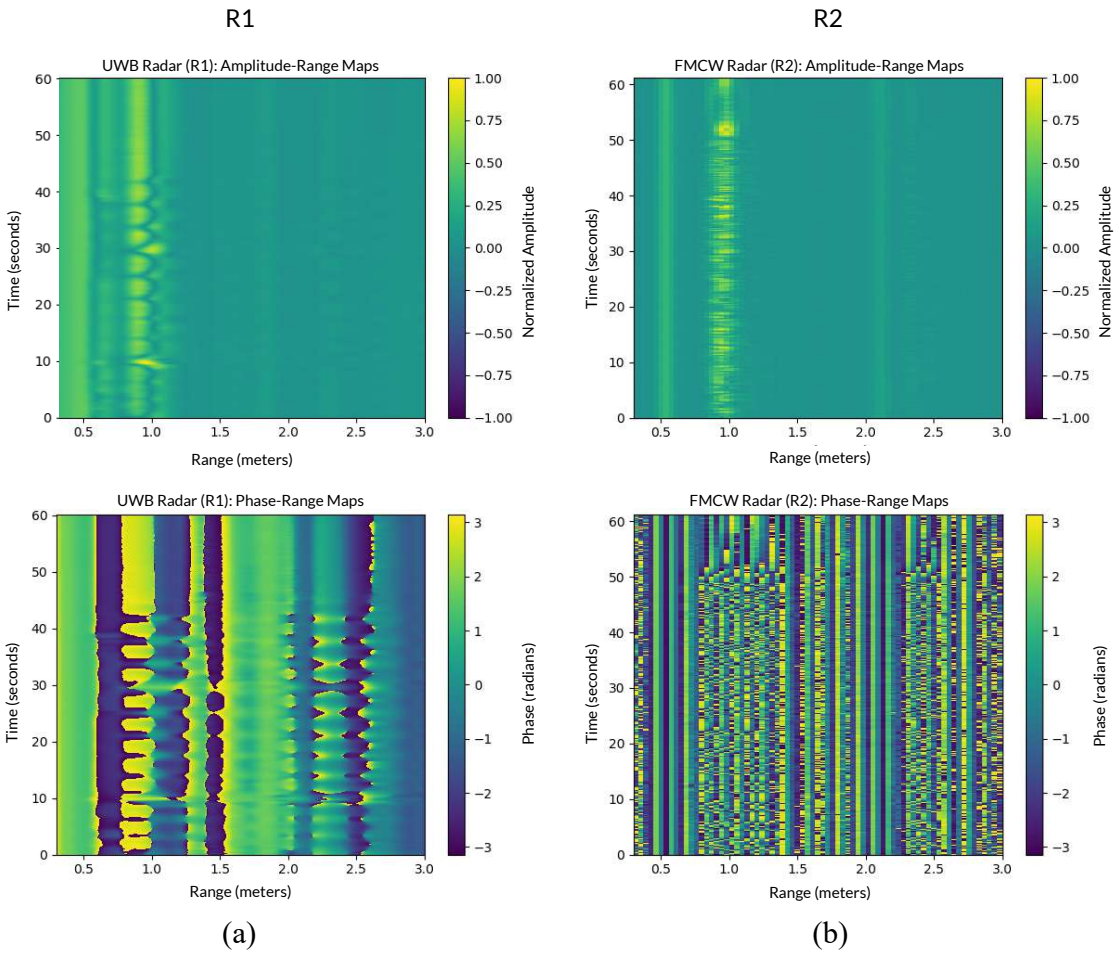

Figure 6.1: Differences between radar range maps acquired with (a) R1 and (b) R2 when a human target (Subject 1) is located at one meter of distance from radars.

Starting by analysing the differences between **amplitude-range maps**, similar patterns are easier to observe - Figure 6.1 (top). These amplitude maps are characterized by the magnitude of reflected signals, where the transmitted power factor has a crucial point in the detection of objects. Higher amplitudes values, corresponding to the RF signals reflected by the Human target, are perceived in both radar maps at 1.0 meters. Even with different transmitted RF powers in R1 and R2, these maps present similar amplitude patterns, except in the first few centimetres, where R1 presents an evident manifestation that does not appear in R2. This is an effect of antenna crosstalk, typical of pulse radar architecture due to the coupling between transmitter and receiver antennas [121]. Nonetheless, this effect is static and consequently can be easily removed as a DC component.

On the other hand, the **phase-range maps** signals of both radar sensors are qualitative more different when compared to range maps - Figure 6.1 (bottom). This visual divergence can be mainly explained by the different wavelength used in each radar. Since FMCW wavelength is 10 times inferior to IR-UWB, for the same distance unit, FMCW

phase maps will present 10 times more phase cycle rotation. Therefore, this effect can be easily understood in the above wrapped phase maps, where phase variation is faster on FMCW than IR-UWB data, represented by narrower columns that give the impression of a faster colour variation.

In addition, the propagation of RF waves in the medium as well as their interaction with materials depends on their frequency. Since R1 has a smaller frequency than R2, its waves have a more significant dispersion in the medium. Moreover, and how it was seen in Subsection 3.5, it is more likely that R1 waves are reflected inside the human body tissues. On the other hand, millimetric frequencies of R2 enable narrower beam, which results in better-quality measurements in R2.

6.2 Target Localization

Although in this experience, the position of the participants was previously known, in real life applications, automatic detection of target's distance is often required for the extraction of vital signs. This can be described as one of the major challenges in human monitoring applications, especially in complex environments. Therefore, an algorithm was developed to detect the target position automatically. Table 6.1 compares the estimated range values obtained by the applied method with the real distance at which the subjects were positioned. A graphical representation of these results is also presented on Figure 6.3.

The maximum error found between the real location and the estimated using radar was 0.2 meters. However, this is not a significant error since this value corresponds to the normal thickness of the human body. Moreover, a small misalignment of the subject when positioned for the experiment can also contribute to this error.

Table 6.1: Estimated range position of human targets in collected radar signals.

		Estimated Range (m)									
Radar	Range (m)	S1	S2	S3	S4	S5	S6	S7	S8	S9	S10
	2.5	2.3	2.4	2.4	2.5	2.6	2.4	2.4	2.4	2.6	2.5
R1	1.0	0.9	1.0	1.0	0.9	0.8	0.9	1.0	1.0	1.0	0.9
	0.5	0.4	0.6	0.5	0.3	0.4	0.5	0.4	0.5	0.5	0.5
	2.5	2.4	2.6	2.5	2.5	2.7	2.5	2.6	2.5	2.6	2.6
R2	1.0	0.9	0.9	0.9	0.9	0.9	0.9	0.9	0.9	0.9	1.0
	0.5	0.5	0.5	0.5	0.5	0.5	0.5	0.5	0.5	0.5	0.5

Figure 6.2 shows a set of range maps obtained after clutter removal at the three different distances, where human presence can be identified and detected.

In real life applications, the applied method might be too simple to remove clutter and detect the target position efficiently. To further improve the algorithm used, there are some details that should be taken into account.

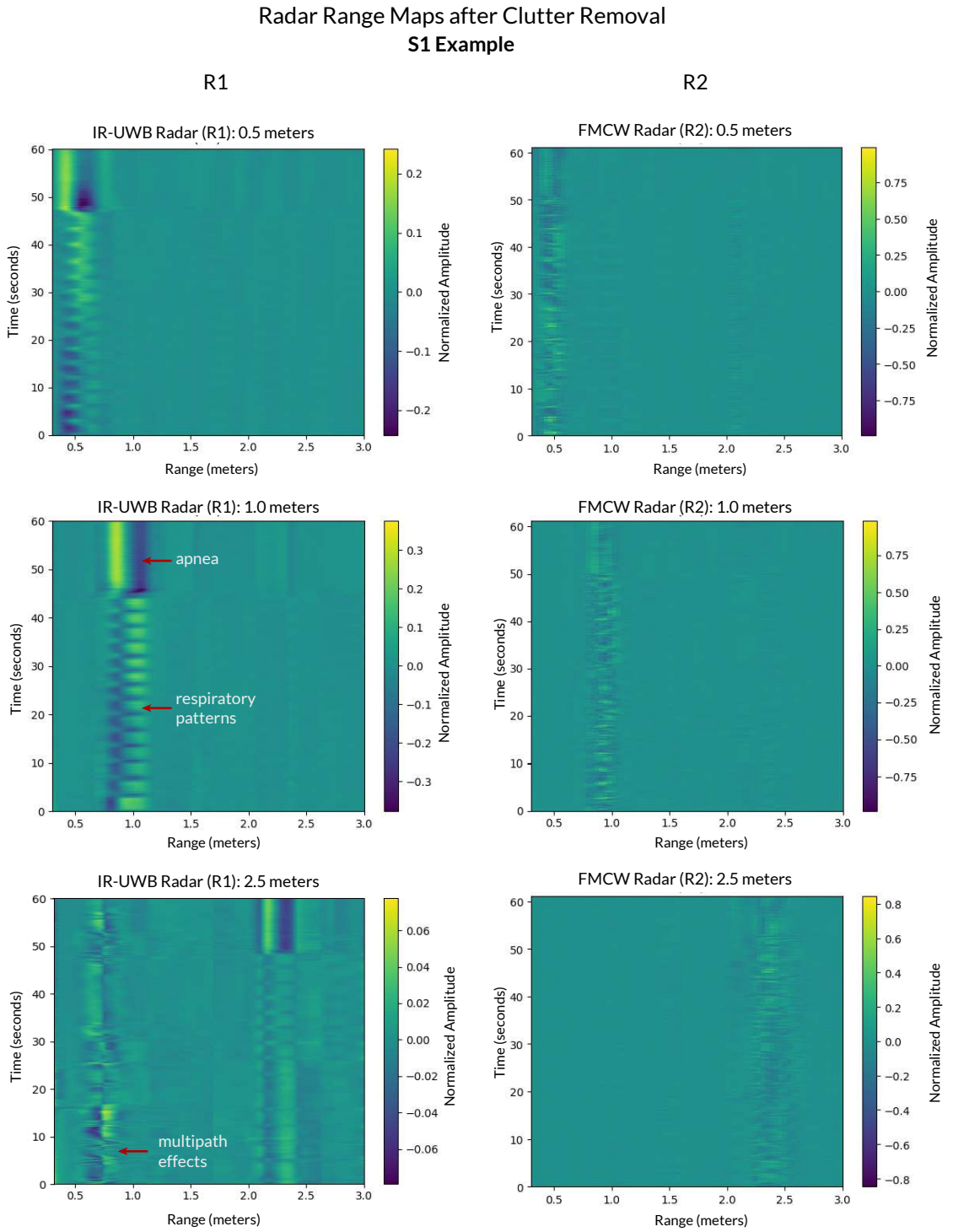

Figure 6.2: Representation of amplitude and phase maps after clutter removal (exemplified by S1 dataset). After clutter removal, subjects are more noticeable on radar maps.

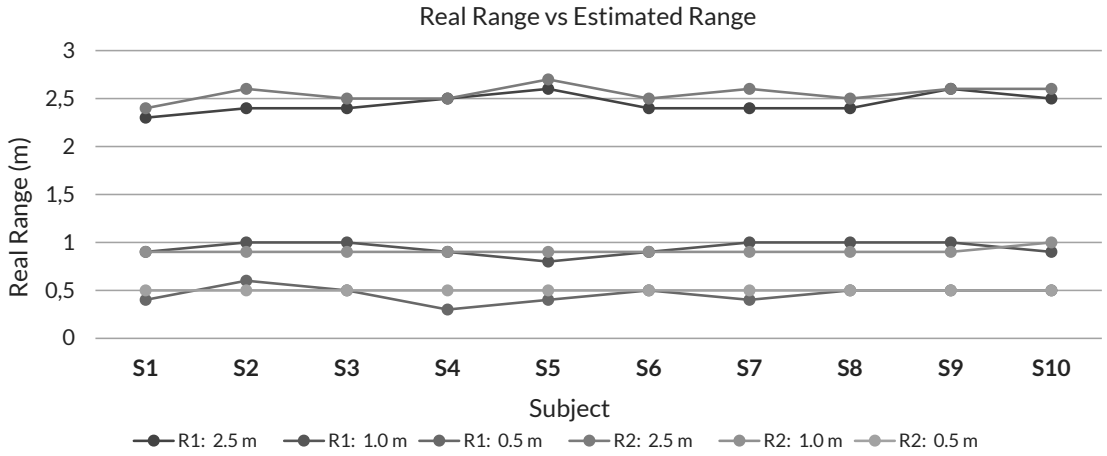

Figure 6.3: Graphic representation of Table 6.1. Each point represents an estimated range by subject and radar used. Each segment follows the reference range lines.

First, and how it was expected, the intensity of the target in maps is inversely proportional with the increase of distance. Bigger distances covered by the RF waves naturally result in higher energy losses. However, and according to the results presented above, this effect is not significant enough to lose target range information up to a distance of 2.5 meters, confirming that both radars, with the configuration proposed in Chapter 4, can be used to track targets up to the referred distance. Notwithstanding, it is important to notice that the maximum established range of 2.5 meters is not a radar limitation, but only a suitable value found to be used in this first experimental approach. The three range intervals (0.5, 1.0 and 2.5 meters) were chosen according to the conditions of the usual distance used in literature (below 1.0 meters) and considering typical daily life situations where a future radar could be used. For example, 2.5 meters is a reasonable value to consider when monitoring a person in front of a TV or lying in bed while sleeping. Notwithstanding, with the current configuration, R1 and R2 can measure ranges up to a distance of 9.90 (Table 4.1) and 3.75 (Table 4.2) meters, respectively. Hence, further studies are recommended with targets positioned at larger distances with the aim of test the viability in vital signs acquisition at longer distances than those used in this study.

Multipath effects were also observed in collected radar data, especially in 2.5 meters maps. In this experience, multipath effects were originated from reflections in the wall, floor and roof, causing a delay in signals detection. These effects must be considered in future applications in order to avoid ambiguities when detecting target location.

Finally, respiratory patterns were also observed in the amplitude maps. This observation goes along with some studies that have shown already the possibility to collect those signals only from the power amplitude of reflected signals [58, 84]. Nevertheless, phased based methods were chosen to be applied in this study to achieve the similarity between the raw radar returned by radars with the aim of using the same offline signal processing techniques in both radars signals.

6.3 Respiratory Signals Evaluation

In the first 40 seconds, respiratory and heartbeat signals were monitored simultaneously. In order to assess the capacity of radars for respiratory sensing, a first qualitative analysis of the unwrapped signals was performed. Thereafter, and for more precise analysis, the respiratory components of the radars signals were assessed through quantitative methods. The estimated breaths events were compared with the reference values extracted from the audio reference in an event-based classification approach. This classification was used to understand if the detection of the physiological radar signals was also dependent on the distance, sensor, or physiology of the monitored participants. Finally, the estimated respiratory rate (RR) values were assessed.
Thus, in the scope of this dissertation hypothesis, the results and discussion present in this section intend to answer the following points:

1. Understand how breathing waveform patterns appear on radar signals;
2. Assess the time-domain accuracy in the detection of the respiratory events;
3. Perceive the viability in the use of radars and proposed methods for RR estimation;
4. Compare R1 and R2 sensors performances in respiratory sensing.

6.3.1 Waveform Pattern Signals Analysis

In general, a quite good correlation between radar and respiratory audio signals was observed in both radar signals. A typical unwrapped and non-processed radar wave recorded in the validation experience, together with its respective respiratory audio ground truth signal, is illustrated on Figure 6.4.

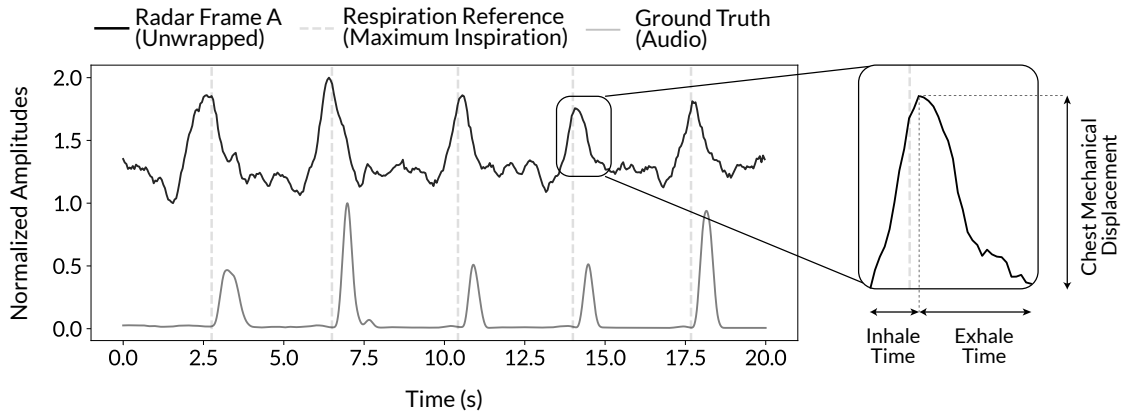

Figure 6.4: Unwrapped radar signal example compared with respective audio ground-truth signal. Respiratory waves are clearly perceived as well inspiration and expiration instants.

Analysing Figure 6.4, it is possible to note that peaks on radar respiratory signals match the respiratory peaks from the reference. As a reminder, the peaks of the audio signal reference corresponds to the maximum expiratory flow and only dashed lines are considered as a reference point for the maximum displacement of the chest. On the other hand, the inspiratory and expiratory moments, corresponding to the mechanical expansion and contraction of the chest, are also present as the positive and negative slopes on radar signals, respectively. Indeed, the radar sensors used seem to be sensible enough to detect physiological differences in the inspiratory/expiratory (I/E) timing ratios, which allows them to be used not only as a tool for RR measurements but also for time-domain volume chest tracking, from where much more information can be extracted [124]. Unfortunately, the microphone used as a reference was not sensible enough, and some of the inspiration events were not correctly captured. Thereby, a more detailed respiratory waveform analysis could not be made due to the lack of a proper inspiratory reference.

Comparing the performance of R1 and R2, in every R1 unwrapped signals, the breath movements were clearly evident without disruption and without any doubt about their physical phenomena origin. In contrast, R2 shown more noisy and shapeless unwrapped signals, where respiration was less evident compared to R1 signals. A more in-depth analysis of this difference will be given in the next section, where respiratory events from each radar were quantitatively classified against their reference signals. Notwithstanding, in a total of 30 recordings per radar, high-quality waveform breath signals were found up to the maximum measurement range of 2.5 meters. Comparative examples of the unwrapped radar and respective processed radar components, recorded with a subject (S6) located at 2.5 metres, are reported in Figure 6.5.

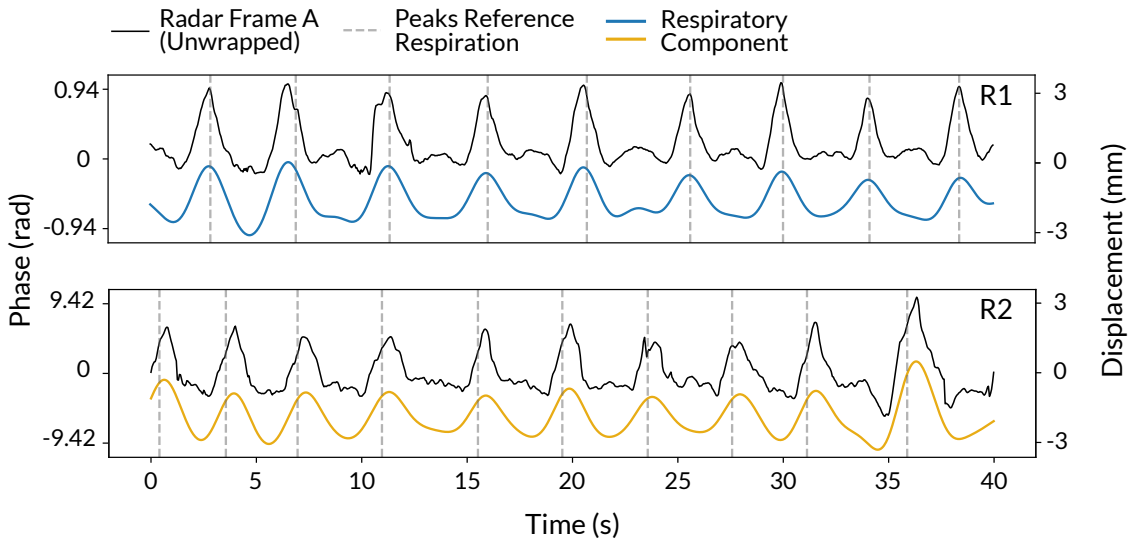

Figure 6.5: Comparison between radar signals extracted from R1 and R2 and the respective processed respiratory component. Despite the different phase scales, both signals have the same millimetric displacement scale.

Despite the differences between radar sensors, similar respiratory parameters could be found in both signals. Note that, even with different phase scales (left axis), R1 and R2 registered concordance values of peak-to-peak displacement variation of the chest (right axis). From both radar, an averaged chest displacement of 3 mm to 4 mm during successive breaths is observed. These values are slightly below the reference interval mentioned on Subsection 3.1.3, but this difference is not significant since chest displacement measures from radars can vary with target posture, the beam incident angle and others.

Note that, R1 and R2 signals were recorded in different instants (see acquisition protocol) and naturally, the above signals are not a representation of the same respiratory moments. However, they were recorded one after the other in a time interval inferior to 1 minute, thus it can be assumed that the subjects maintained similar respiratory parameters such as RR and chest volume variations.

6.3.2 Event-Based Classification

For a quantitative assessment of breath radar expression in time-domain, a direct comparison between the peaks from the radars and the reference signal was performed. Radar breath events were classified according to TP, FN and FP metrics. Results per recording are shown in Table A.1 on Appendix A.

6.3.2.1 Radar Centered Analysis

Table 6.2 summarises the metrics obtained per radar and associated error rate. A more in-depth explanation about error rates origin can be given taking into account Table A.1 and considering the notes taken during the subject's monitorization.

Table 6.2: Classified metrics events sorted per radar and associated error rates (rounded to 3 significant digits).

Radar	REAL	EST	FP	FN	TP	**Error (%)**
R1	313	312	2.00	3.00	310	**1.60**
R2	309	309	26.0	26.0	283	**16.8**

Examining **R1** results, only 5 in 313 events were not correctly identified as breath events resulting in a hit rate of 98% (approximately) for the 20 minutes of radar monitoring. Misclassified events were found in S2, S4 and S6 records. By looking in detail to their signals, it is possible to see that these did not maintain a regular respiratory pattern as it was asked or presented increased body movements that disrupted the signals. These observations could also be confirmed by the notes taken during the monitorization: S2 reported some dyspnea problems, S4 yawned during one of the records and, was not capable of being relaxed and static during recording as it was previously requested, and finally, S6 exhibited an anxiety status during the monitorization, perceived as sporadic random body movements on the signals. As mentioned before, these last referred events

were punctual events that were not anticipated in the algorithm design since it was constructed to find events in a regular respiratory signal. Nevertheless, even with these minimal human errors, R1 showed a good performance in respiratory signals sensing.

In contrast, 52 in 309 events were incorrectly classified in **R2** signals. Beyond the human error already identified above, two other causes were identified. First, in two R2 frame recordings, only pure noise was identified without any sign of respiratory patterns. Secondly, some of the non-identified events are due to errors in the unwrapping phase step of R2 signals. Indeed, and as indicated previously, R2 is characterized by a RF wavelength 10 times smaller than R1, which means that for the same millimetric movement captured with both sensors, R2 phase varies 10 times more. Consequently, phase displacements caused by thorax breath movements have a higher probability of overcoming $\pm\pi$ interval, leading to phase ambiguities that could be not distinguished by the applied unwrapping function.

Notwithstanding, even with a higher error rate when compared with R1, R2 still have a considerable hit rate of 83% (approximately) in respiratory detection that could be increased in the future with some improvements in the unwrapping function. Moreover, DC compensation and I/Q imbalance are commonly signal pre-processing steps usually applied to signals from CW radar [125] but that were not used in this work due to signal processing equivalence reasons. Therefore, the application of these techniques in future works may improve the quality and detection of respiratory events.

6.3.2.2 Subject and Distance Centered Analysis

The relationship between the error rate versus the subjects or versus the distance from the radars for both is shown in Figure 6.6. This analysis is very important to understand if the detection of respiratory events could be dependent on one of these parameters.

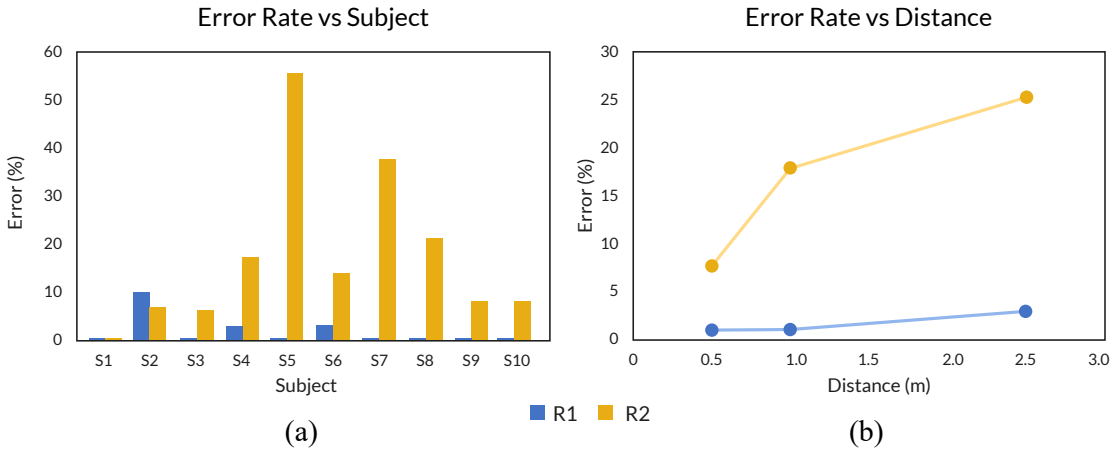

Figure 6.6: Classified metrics events and associated errors rates sorted per (a) subject and (b) distance.

As it was discussed in Subsection 3.5, the interaction of emitted RF waves with the

human body depends on the composition of the tissues. Thereby, individual parameters of the monitoring subjects such as the different levels of fat, muscle density and body position should have an influence on the quality of the radar signals. In order to test if this previous statement has a significant effect in practical terms, the classification events errors, displayed in Table A.1, were sorted by subject and presented in Figure 6.6 (a). Observing the plot, subject S5 and S7 stand out since they reported an error superior to 30%, which no other subject had. However, these high errors are only observed for R2 signals, whereas in R1, the signals were correctly classified. This means that the origin of the error is not directly related to the specific physiological characteristics of subjects S5 and S7, but most probably with a R2 parameter. Otherwise, a similar error should have been observed in the signals of R1, what did not happen.

As previously mentioned, SNR decreases when the target is situated at longer distances from radars. Consequently, it is important to assess the impact that the target distance have in the detection of respiratory events. Thus, error rates sorted by distance and radars were computed. Results are shown in Figure 6.6 (b). It was detected a significant number of errors in respiratory events classification with the increase of the distance from the R2 radar, while the R1 radar had values below 5%. This agrees with what has been found in some previous works such as in [126]. However, the number of recordings and population analyzed in the present study, is not significantly high to affirm that signals recorded further from the radar will have a lower quality and be more prone to errors in detecting respiration events.

6.3.3 Respiratory Rate Estimation

For estimation of RR from the radar signals, two typical peaks techniques in time and frequency domain were used, based on a inter-distance peak method (M1) and FFT (M2). The RR estimated values fall within a 9 and 27 RPM range in the studied population. All the estimated values and respective absolute errors AE are reported in Table A.2 on Appendix A. Table 6.3 below summarizes the performance of both methods per radar used.

Table 6.3: Estimated RR Mean Absolute Error (MAE) and Standard Deviation (SD) of the Absolute Errors (AE) values obtained for each radar-method combination.

Radar	M1 (RPM)	M2 (RPM)
R1	0.33 ± 0.47	1.3 ± 1.1
R2	1.0 ± 2.0	2.1 ± 1.2

Comparing the mean absolute errors (MAE) obtained using either method for both radars and their reference value, a minimum MAE of 0.33 ± 0.47 RPM was obtained applying M1 to R1 signals, whereas a maximum MAE of 2.1 ± 1.2 RPM was achieved applying M2 to R2 signals.

Notwithstanding, larger MAE values were obtained for R2 when comparing between radar performance, whereas larger MAE values were obtained with M2 method when comparing methods performance values. Despite the apparently small difference between estimated radar-method pair errors, it should be taken into account that R2-M2 error is much more significant than R1-M1 when those are compared with the reference RR range values presented in Table 3.1. That is, in a interval range of 8 RPM (considering the 12 to 20 RPM reference range), R2-M2 can present a roughly and significantly absolute error of 3 RPM in 8 RPM (reference values), whereas R1-M1 can present less than 1 RPM error in a range of 8 possible values. Moreover, an additional round-off error of 2 RPM resulted from the rounding of estimated RR values should be also taken into account in this analysis.

Figure 6.7 presents four dispersion plots that compare both methods, applied to the 30 signals obtained with each radar, R1 and R2. To each graph, the regression line associated with the coloured line is shown.

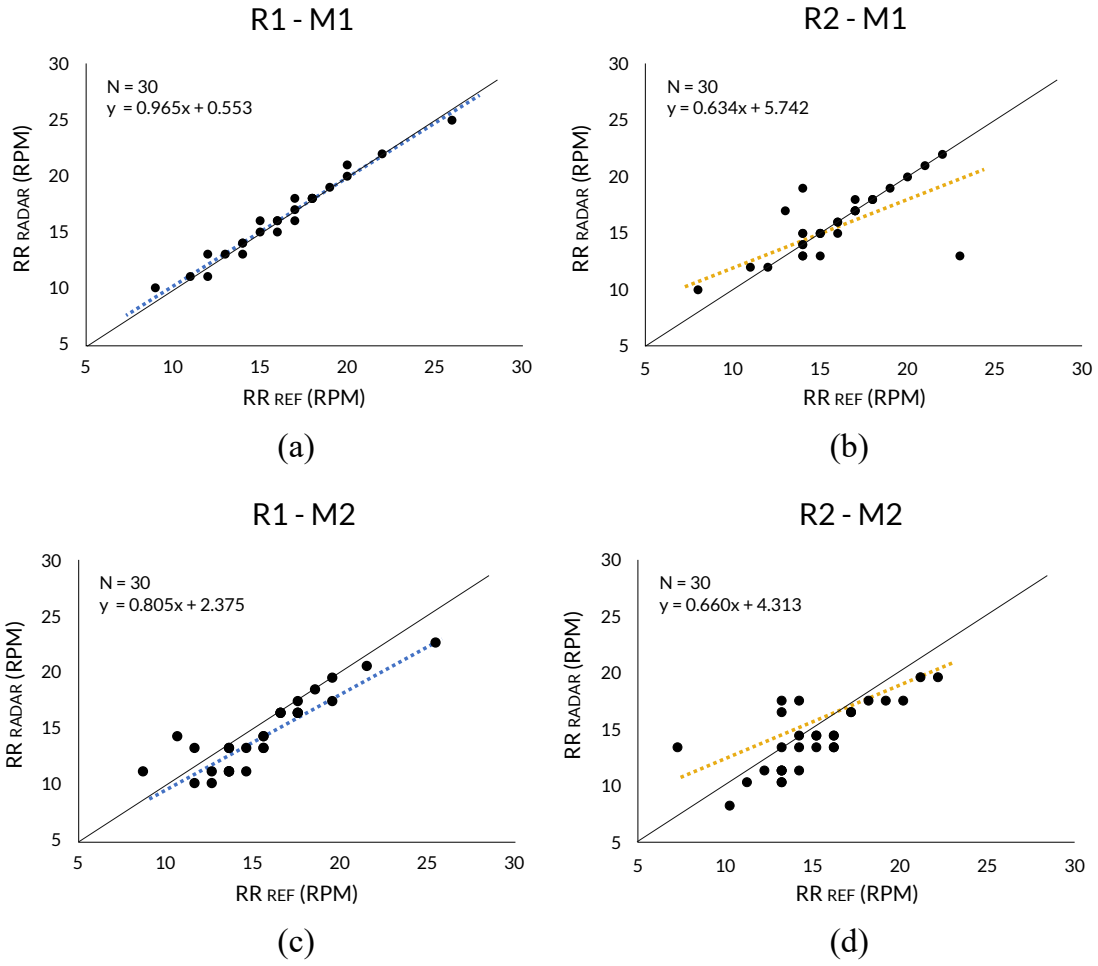

Figure 6.7: Dispersion plot comparing RR references values and estimated RR values obtained with M1 and M2 methods applied to R1 and R2 radar signals.

Observing the four dispersion maps, it is evident that R1-M1 points, Figure 6.7 (a), fit better the reference curve when compared with the other radar-method pairs. The regression line of R1-M1 has a slope almost equal to one, indicating an excellent agreement between radar and reference measurement, with low scatter. On the other hand, despite the R2-M1 present the lowest slope value in the set of the four plots, this result could be neglected since the majority of R2-M1 points still overlapping the reference (black) line. As can be observed in Figure 6.7 (b), the low slope value was obtained due to the presence of an evident outlier in R2-M1 data and some scattering points above the reference line. For reasons of timing and work priorities, the outlier value was not removed from data in this results, and therefore it is recommended, in the future, the recalculation of all the presented metrics excluding this outlier from R2-M1 data.

Concerning M2 method, R1-M2 (c) and R2-M2 (d) plots illustrate an underreporting pattern with a negative bias. A more prominent dispersion is observed when compared with the M1 method plots. Notwithstanding, despite the lower performance comparison of M2 when compared to M1, M2 still presents a considerable correlation between estimated and reference RR values. In the future, M2 performance should be again tested with larger time frames since the scattering observed in M2 plots may be associated with the low-frequency resolution of the computed Frame A spectrums (40 seconds). Frequency resolution is defined as the ratio between sampling frequency and the number of data points in frames, and therefore the number of data points used may not have been enough to estimate RR accurately.

Using the latter conclusion, a Bland-Altman analysis was performed using the M1 method between both radars and their references. Plots can be seen in Figure 6.8.

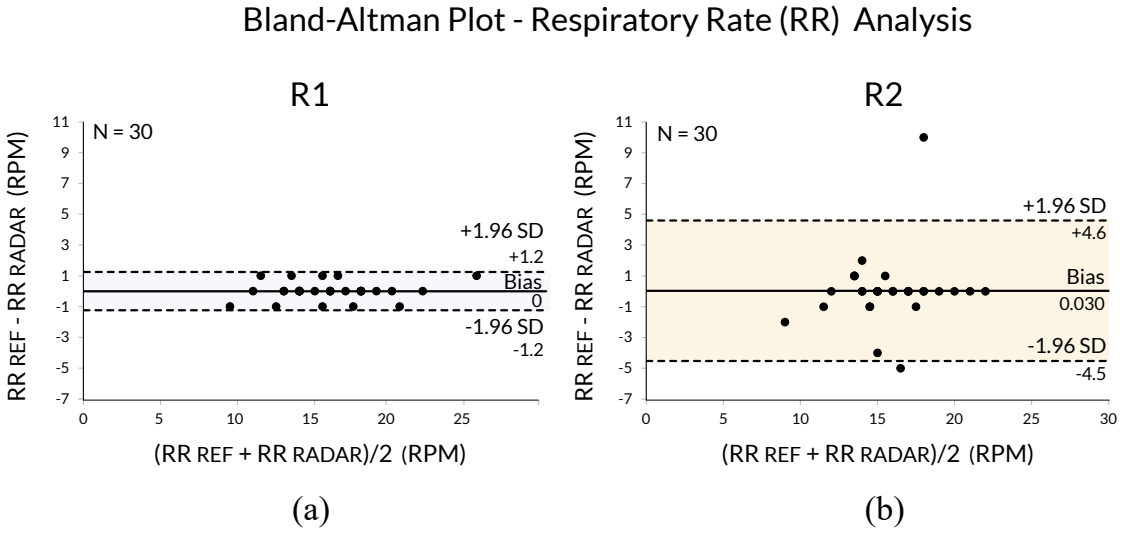

Figure 6.8: Bland-Altman comparison between respiratory rate measured reference and radar value obtained with method M1 applied to signals recorded with (a) R1 and (b) R2.

R1 Bland-Altman plot - Figure 6.8 (a), shows a quite good agreement between the RR values estimated in R1 signal (RR_{RADAR}) and RR values reference (RR_{REF}) with a systematic error (Bias) equal to zero. All samples are contained inside the 95% limits of confidence ranging from -1.2 to +1.2 RPM. On the other hand, a lower concordance in R2 Bland-Altman plot - Figure 6.8 (b) - is clearly observed with a confidence interval now ranging from -4.5 and 4.6 RPM and two samples located outside the limits of this interval. Despite the larger spread for the points compared with R1, bias is still close to zero what proves the consistency of the analyzed system. Moreover, most of the samples are distributed centrally around zero, which provides reasonable confidence in this radar-method technique.

For both radars, the same general pattern is maintained along with the horizontal axis values. This indicates that there is no variability dependence on the RR radar estimated values in the measured RR reference ranges. Finally, from this Bland-Altman analysis, it can be concluded that both R1 and R2 sensors can provide accurate measurements of RR, however, R1 was shown to have a more outstanding performance compared with R2.

6.4 Heartbeat Signals Evaluation

Heartbeat activity in radar signals can be measured using radar sensors due to the small displacement of cardiac muscles and also the wave pulse created by the ejection of blood from the heart. However, their expression is not as evident as the respiratory cycle, since the tissue's displacement due to cardiac activity is 10 times smaller to that created by the respiration. Thus, each subject was asked to sustain their respiration for a certain period to more easily detect the cardiac cycles using a radar. These apnea signals (Frame B) were only used for a qualitative assessment. Nevertheless, the detection of cardiac activity in the "normal"signals (Frame A), that is during respiration, was also performed from where HR values were estimated.
Hence, the results and discussion presented in this section, intend to answer the following questions about heartbeat detection using radars:

1. Understand how heartbeat waveform patterns appear on radar signals;
2. Perceive the viability for the use of radar in HR detection;
3. Compare the performance of R1 and R2 radar sensors in the cardiac activity sensing.

6.4.1 Heartbeat in a Normal Condition

Figure 6.9 reports the same cropped signals shown in the respiratory section (Figure 6.4), compared against its ECG ground truth signal. As it can be observed, small peaks arising between respiratory peaks (which at first glance can be perceived as noise) have a relation with R peaks of the ECG reference.

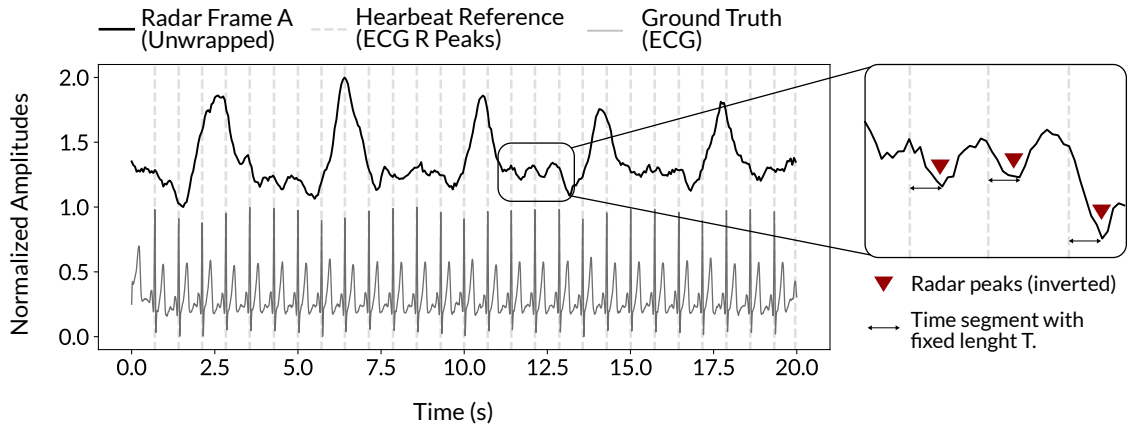

Figure 6.9: Unwrapped radar signal examples compared with respective ECG ground-truth signal. Small heart peaks are perceived between respiratory events.

As seen in the vital signs model presented in Subsection 3.3.3 and Subsection 3.4.2, in perfect conditions, radar signals should be composed of a sum of respiratory and heartbeat signals when monitoring a unique and static target. However, in real-life situations and commonly reported in the literature [62, 63], the weak cardiac signals can be easily masked by the strong respiratory wave. In fact, we can relate this statement with the collected radar data of this study, where most of the heartbeat activity was found between the respiratory moments, where the chest is static. In general, heartbeat expression was not evident in more than 50% of the unwrapped Frame A signals.

Comparing radar sensors performance, a larger manifestation of the heart activity (represented by small peaks in Figure 6.9) was found in R2 signals, rather than R1. This result is opposite to the one done in respiratory analysis, where R2 presented larger errors in respiratory activity detection. Once more, the possible reason can be encountered in the RF wavelength used in each radar. Since R2 uses a wavelength ten times smaller than R1, this makes R2 more sensible to capture small millimetric movements. In addition, the unwrapping of the R2 signals have less ambiguities when detecting heartbeat, since phase variation rarely exceed the $\pm\pi$ interval.

Figure 6.12 reports an example of signals extracted from subject S4 at 2.5 metres. In this example, the subject did not followed the protocol as it was expected, sustaining the respiration during the first acquisition phase (Frame A) as can be seen in unwrapped signal (top subplot) between the 9 and 20 seconds. This recording allowed us to realize that the highest amount of heartbeat was actually found between breathing cycles when chest did not move, that is in motionless conditions. This fact was observed in most of the collected data.

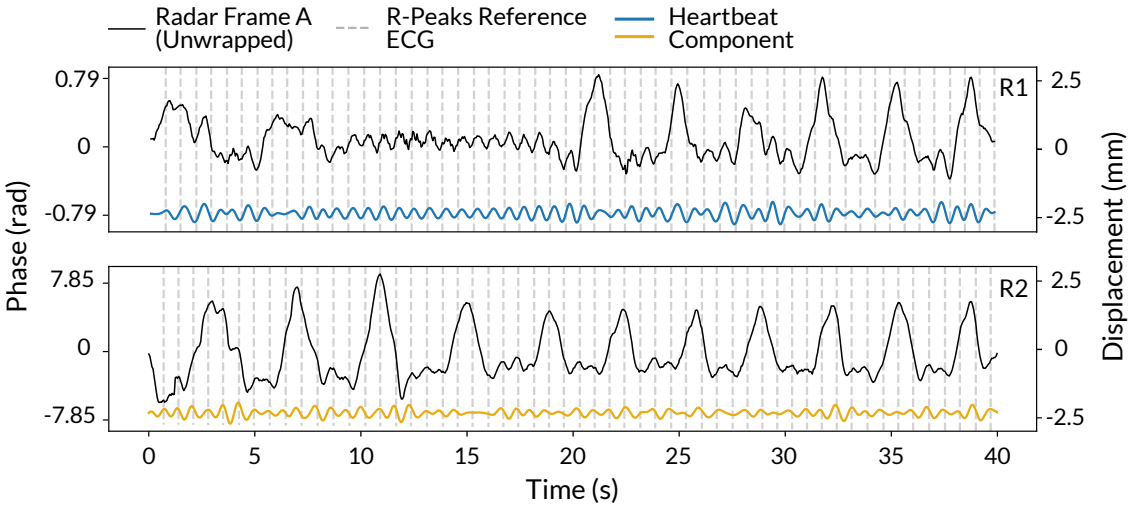

Figure 6.10: Comparison between radar signals extracted from R1 and R2 and respective heartbeat processed component.

In the frequency domain, spectrums of the collected signals on Frame A were computed. Figure 6.11 shows a typical spectrum representation of an unwrapped radar signal recorded from S1. Grey points represent the respiratory frequency and its respective harmonics, whereas the red point represents the reference heart frequency. As it can be noticed, respiratory harmonics fall within the heartbeat expression on the frequency-domain, making difficult the extraction of heartbeats through a simple spectrum inspection, a widely reported issue in the literature [63].

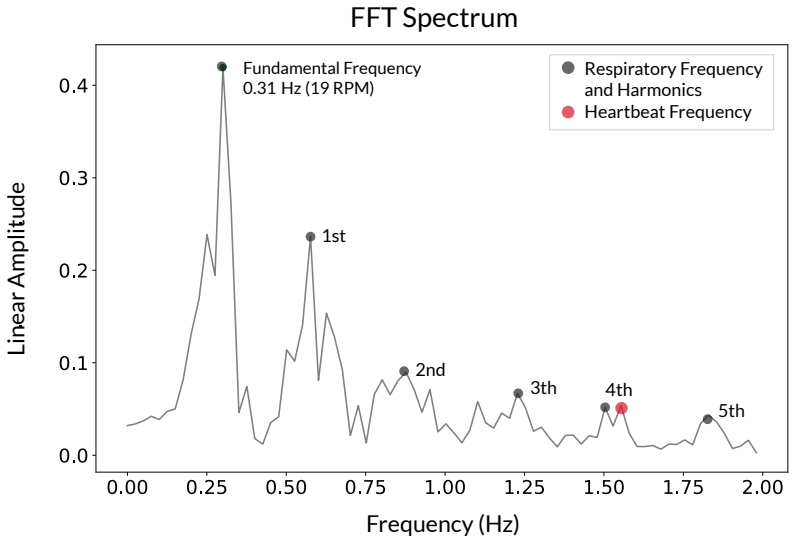

Figure 6.11: Spectrum of an unwrapped Frame A signal computed using FFT. Frequencies below 0.1 Hz were removed. Grey dots represent respiratory frequency peaks and respective harmonics. The red dot is related to heart frequency reference value.

6.4.2 Heartbeat in Apnea

In order to understand the real sensibility of the radars in the measurement of cardiac activity, it was asked to participants to hold their breath in the last 45 seconds of the protocol (Frame B). Being the respiratory signals the principal cause of noise, the voluntary apnea allowed a better measurement of the beats while also help to understand how much other noises sources could affect the heartbeat measurement. Notwithstanding, as this non-breathing state does not provide a realistic representation of human cardiorespiratory cycle in a daily life situation, this data frame was only bound to qualitative assessment. Therefore, by visual inspection, three types of heartbeat radar signals were identified from R1 and R2 recorded apnea frames:

1. **High-quality heartbeat**: clear heartbeat peaks on radar signals are in concordance with all ECG peaks reference - Figure 6.12 (a);
2. **Median-quality heartbeat**: some heart peaks are evident with ECG peaks whereas others are nonexistent due to noise - Figure 6.12 (b);
3. **Low-quality heartbeat**: no heart event is detected - Figure 6.12 (c);

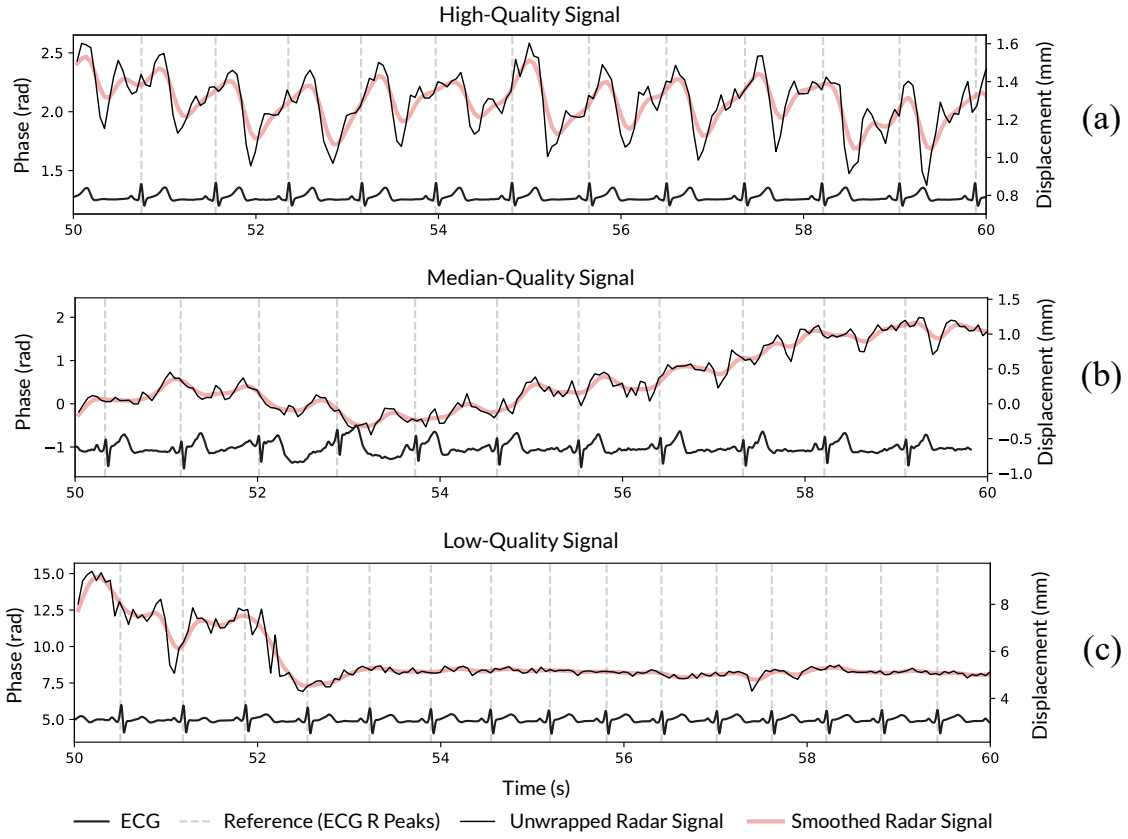

Figure 6.12: Examples of the three types of radar quality signals observed when subjects were in a voluntary apnea condition (Frame B). All examples are from R2 recordings.

These results seemed to be dependent on the measurement conditions as well as the monitored subject. For both sensors, high-quality signals were found more often for closer distances while low-quality signals were found frequently for farther distances. Notwithstanding, at least one record in the set of the collected data was classified as a high-quality heartbeat for each one of the radar sensors, proving the capacity of both sensors to measure cardiac signals up to 2.5 meters. Despite Figure 6.12 only presents R2 records, similar waveform patterns were found in R1, and therefore it is important to note that all the analysis performed in this subsection are related with events observed in both sensors.

Observing the high-quality signal in Figure 6.12 (a), it is possible to see that a significant amount of noise overlaps the cardiac curve. However, this was not a standard pattern observed in all high-quality signals, since some of them showed up signals with higher SNR and different morphologies. These differences could be related to two main factors: phase jitter and the different body points from where waves are reflected [127, 128].

Phase jitter [129] is a term used to describe phase fluctuations, commonly observed in RF systems, in time-domain. These phase deviations could be either deterministic, for example when it is originated by interference from other operating systems, or random, for example when it results from instabilities of oscillators or the temperature of components (Gaussian noise). Although this effect is not so noticeable in Frame A signals (e.g Figure 6.9) due to the presence of respiration patterns, the phase jitter should be considered since it can affect the quality of the small heartbeat peaks. Hence, it is recommended in future applications, the use of calibration routines [130] and/or the development of phase noise correction algorithms [128] in order to increase the heartbeat-to-noise quality in the radar signals.

As mentioned before, different heartbeat morphologies were observed in high-quality signals. Beyond phase noise, the morphologies of the signals can be affected by targets factors, such as their posture, clothes, fat and muscular compositions. Contrarily to breath, which causes a large displacement of the chest, the amount of skin (or cross-section area) available is essential in the measurement of sub-millimetric displacements caused by the cardiac muscle contractions and/or skin pulse propagation. For example, if the aim of this work was only to detect the heart rate of a subject, a better target would be the neck, since the carotid pulse appears very close to the surface and is easily viewed by the naked eye [131].

Finally, the failure to capture all the cardiac events in some medium and low-quality signals can be related to the previous statements but also with occasional and random body movements [132]. For the reasons mentioned above, the Human target's characteristics may have a more significant influence on the signal quality. However, more in-depth analysis of these apnea signals is needed to understand if some relation between subjects and low-quality signals exists.

6.4.3 Heart Rate Estimation

As mentioned before, the simplest method to obtain a heart rate estimative is to calculate the distance between adjacent peaks (M1). However, and in order to obtain estimated reliable HR values from radar, the selective short-term autocorrelation (SSAC) method was proposed (M2). With SSAC, the HR value is only returned when the selective algorithm considers that it could be a reliable value, otherwise a NULL (N) output is returned. All the estimated HR values and respective absolute errors (AE) can be found in Table A.3 on Appendix A. Table 6.4 below summarizes the performance of both methods per radar used.

Table 6.4: Estimated HR Mean Absolute Error (MAE) and Standard Deviation (SD) of the Absolute Errors (AE) values obtained for each radar-method combination.

Radar	M1 (BPM)	M2 (BPM)
R1	6.7 ± 5.7	2.0 ± 2.4
R2	5.2 ± 4.3	1.8 ± 2.2

The HR reference values of the analyzed population were within a range between 61 and 94 BPM. Comparing MAE values using the M1 or the M2 method, there is an approximately 3 BPM error decrease when using the M2 method for both radars. Notwithstanding, the better results of SSAC were only obtained because this method rejected a large number of segments, where heartbeats were determined to be nonexistent. In a total of 60 recorded signals (Frame A), SSAC did not identify a reliable HR estimated value in 14 signals using R1 and 9 using R2.

Figure 6.13 depicts the dispersion plot of both methods comparing the estimated and reference BPM values. The N parameter, presented in each plot is the total number of samples assessed using each radar-method combination. Observing the four plots, it is clear the better performance of M2 method (bottom subplots) when compared with M1 (top subplots).

The big dispersion observed in R1-M1 and R2-M1 plots confirm that M1 is not a suitable methods to be used in the estimation of HR parameters extracted from radar signals. The weak correlation of R1-M1 method is reflected in its flat fitted line and slope coefficient nearest to zero. Although R2-M1 plot also presents a high scatter pattern, it seems to follow an overreporting pattern with a positive trend. Concerning the nature of M1 method, these results suggest that R2 signals may have a greater heartbeat-to-noise ratio quality compared with R1. That is, since M1 compute the rates using only the mean value between the peaks of heartbeat component signal, this method will work better on signals where the small peaks are more evident.

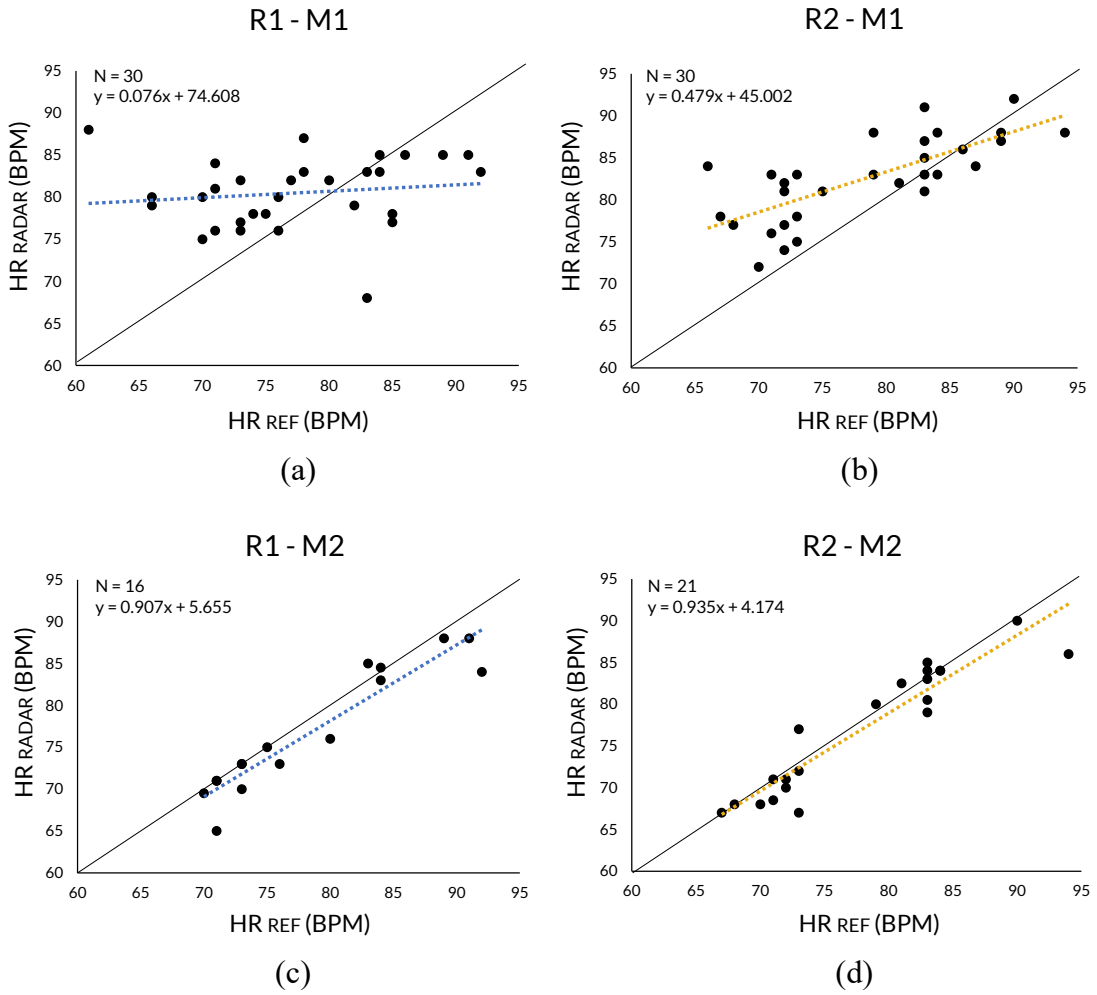

Figure 6.13: Dispersion plot comparing HR references values and estimated HR values obtained with M1 and M2 methods applied to R1 and R2 radar signals.

Overall, the first M1 results are in line with the general concern assumed in literature and highlighted in the state-of-the-art chapter: simple peaks technique with FIR filter applications are not good enough to extract the cardiac information from radar signals. Most of the proposed solutions in literature are based on signal decompositional methods for HR estimation [59, 73, 75]. However, these approaches are computationally heavy what makes them unsuitable for real-time application and streaming processing. For this reason, we decided to follow a different direction and design this new and less complex SSAC algorithm (M2).

Observing R1-M2 and R2-M2 plots, a better correlation between the estimated and reference HR values is evident. It is important to notice that only the estimated HR values accepted by M2 method are shown. Considering the weak and unpredictable expression of the heartbeats in the signals, M2 shows to be a reasonable solution to measure the HR parameter in cardiovascular applications periodically. Hence, it is recommended the use of this algorithm in applications where HR readings are not needed continuously over

time. For example, SSAC could be applied in sleeping monitoring applications where RR and motion are usually low, and therefore HR expression could be extracted from more prolonged time intervals between respiratory cycles, where their expression is more clear (see Figure 6.9). Nevertheless, in the future, SSAC should be again tested with a higher population.

To conclude this discussion about the detection of HR using radar, Bland-Altman analysis was performed for the M2 method.

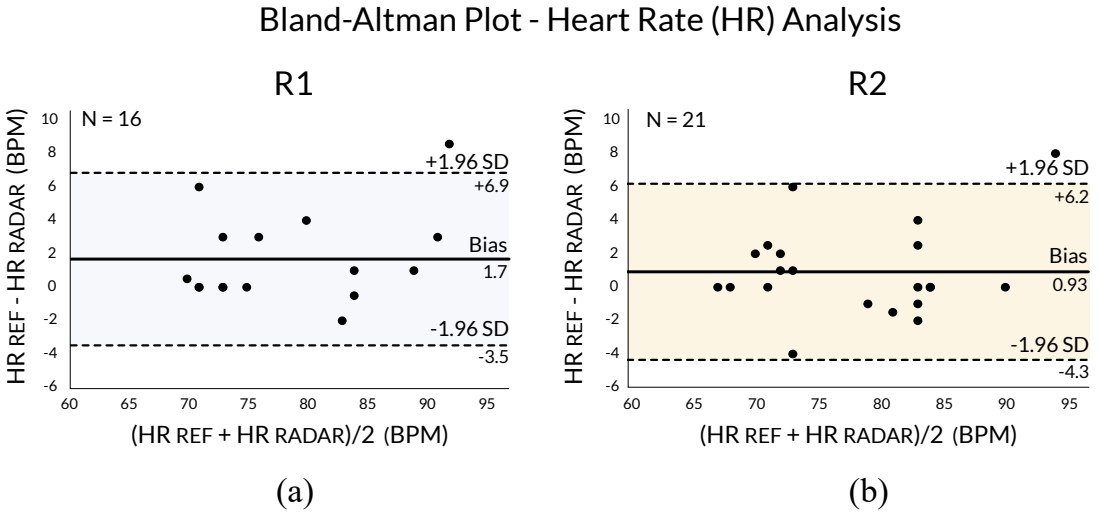

Figure 6.14: Bland-Altman comparison between heart rate measured reference and radar values obtained with method M2 applied to signals recorded with (a) R1 and (b) R2.

Observing both R1 and R2 Bland-Altman plots, it is possible to find similar ranges for the confidence interval: -3.5 to +6.9 BPM to R1 and -4.3 to 6.2 BPM to R2. Also, in each radar plot, all the sample are contained within the referred 95% confidence interval with the exception of one unique outlier. Although the wide range for the agreement limits, and taking into account the nonexistence presence of heartbeat expression on these signals, the tolerance limits are assumed as acceptable BPM errors, especially due to the difficulty in detecting this small expression on signals.

A bias of 0.9 and 1.7 BPM was found for R1 and R2, respectively. This indicates that estimated RR values may lie above these bias, which can point to the existence of a systematic error near to one. However, in the context of this analysis, this bias between estimated (HR_{RADAR}) and reference (HR_{REF}) values does not have great signification. Since the estimated frequency values are directly rounded to BPM integer values, the error could increase during this process up to 1 BPM. Second, the reduced number of samples used might influence the increase of bias. Also, this first approach only wanted to demonstrate that radar could be used to detect vital signs with a good enough accuracy, and a difference of 1 BPM to the reference (Table 3.1) is not a significant amount.

Finally, no trend is observed for any of the sensors plots. However, estimated HR values for the R2 radar are closer to zero (in the y axis) when compared to R1, indicating that the HR were found with smaller error using R2. Hence, we can consider that R2 had a slightly better performance in the measurement of RR than R1 radar, in agreement with the first qualitative analysis where more visible heartbeat activity seemed to be present in the R2 signals.

Chapter 7

Conclusion

This concluding chapter summarizes the developed work and presents an overview of its achievements. Based on this thesis accomplishments, we first conclude about the viability of using radar for remote respiratory and heartbeat monitoring. Then, we extend our findings into a commercial report where the strengths and weaknesses of sensors used are identified in order to make a decision about which one is the most suitable to be integrated into a PLUX product. Some application scenarios are also proposed, followed by some guidelines and future developments. Finally, a reflection about remote vital signs application in the world and how this work can contribute to it is given.

7.1 Thesis Summary and Overall Results

This study aimed to assess the feasibility of using radar sensors for remote vital signs monitoring. To this purpose, two multi-purpose commercial radar, based on IR-UWB, a pulse emitting radar, and FMCW technology, which send a chirp to detect objects, were acquired and adapted to be used as bio-radar sensors. Then, an acquisition protocol was developed, and radar data were collected from 10 subjects in a relaxed position located up to a distance of 2.5 meters away from the sensors. Finally, signal processing methods were developed to extract and assess the cardiorespiratory signals, concluding about which are the best method-sensors combination to extract respiratory rate and heart rate accurately.

Overall, the set of algorithms developed together with the radar configuration used, proved to be sufficiently accurate for non-contact respiratory and heart rate monitoring applications.

Considering the initial proposed goals, a more detail overview of results achievement is given in detail below.

7.1.1 Respiratory Remote Sensing

In a first qualitative analysis, the respiratory activity was observed in the majority of the collected radar data. Inspiratory and expiratory timings were clearly extracted, since respiratory cycles on radar signals are successive contractions and relaxations of the thorax.

Using a peak finding algorithm, the respiratory events were estimated in signals and were directly compared against their reference, recorded using a microphone. In total, 625 respiratory events were classified. The metrics extracted were analyzed by radar type, subject and distance. A minimum error of 1.6% was obtained for signals extracted using the IR-UWB radar. Different distances or subjects do not appear to play a significant role in the error rate for respiration cycles detection.

To extract the respiration rate from the signals, two methods in time and frequency domain were used and applied to signals acquired with IR-UWB and FMCW. In the four radar-method configurations evaluated, a maximum mean absolute error of 2.1 RPM was obtained. Minor estimated respiratory rate errors were found when the first time-domain method was applied to radar signals extracted from IR-UWB radar.

In summary, methods for respiratory detection and respiratory rate estimation were successfully developed in this work. The achieved results are in agreement with previous studies, confirming that radars can be used for tracking respiration over time.

7.1.2 Heartbeat Remote Sensing

Contrarily to current studies, that usually assess radar heartbeats in short and real-life situations, in this study, we analyzed approximately one hour of heartbeat signals in both contexts: a relaxed situation and a voluntary apnea state.

By a first visual inspection of the signals, it was clear that the small peaks of the heartbeat were not present, masked by the respiration component, in more than 50% of the signals. Therefore, visually the only detected peaks where in the regions between respiratory cycles, where the influence by the chest displacement during those cycles was less prone to cover the millimetric movements of the heart muscles and pulse skin displacement. Further, apnea frames were used to confirm the viability of using radars for heartbeat sensing. In apnea, only random noise was present, and therefore it was confirmed that both radars used are sensible to measure the sub-millimetric tissues displacements caused by cardiovascular activity. Notwidhtstaing, the heartbeat was not also observed in all apnea frames.

Concerning the previous observations, a novel heart rate estimation approach was developed to extract this parameter from the weak heartbeat signal: the Selective Short-Term Autorcorrelation (SSAC). Contrarily to the high computational complexity techniques based on decomposition algorithms, commonly used on literature, SSAC was proposed with the aim of being implemented in further real-time algorithms. Although heartbeats can be extracted from these weak signals, SSAC was designed to only return a rate when

relevant heartbeat expression is on the signals, that is when the subject is in a favourable position to this measurement. To check the accuracy of the proposed method, a reference ECG was recorded at the same time and, SSAC was compared with a traditional mean peak method, where the proposed method was more accurate that this metric when a valid heart rate was returned. Besides the improvement, a minimum mean absolute error of 1.8 BPM was still found when using the FMCW radar.

Comparing to the state of art, the developed SSAC approach has a higher error rate, although a direct comparison should not be made. Most of the studies in the literature are made in very restricted conditions such as apnea or directing the radar cross-section directly to favourable zones such as the carotid, where only the heart rate can be extracted, ignoring the respiration component.

In summary, this work was demonstrated a general complexity in acquiring high-quality heartbeat signals with radars in real environments. Concerning the results achieved in this work, it is not recommended the use of radars for heart signal activity tracking in complex environments of daily life. However, the developed algorithm presented in this thesis was shown as an alternative for periodically heart rate measurements with radars.

7.1.3 Radars Perfomance

In the conditions of the experimental setup, IR-UWB demonstrated a greater capability in respiratory sensing, whereas heartbeat activity was found more often in signals recorded using FMCW. Although R2 had presented a slightly better heart rate acquisition performance, this needs to be further confirmed in a future study with a higher number of subjects, since not every signal provided a valid heart rate. Hence, in overall IR-UWB presented better quality cardiorespiratory measurements.

7.1.4 Commercial Considerations

In addition to the main goal of this dissertation, this research was also done to find a commercial off-the-shelf radar that, together with the developed algorithms, could be used in a novel Bio-Radar to be introduced in PLUX's commercial catalogue. Therefore, the methods and algorithms applied in this research were chosen considering this possible future commercialization. For example, radar sensors were chosen taking into account some commercial requirements (enumerated in Chapter 4) whereas the developed signal processing algorithms were built to be integrated into future real-time or post-processing plugins applications.

Thus, concerning the results achieved in this study, a commercially oriented analysis was performed on which could be the most suitable sensor to be integrated into a future PLUX Bio-Radar. In order to make this analysis, seven radar sensors features were considered. This small commercial analyse is reported in Appendix C. Although IR-UWB from a pure vital signal sensing standpoint has better performance, FMCW can be considered more suitable to be used in a commercial application.

7.1.5 Work Contributions

The principal contributions of this work for the development of contactless vital signs techniques using radar technology are listed below:

- **A comparison between the performance of current off-the-shelf radars in the market for vital sings applications:** For a non-specialist in radar field, the large number of studies incorporating different radar types and concepts can be confused. Most of the vital signs studies are focused on the use of one only radar type, and review papers did not exhibit the practical differences and concerns to take into account when choosing a model, or a certain technology. In this study, two of the most popular radar technologies (IR-UWB and FMCW) used in vital signs radar studies were used, configurated and compared in similar real-life situations. The developed python scripts used for the configuration and adjustment of both sensors are made available online in the following link: https://github.com/alexandrasdl/RADAR-WORLD.

- **A new vital signs radar dataset:** More than 1 hour of collected radar signal are made available on shorturl.at/drHSZ. Beyond the methods applied in this dissertation, this dataset could also be used to test new approaches and algorithms in this field.

- **A detailed respiratory study:** Contrary to conventional studies, which are focused on in the extraction of RR parameters from radar signals, in this study, the quality of respiratory detection was also assessed following an event-based classification approach.

- **A new approach for Heart Rate monitoring:** The most popular methods used to extract the heart activity from the weak radar signals are based on decomposition algorithms. However in this study, a novel algorihtm called SSAC was proposed to estimate HR in signals with considerable heartbeat presence.

- **A concept for a Wireless Bio-Radar Sensor:** Finally, based on the results achieved of this dissertation, a small and illustrative concept application of the future bio-Radar PLUX was developed. A demonstration of this is in Appendix D.

7.2 Future Work

Despite the promising results presented in this work for non-contact measurement of respiratory and heart parameters, further work is required to improve the developed techniques and obtain more accurate systems. Some potential solutions are presented below:

Additional Validation: Although this study was carried out in a more realistic environment than most of the previous studies, it is important to validate the algorithms used in a larger population and different environments conditions. For example, it is recommended the application of the developed algorithms in motionless scenarios such as a person working on a computer or sleeping.

Beyond new environments studies, further studies to assess the quality of radar signals when applied to subjects with different physiological characteristics are recommended, since it is an important parameter that lacks in literature. In this study, some considerations about this topic were made, however, due to the reduced number of the population tested, no relevant patterns between subject characteristics and the quality of the signal were observed.

It is also recommended to use a more precise breath reference tool than audio for further assessment of inspiratory and expiratory moments. As mentioned before, the inspiration-to-expiration ratio is a significant parameter since variations in this ratio may be related to the presence of respiratory diseases [124]. Moreover, although its potential to perceive acute changes in a patient's condition, respiratory rate is still the most neglected vital sign in practice clinic mainly due to time constraints that this activity requires for medical staff [3, 133]. As seen in this study, radar technology can provide high quality breath measures, and therefore radar may be the new solution to solve this problem in medical context. For these reasons, the need for more profound studies in the analysis of this parameter by radar applications is reinforced.

Algorithms Improvements: Since one of the objectives of this study was to understand the differences between the two implemented radars, the same signal processing chain was used to make the process more effective in the available time (see a general overview in Appendix C). However, some additional signal processing steps are recommended to be added according to the operation mode of the radar used.

To improve the quality of FMCW signals, unwrapping function should be improved to avoid ambiguities in respiratory signals. I/Q imbalance and DC offset [54] were also not considered, and therefore these steps should be added to improve algorithms accuracy.

In this work, a method for automatic target detection was developed. However, the methods implemented could be not enough when there is motion in the background. Hence, it is recommended additional processing to algorithms to detect targets even when external or random body movements occurs [132]. The radars sensors selected were also choosen according to their capacity to measure activity in different ranges and therefore, signal processing techniques for multi-target tange detection and vital signs sensing can be further developed using the configurated radars.

Hardware Improvements: The quality of signals is also dependent on the configuration performed on radars. In this work, IR-UWB demonstrated a better performance than

FMCW radar in vital signs sensing. However, the FMCW sensor has potential features that can be used to improve the quality of the signals.

As seen in Chapter 4, FMCW chip has an excellent processing capacity for embedded applications, which can be leveraged to perform some of the computation needs for respiration and heart rate estimation. Similar to the coherent processing used in IR-UWB, an equivalent technique is suggested to be implemented in the signal processing chain of FMCW.

In this work, only one pair in a total of four TX/RX antennas pairs were used. However, the activation of more than one pair of antennas allows performing angular measurements that could be introduced as parameters in novel algorithms to increase the precision of the physiological measurements. Nevertheless, the solutions proposed above should be implemented concerning the mandatory local rules of radiation emission.

7.3 Application: Wireless Bio-Radar

The developed work in this dissertation served as a proof of concept of a possible new sensor for PLUX catalogue. Following the wireless approach employed by PLUX when designing new products, this should also be a completely wireless bio-radar being able to be positioned in any part of a room without any wire. To demonstrate this concept, and using the signals processing techniques developed in this work, a small mockup of this future product was developed and presented in Appendix D. Figure 7.1 illustrate a potential scenario application where a PLUX module is used in conjuction with a wireless Bio-Radar.

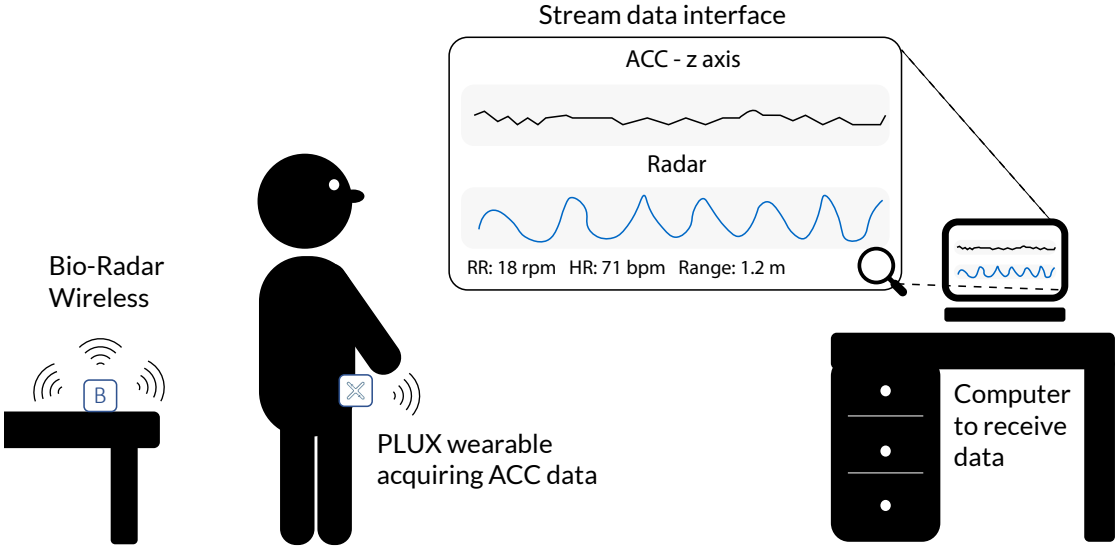

Figure 7.1: Example of an application scenario using a wireless bio-radar module integrated into a PLUX product. In the schema, a subject is simultaneously monitored by the radar module (on table) and an accelerometer PLUX wearable module.

The algorithms developed in this work can be used along with the bio-radar system, in offline and/or real-time processing. The implemented algorithms are crucial for the decoding of the radar signals. These algorithms will be implemented on PLUX's opensignal software as an plugin, either in real time and offline mode, thus enabling the user to get the RR and HR from the signals, while also recording the raw data.

According to the commercial report presented in Appendix C, R2 can be considered the best option to be used in this future product. Notwithstanding, other hardware requirements have to be considered such as the integration of R2 in a new board where a battery, antennas designs and the wireless communication module.

7.4 Future of Remote Vital Signs Sensing

Although favourable results were achieved in remote measurement of vital signs by the present study, and similarly to a vast majority of the reviewed literature, was performed with static target conditions. Large motion is appointed at one of the biggest limitations in the bio-radar system since its activity can mask the vital signs expressions.

The motion noise problem in radar signals is not trivial. Nevertheless, today's radar technology can be applied in a considerable number of situations without major hindrance such as sleep monitoring applications, driver's monitoring in automotive contexts, research applications and others, where respiratory and heart rate parameters are recorded in an immobile or quasi immobile environments.

Whereas most of the studies are focused on the removing of external noise, in our study, we have assumed this current limitation and adapted our methods to be applied scenarios where the subject would be in a real and motionless situation. Similarly to smartwatches that make measurements of vital signs over the day periodically, we assumed that a future iteration of this work could also be used to collect RR and HR parameters periodically and remotely. Since in everyday life, there are always periods where the human being is static or has small movements, that can be used to extract vital signs values.

In conclusion, although there is not yet possible the use of radar for an accurately 24/7 monitoring applications with current algorithms, this study as shown that radar technology is sufficiently reliable to pass from board into more practical and real remote vital signs sensing applications in this new and extincting field. In the future, it is expected improvements of these non-contact applications with the developments of new and more robust algorithms, enabling remote monitoring in environments where today contact based approach are still tried to be used for continuous monitoring, such as nursing homes, or independent senior living. By providing a completely hands free, where the user does not have to interact with the device for it to be sensing vital signs could be a game changer in this field, where user adoption tends to be the biggest issue.

Bibliography

[1] J. Kellett and F. Sebat. "Make vital signs great again – A call for action." In: *European Journal of Internal Medicine* 45 (2017), pp. 13–19. ISSN: 09536205. DOI: 10.1016/j.ejim.2017.09.018. URL: http://www.sciencedirect.com/science/article/pii/S0953620517303679https://linkinghub.elsevier.com/retrieve/pii/S0953620517303679.

[2] M. M. Churpek, R. Adhikari, and D. P. Edelson. "The value of vital sign trends for detecting clinical deterioration on the wards." In: *Resuscitation* 102 (2016), pp. 1–5. ISSN: 03009572. DOI: 10.1016/j.resuscitation.2016.02.005. URL: http://www.sciencedirect.com/science/article/pii/S0300957216000770https://linkinghub.elsevier.com/retrieve/pii/S0300957216000770.

[3] R. Parkes. "Rate of respiration: the forgotten vital sign." In: *Emergency Nurse* 19.2 (2011), pp. 12–17. ISSN: 1354-5752. DOI: 10.7748/en2011.05.19.2.12.c8504. URL: http://rcnpublishing.com/doi/abs/10.7748/en2011.05.19.2.12.c8504.

[4] M. R. Neuman. "Vital Signs: Heart Rate." In: *IEEE Pulse* 1.3 (2010), pp. 51–55. ISSN: 2154-2287. DOI: 10.1109/MPUL.2010.939179. URL: http://ieeexplore.ieee.org/document/5642169/.

[5] S. C. Verrillo, M. Cvach, K. W. Hudson, and B. D. Winters. "Using Continuous Vital Sign Monitoring to Detect Early Deterioration in Adult Postoperative Inpatients." In: *Journal of Nursing Care Quality* 34.2 (2019), pp. 107–113. ISSN: 1057-3631. DOI: 10.1097/NCQ.0000000000000350. URL: http://journals.lww.com/00001786-201904000-00004.

[6] *Cardiovascular diseases*. URL: https://www.who.int/health-topics/cardiovascular-diseases/.

[7] J. M. Rothschild, E. Gandara, S. Woolf, D. H. Williams, and D. W. Bates. "Single-Parameter Early Warning Criteria to Predict Life-Threatening Adverse Events." eng. In: *Journal of Patient Safety* 6.2 (2010), pp. 97–101. ISSN: 1549-8417. DOI: 10.1097/PTS.0b013e3181dcaf32. URL: http://journals.lww.com/01209203-201006000-00007.

[8] J. P. L. Leenen, C. Leerentveld, J. D. van Dijk, H. L. van Westreenen, L. Schoonhoven, and G. A. Patijn. "Current Evidence for Continuous Vital Signs Monitoring by Wearable Wireless Devices in Hospitalized Adults: Systematic Review." In: *Journal of Medical Internet Research* 22.6 (2020), e18636. ISSN: 1438-8871. DOI: 10.2196/18636. URL: http://www.jmir.org/2020/6/e18636/.

[9] R. S. Ravindran. "A Solution to Monitoring the Electrocardiograph in Patients with Extensive Burn Injury." In: *Anesthesiology* 87.3 (1997), pp. 711–712. ISSN: 0003-3022. DOI: 10.1097/00000542-199709000-00041. URL: https://doi.org/10.1097/00000542-199709000-00041https://pubs.asahq.org/anesthesiology/article/87/3/711/36269/A-Solution-to-Monitoring-the-Electrocardiograph-in.

[10] E. McAdams et al. "Wearable sensor systems: The challenges." In: *2011 Annual International Conference of the IEEE Engineering in Medicine and Biology Society* 2011 (2011), pp. 3648–3651. DOI: 10.1109/IEMBS.2011.6090614. URL: http://ieeexplore.ieee.org/document/6090614/.

[11] M. Hirshkowitz. "Polysomnography Challenges." In: *Sleep Medicine Clinics* 11.4 (2016), pp. 403–411. ISSN: 1556407X. DOI: 10.1016/j.jsmc.2016.07.002. URL: https://linkinghub.elsevier.com/retrieve/pii/S1556407X16300601.

[12] S. Leem, F. Khan, and S. Cho. "Vital Sign Monitoring and Mobile Phone Usage Detection Using IR-UWB Radar for Intended Use in Car Crash Prevention." In: *Sensors* 17.6 (2017), p. 1240. ISSN: 1424-8220. DOI: 10.3390/s17061240. URL: http://www.mdpi.com/1424-8220/17/6/1240.

[13] E. G. Ziganshin, M. A. Numerov, and S. A. Vygolov. "UWB Baby Monitor." In: *2010 5th International Confernce on Ultrawideband and Ultrashort Impulse Signals*. IEEE, 2010, pp. 159–161. ISBN: 978-1-4244-7470-7. DOI: 10.1109/UWBUSIS.2010.5609156. URL: http://ieeexplore.ieee.org/document/5609156/.

[14] M. G. Amin, Y. D. Zhang, F. Ahmad, and K. D. Ho. "Radar Signal Processing for Elderly Fall Detection: The future for in-home monitoring." In: *IEEE Signal Processing Magazine* 33.2 (2016), pp. 71–80. ISSN: 1053-5888. DOI: 10.1109/MSP.2015.2502784. URL: http://ieeexplore.ieee.org/document/7426551/.

[15] *PLUX - About Us*. URL: https://plux.info/content/9-about-us (visited on 03/30/2020).

[16] S. Okutucu and A. Oto. *Interpreting ECGs in Clinical Practice*. 1st. Cham, Switzerland: Springer International Publishing AG, 2018, p. 117.

[17] A. Rosiek and K. Leksowski. "The risk factors and prevention of cardiovascular disease: the importance of electrocardiogram in the diagnosis and treatment of acute coronary syndrome." eng. In: *Therapeutics and Clinical Risk Management* Volume 12 (2016), pp. 1223–1229. ISSN: 1178-203X. DOI: 10.2147/TCRM.S107849.

URL: https://www.dovepress.com/the-risk-factors--and-prevention-of-cardiovascular-disease-the-importa-peer-reviewed-article-TCRM.

[18] L. Su, S. Borov, and B. Zrenner. "12-lead Holter electrocardiography." eng. In: *Herzschrittmachertherapie + Elektrophysiologie* 24.2 (2013), pp. 92–96. ISSN: 0938-7412. DOI: 10.1007/s00399-013-0268-4. URL: http://link.springer.com/10.1007/s00399-013-0268-4.

[19] H. L. Kennedy. "The Evolution of Ambulatory ECG Monitoring." eng. In: *Progress in Cardiovascular Diseases* 56.2 (2013), pp. 127–132. ISSN: 00330620. DOI: 10.1016/j.pcad.2013.08.005. URL: https://linkinghub.elsevier.com/retrieve/pii/S0033062013001503.

[20] J. S. Steinberg et al. "2017 ISHNE-HRS expert consensus statement on ambulatory ECG and external cardiac monitoring/telemetry." eng. In: *Heart Rhythm* 14.7 (2017), e55–e96. ISSN: 15475271. DOI: 10.1016/j.hrthm.2017.03.038. URL: https://linkinghub.elsevier.com/retrieve/pii/S1547527117304150.

[21] S. Majumder, L. Chen, O. Marinov, C.-H. Chen, T. Mondal, and M. J. Deen. "Noncontact Wearable Wireless ECG Systems for Long-Term Monitoring." In: *IEEE Reviews in Biomedical Engineering* 11 (2018), pp. 306–321. ISSN: 1937-3333. DOI: 10.1109/RBME.2018.2840336. URL: https://ieeexplore.ieee.org/document/8368254/.

[22] A. Reisner, P. A. Shaltis, D. McCombie, H. H. Asada, D. S. Warner, and M. A. Warner. "Utility of the Photoplethysmogram in Circulatory Monitoring." eng. In: *Anesthesiology* 108.5 (2008), pp. 950–958. ISSN: 0003-3022. DOI: 10.1097/ALN.0b013e31816c89e1. URL: https://pubs.asahq.org/anesthesiology/article/108/5/950/8368/Utility-of-the-Photoplethysmogram-in-Circulatory.

[23] J. Allen. "Photoplethysmography and its application in clinical physiological measurement." eng. In: *Physiological measurement* 28.3 (2007), R1–39. ISSN: 0967-3334 (Print). DOI: 10.1088/0967-3334/28/3/R01.

[24] D. Biswas, N. Simoes-Capela, C. Van Hoof, and N. Van Helleputte. "Heart Rate Estimation From Wrist-Worn Photoplethysmography: A Review." In: *IEEE Sensors Journal* 19.16 (2019), pp. 6560–6570. ISSN: 1530-437X. DOI: 10.1109/JSEN.2019.2914166. URL: https://ieeexplore.ieee.org/document/8703846/.

[25] Y Maeda, M Sekine, T Tamura, A Moriya, T Suzuki, and K Kameyama. "Comparison of reflected green light and infrared photoplethysmography." In: *2008 30th Annual International Conference of the IEEE Engineering in Medicine and Biology Society*. IEEE, 2008, pp. 2270–2272. ISBN: 978-1-4244-1814-5. DOI: 10.1109/IEMBS.2008.4649649. URL: https://ieeexplore.ieee.org/document/4649649/.

[26] M. Ghamari. "A review on wearable photoplethysmography sensors and their potential future applications in health care." eng. In: *International Journal of Biosensors & Bioelectronics* 4.4 (2018), pp. 195–202. ISSN: 25732838. DOI: 10.15406/ijbsbe.2018.04.00125. URL: https://medcraveonline.com/IJBSBE/a-review-on-wearable-photoplethysmography-sensors-and-their-potential-future-applications-in-health-care.html.

[27] F. AL-Khalidi, R Saatchi, D Burke, H Elphick, and S Tan. "Respiration rate monitoring methods: A review." eng. In: *Pediatric Pulmonology* 46.6 (2011), pp. 523–529. ISSN: 87556863. DOI: 10.1002/ppul.21416. URL: http://doi.wiley.com/10.1002/ppul.21416.

[28] C. Massaroni, A. Nicolò, D. Lo Presti, M. Sacchetti, S. Silvestri, and E. Schena. "Contact-Based Methods for Measuring Respiratory Rate." eng. In: *Sensors* 19.4 (2019), p. 908. ISSN: 1424-8220. DOI: 10.3390/s19040908. URL: http://www.mdpi.com/1424-8220/19/4/908.

[29] Y. Nam, B. A. Reyes, and K. H. Chon. "Estimation of Respiratory Rates Using the Built-in Microphone of a Smartphone or Headset." In: *IEEE Journal of Biomedical and Health Informatics* 20.6 (2016), pp. 1493–1501. ISSN: 2168-2194. DOI: 10.1109/JBHI.2015.2480838. URL: http://ieeexplore.ieee.org/document/7273825/.

[30] T. Daiana da Costa, M. de Fatima Fernandes Vara, C. Santos Cristino, T. Zoraski Zanella, G. Nunes Nogueira Neto, and P. Nohama. "Breathing Monitoring and Pattern Recognition with Wearable Sensors." In: *Wearable Devices - the Big Wave of Innovation*. IntechOpen, 2019. ISBN: 978-1-78984-496-2. DOI: 10.5772/intechopen.85460. URL: https://www.intechopen.com/books/wearable-devices-the-big-wave-of-innovation/breathing-monitoring-and-pattern-recognition-with-wearable-sensors.

[31] D. Dias and J. Paulo Silva Cunha. "Wearable Health Devices—Vital Sign Monitoring, Systems and Technologies." eng. In: *Sensors* 18.8 (2018), p. 2414. ISSN: 1424-8220. DOI: 10.3390/s18082414. URL: http://www.mdpi.com/1424-8220/18/8/2414.

[32] B. Reeder and A. David. "Health at hand: A systematic review of smart watch uses for health and wellness." eng. In: *Journal of Biomedical Informatics* 63 (2016), pp. 269–276. ISSN: 15320464. DOI: 10.1016/j.jbi.2016.09.001. URL: https://linkinghub.elsevier.com/retrieve/pii/S1532046416301137.

[33] S. A. Siddiqui, Y. Zhang, Z. Feng, and A. Kos. "A Pulse Rate Estimation Algorithm Using PPG and Smartphone Camera." eng. In: *Journal of Medical Systems* 40.5 (2016), p. 126. ISSN: 0148-5598. DOI: 10.1007/s10916-016-0485-6. URL: http://link.springer.com/10.1007/s10916-016-0485-6.

[34] C Michailidis, I Smanis, K Stamatis, C Bergeles, and A Kouris. "Development of a smartphone-enabled spirometer for personalised respiratory health." In: *2014 4th International Conference on Wireless Mobile Communication and Healthcare - Transforming Healthcare Through Innovations in Mobile and Wireless Technologies (MOBIHEALTH)*. 2014, pp. 67–70. DOI: 10.1109/MOBIHEALTH.2014.7015911.

[35] R. S. GUBNER, M. RODSTEIN, and H. E. UNGERLEIDER. "Ballistocardiography." und. In: *Circulation* 7.2 (1953), pp. 268–286. ISSN: 0009-7322. DOI: 10.1161/01.CIR.7.2.268. URL: https://www.ahajournals.org/doi/10.1161/01.CIR.7.2.268.

[36] W. Dock. "BALLISTOCARDIOGRAPHY IN MEDICAL PRACTICE." eng. In: *Journal of the American Medical Association* 146.14 (1951), p. 1284. ISSN: 0002-9955. DOI: 10.1001/jama.1951.03670140010003. URL: http://jama.jamanetwork.com/article.aspx?doi=10.1001/jama.1951.03670140010003.

[37] E. Pinheiro, O. Postolache, and P. Girão. "Theory and Developments in an Unobtrusive Cardiovascular System Representation: Ballistocardiography." eng. In: *The Open Biomedical Engineering Journal* 4.1 (2010), pp. 201–216. ISSN: 1874-1207. DOI: 10.2174/1874120701004010201. URL: https://openbiomedicalengineeringjournal.com/VOLUME/4/PAGE/201/.

[38] A. Albukhari, F. Lima, and U. Mescheder. "Bed-Embedded Heart and Respiration Rates Detection by Longitudinal Ballistocardiography and Pattern Recognition." eng. In: *Sensors* 19.6 (2019), p. 1451. ISSN: 1424-8220. DOI: 10.3390/s19061451. URL: https://www.mdpi.com/1424-8220/19/6/1451.

[39] W. Zhao, H. Ni, X. Zhou, Y. Song, and T. Wang. "Identifying sleep apnea syndrome using heart rate and breathing effort variation analysis based on ballistocardiography." In: *2015 37th Annual International Conference of the IEEE Engineering in Medicine and Biology Society (EMBC)*. IEEE, 2015, pp. 4536–4539. ISBN: 978-1-4244-9271-8. DOI: 10.1109/EMBC.2015.7319403. URL: https://ieeexplore.ieee.org/document/7319403/.

[40] *{EMFIT} Science of Ballistocardiography*. URL: https://www.emfit.com/science-of-ballistocardiography (visited on 09/30/2020).

[41] N. Wadhwa et al. "Eulerian video magnification and analysis." In: *Communications of the ACM* 60.1 (2016), pp. 87–95. ISSN: 0001-0782. DOI: 10.1145/3015573. URL: https://dl.acm.org/doi/10.1145/3015573.

[42] P. B. Chambino. "No Title." Master's thesis.

[43] C. Massaroni, D. S. Lopes, D. Lo Presti, E. Schena, and S. Silvestri. "Contactless Monitoring of Breathing Patterns and Respiratory Rate at the Pit of the Neck: A Single Camera Approach." In: *Journal of Sensors* 2018 (2018), pp. 1–13. ISSN: 1687-725X. DOI: 10.1155/2018/4567213. URL: https://www.hindawi.com/journals/js/2018/4567213/.

[44] C. Luca, C. Corciovă, D. Andriţoi, and R. Ciorap. "The Use of Thermal Imaging Techniques as a Method of Monitoring the New Born." In: 2019, pp. 35–39. ISBN: 978-981-13-6206-4. DOI: 10.1007/978-981-13-6207-1_6. URL: http://link.springer.com/10.1007/978-981-13-6207-1{_}6.

[45] K Mutlu, J. E. Rabell, P. Martin del Olmo, and S Haesler. "IR thermography-based monitoring of respiration phase without image segmentation." eng. In: *Journal of Neuroscience Methods* 301 (2018), pp. 1–8. ISSN: 01650270. DOI: 10.1016/j.jneumeth.2018.02.017. URL: https://linkinghub.elsevier.com/retrieve/pii/S0165027018300591.

[46] J. Lin. "Noninvasive microwave measurement of respiration." In: *Proceedings of the IEEE* 63.10 (1975), pp. 1530–1530. ISSN: 0018-9219. DOI: 10.1109/PROC.1975.9992. URL: http://ieeexplore.ieee.org/document/1451922/.

[47] J. Y. Lee and J. C. Lin. "A Microcprocessor-Based Noninvasive Arterial Pulse Wave Analyzer." In: *IEEE Transactions on Biomedical Engineering* BME-32.6 (1985), pp. 451–455. ISSN: 0018-9294. DOI: 10.1109/TBME.1985.325454. URL: http://ieeexplore.ieee.org/document/4122086/.

[48] S. M. Sharpe, J. Seals, A. H. MacDonald, and S. R. Crowgey. *Non-contact vital signs monitor*. 1990.

[49] T. E. Mcewan. *Ultra-wideband radar motion sensor*. 1994.

[50] V. L. Petrovic, M. M. Jankovic, A. V. Lupsic, V. R. Mihajlovic, and J. S. Popovic-Bozovic. "High-Accuracy Real-Time Monitoring of Heart Rate Variability Using 24 GHz Continuous-Wave Doppler Radar." In: *IEEE Access* 7 (2019), pp. 74721–74733. ISSN: 2169-3536. DOI: 10.1109/ACCESS.2019.2921240. URL: https://ieeexplore.ieee.org/document/8732355/.

[51] J.-H. Park, Y.-J. Jeong, G.-E. Lee, J. Oh, and J.-R. Yang. "915-MHz Continuous-Wave Doppler Radar Sensor for Detection of Vital Signs." In: *Electronics* 8.5 (2019), p. 561. ISSN: 2079-9292. DOI: 10.3390/electronics8050561. URL: https://www.mdpi.com/2079-9292/8/5/561.

[52] V. C. Chen. *The Micro-doppler Effect in Radar*. Artech House radar library. Artech House, 2011. ISBN: 9781608070589. URL: https://books.google.nl/books?id=eJ7eMHpxt30C.

[53] D. Girbau, A. Lazaro, Á. Ramos, and R. Villarino. "Remote Sensing of Vital Signs Using a Doppler Radar and Diversity to Overcome Null Detection." In: *IEEE Sensors Journal* 12.3 (2012), pp. 512–518. ISSN: 1530-437X. DOI: 10.1109/JSEN.2011.2107736. URL: http://ieeexplore.ieee.org/document/5699436/.

[54] A. Droitcour, O Boric-Lubecke, V. Lubecke, J Lin, and G. Kovacs. "Range correlation and I/Q performance benefits in single-chip silicon Doppler radars for noncontact cardiopulmonary monitoring." In: *IEEE Transactions on Microwave Theory and Techniques* 52.3 (2004), pp. 838–848. ISSN: 0018-9480. DOI: 10.1109/TMTT.2004.823552. URL: http://ieeexplore.ieee.org/document/1273725/.

[55] Siying Wang et al. "A novel ultra-wideband 80 GHz FMCW radar system for contactless monitoring of vital signs." In: *2015 37th Annual International Conference of the IEEE Engineering in Medicine and Biology Society (EMBC)*. Vol. 2015. IEEE, 2015, pp. 4978–4981. ISBN: 978-1-4244-9271-8. DOI: 10.1109/EMBC.2015.7319509. URL: http://ieeexplore.ieee.org/document/7319509/.

[56] J.-M. Munoz-Ferreras, J. Wang, Z. Peng, C. Li, and R. Gomez-Garcia. "FMCW-Radar-Based Vital-Sign Monitoring of Multiple Patients." In: *2019 IEEE MTT-S International Microwave Biomedical Conference (IMBioC)*. Vol. 1. IEEE, 2019, pp. 1–3. ISBN: 978-1-5386-7395-9. DOI: 10.1109/IMBIOC.2019.8777845. URL: https://ieeexplore.ieee.org/document/8777845/.

[57] M. Alizadeh, G. Shaker, J. C. M. D. Almeida, P. P. Morita, and S. Safavi-Naeini. "Remote Monitoring of Human Vital Signs Using mm-Wave FMCW Radar." In: *IEEE Access* 7 (2019), pp. 54958–54968. ISSN: 2169-3536. DOI: 10.1109/ACCESS.2019.2912956. URL: https://ieeexplore.ieee.org/document/8695699/.

[58] S. Abdulatif, F. Aziz, P. Alu1ner, B. Kleiner, and U Schneider. "Power-Based Real-Time Respiration Monitoring Using FMCW Radar." In: *arXiv: Signal Processing* (2017).

[59] G.-W. Fang, C.-Y. Huang, and C.-L. Yang. "Simultaneous Detection of Multi-Target Vital Signs Using EEMD Algorithm Based on FMCW Radar." In: *2019 IEEE MTT-S International Microwave Biomedical Conference (IMBioC)*. IEEE, 2019, pp. 1–4. ISBN: 978-1-5386-7395-9. DOI: 10.1109/IMBIOC.2019.8777810. URL: https://ieeexplore.ieee.org/document/8777810/.

[60] M. Mercuri, D. Schreurs, and P. Leroux. "SFCW microwave radar for in-door fall detection." In: *2012 IEEE Topical Conference on Biomedical Wireless Technologies, Networks, and Sensing Systems (BioWireleSS)* (2012), pp. 53–56. DOI: 10.1109/BioWireless.2012.6172729. URL: http://ieeexplore.ieee.org/document/6172729/.

[61] L. Anishchenko and E. Gaysina. "Comparison of 4 GHz and 14 GHz SFCW radars in measuring of small laboratory animals vital signs." In: *2015 IEEE International Conference on Microwaves, Communications, Antennas and Electronic Systems (COMCAS)*. IEEE, 2015, pp. 1–3. ISBN: 978-1-4799-7473-3. DOI: 10.1109/COMCAS.2015.7360388. URL: http://ieeexplore.ieee.org/document/7360388/.

[62] M. Chia, S. Leong, C. Sim, and K. Chan. "Through-Wall UWB Radar Operating Within FCC's Mask for Sensing Heart Beat and Breathing Rate." In: *European Radar Conference, 2005. EURAD 2005.* IEEE, 2005, p. 283. ISBN: 2-9600551-3-6. DOI: 10.1109/EURAD.2005.1605615. URL: http://ieeexplore.ieee.org/document/1605615/.

[63] A. Lazaro, D. Girbau, and R. Villarino. "ANALYSIS OF VITAL SIGNS MONITORING USING AN IR-UWB RADAR." In: *Progress In Electromagnetics Research* 100 (2010), pp. 265–284. ISSN: 1559-8985. DOI: 10.2528/PIER09120302. URL: http://www.jpier.org/PIER/pier.php?paper=09120302.

[64] F. C. Commission and Others. "In the matter of revision of part 15 of the commission's rules regarding ultra-wideband transmission systems." In: *First Report And Order, ET Docket 98-153* (2002).

[65] J. Pan. "Medical Applications of Ultra-WideBand (UWB)." In: (2007).

[66] S. Pisa, E. Pittella, and E. Piuzzi. "A survey of radar systems for medical applications." In: *IEEE Aerospace and Electronic Systems Magazine* 31.11 (2016), pp. 64–81. ISSN: 0885-8985. DOI: 10.1109/MAES.2016.140167. URL: http://ieeexplore.ieee.org/document/7771668/.

[67] Y. Xu, S. Dai, S. Wu, J. Chen, and G. Fang. "Vital Sign Detection Method Based on Multiple Higher Order Cumulant for Ultrawideband Radar." In: *IEEE Transactions on Geoscience and Remote Sensing* 50.4 (2012), pp. 1254–1265. ISSN: 0196-2892. DOI: 10.1109/TGRS.2011.2164928. URL: http://ieeexplore.ieee.org/document/6026944/.

[68] L. Liu, Z. Liu, and B. E. Barrowes. "Through-Wall Bio-Radiolocation With UWB Impulse Radar: Observation, Simulation and Signal Extraction." In: *IEEE Journal of Selected Topics in Applied Earth Observations and Remote Sensing* 4.4 (2011), pp. 791–798. ISSN: 1939-1404. DOI: 10.1109/JSTARS.2011.2157461. URL: http://ieeexplore.ieee.org/document/5898435/.

[69] L. Liu, Z. Liu, H. Xie, B. Barrowes, and A. C. Bagtzoglou. "Numerical simulation of UWB impulse radar vital sign detection at an earthquake disaster site." In: *Ad Hoc Networks* 13.Part A (2014), pp. 34–41. ISSN: 15708705. DOI: 10.1016/j.adhoc.2012.08.006. URL: https://linkinghub.elsevier.com/retrieve/pii/S1570870512001539.

[70] A. Tariq, A. Zahid, U. Khan, N. Khan, and F. Khan. "Implementation of Wavelet transform for monitoring of vital signs through IR-UWB Radar." In: *2017 International Conference on Communication, Computing and Digital Systems (C-CODE)*. IEEE, 2017, pp. 337–340. ISBN: 978-1-5090-4448-1. DOI: 10.1109/C-CODE.2017.7918953. URL: http://ieeexplore.ieee.org/document/7918953/.

[71] X. Hu and T. Jin. "Short-Range Vital Signs Sensing Based on EEMD and CWT Using IR-UWB Radar." In: *Sensors* 16.12 (2016), p. 2025. ISSN: 1424-8220. DOI: 10.3390/s16122025. URL: http://www.mdpi.com/1424-8220/16/12/2025.

[72] H Shen et al. "Respiration and Heartbeat Rates Measurement Based on Autocorrelation Using IR-UWB Radar." In: *IEEE Transactions on Circuits and Systems II: Express Briefs* 65.10 (2018), pp. 1470–1474. ISSN: 1558-3791.

[73] H.-S. Cho and Y.-J. Park. "Detection of Heart Rate through a Wall Using UWB Impulse Radar." In: *Journal of Healthcare Engineering* 2018 (2018), pp. 1–7. ISSN: 2040-2295. DOI: 10.1155/2018/4832605. URL: https://www.hindawi.com/journals/jhe/2018/4832605/.

[74] Z. Duan and J. Liang. "Non-Contact Detection of Vital Signs Using a UWB Radar Sensor." In: *IEEE Access* 7 (2019), pp. 36888–36895. ISSN: 2169-3536. DOI: 10.1109/ACCESS.2018.2886825. URL: https://ieeexplore.ieee.org/document/8581412/.

[75] P. Wang et al. "Non-Contact Vital Signs Monitoring of Dog and Cat Using a UWB Radar." In: *Animals* 10.2 (2020), p. 205. ISSN: 2076-2615. DOI: 10.3390/ani10020205. URL: https://www.mdpi.com/2076-2615/10/2/205.

[76] Wang et al. "Method for Distinguishing Humans and Animals in Vital Signs Monitoring Using IR-UWB Radar." In: *International Journal of Environmental Research and Public Health* 16.22 (2019), p. 4462. ISSN: 1660-4601. DOI: 10.3390/ijerph16224462. URL: https://www.mdpi.com/1660-4601/16/22/4462.

[77] L. Ren, Y. S. Koo, Y. Wang, and A. E. Fathy. "Noncontact heartbeat detection using UWB impulse doppler radar." In: *2015 IEEE Topical Conference on Biomedical Wireless Technologies, Networks, and Sensing Systems (BioWireleSS)*. IEEE, 2015, pp. 1–3. ISBN: 978-1-4799-5511-4. DOI: 10.1109/BIOWIRELESS.2015.7152128. URL: http://ieeexplore.ieee.org/document/7152128/.

[78] L. Ren, H. Wang, K. Naishadham, O. Kilic, and A. E. Fathy. "Phase-Based Methods for Heart Rate Detection Using UWB Impulse Doppler Radar." In: *IEEE Transactions on Microwave Theory and Techniques* 64.10 (2016), pp. 3319–3331. ISSN: 0018-9480. DOI: 10.1109/TMTT.2016.2597824. URL: http://ieeexplore.ieee.org/document/7547380/.

[79] L. Ren, Y. S. Koo, H. Wang, Y. Wang, Q. Liu, and A. E. Fathy. "Noncontact Multiple Heartbeats Detection and Subject Localization Using UWB Impulse Doppler Radar." In: *IEEE Microwave and Wireless Components Letters* 25.10 (2015), pp. 690–692. ISSN: 1531-1309. DOI: 10.1109/LMWC.2015.2463214. URL: http://ieeexplore.ieee.org/document/7194855/.

[80] A Nezirovic, A. Yarovoy, and L. Ligthart. "Signal Processing for Improved Detection of Trapped Victims Using UWB Radar." In: *IEEE Transactions on Geoscience and Remote Sensing* 48.4 (2010), pp. 2005–2014. ISSN: 0196-2892. DOI: 10.1109/TGRS.2009.2036840. URL: http://ieeexplore.ieee.org/document/5371937/.

[81] X. Liang, J. Deng, H. Zhang, and T. A. Gulliver. "Ultra-Wideband Impulse Radar Through-Wall Detection of Vital Signs." In: *Scientific Reports* 8.1 (2018), p. 13367. ISSN: 2045-2322. DOI: 10.1038/s41598-018-31669-y. URL: http://www.nature.com/articles/s41598-018-31669-y.

[82] Changzhi Li and Jenshan Lin. "Random Body Movement Cancellation in Doppler Radar Vital Sign Detection." In: *IEEE Transactions on Microwave Theory and Techniques* 56.12 (2008), pp. 3143–3152. ISSN: 0018-9480. DOI: 10.1109/TMTT.2008.2007139. URL: http://ieeexplore.ieee.org/document/4682605/.

[83] W. Yin, X. Yang, L. Li, L. Zhang, N. Kitsuwan, and E. Oki. "HEAR: Approach for Heartbeat Monitoring with Body Movement Compensation by IR-UWB Radar." In: *Sensors* 18.9 (2018), p. 3077. ISSN: 1424-8220. DOI: 10.3390/s18093077. URL: http://www.mdpi.com/1424-8220/18/9/3077.

[84] J. D. Kim et al. "Non-contact respiration monitoring using impulse radio ultra-wideband radar in neonates." In: *Royal Society Open Science* 6.6 (2019), p. 190149. ISSN: 2054-5703. DOI: 10.1098/rsos.190149. URL: https://royalsocietypublishing.org/doi/10.1098/rsos.190149.

[85] Y. Lee et al. "A Novel Non-contact Heart Rate Monitor Using Impulse-Radio Ultra-Wideband (IR-UWB) Radar Technology." In: *Scientific Reports* 8.1 (2018), p. 13053. ISSN: 2045-2322. DOI: 10.1038/s41598-018-31411-8. URL: http://www.nature.com/articles/s41598-018-31411-8.

[86] S.-H. Kim, Z. W. Geem, and G.-T. Han. "A Novel Human Respiration Pattern Recognition Using Signals of Ultra-Wideband Radar Sensor." In: *Sensors* 19.15 (2019), p. 3340. ISSN: 1424-8220. DOI: 10.3390/s19153340. URL: https://www.mdpi.com/1424-8220/19/15/3340.

[87] W. Yin, X. Yang, L. Zhang, and E. Oki. "ECG Monitoring System Integrated with IR-UWB Radar Based on CNN." In: *IEEE Access* 4 (2016), pp. 1–1. ISSN: 2169-3536. DOI: 10.1109/ACCESS.2016.2608777. URL: http://ieeexplore.ieee.org/document/7576640/.

[88] V. D. Kuptsov, S. I. Ivanov, A. A. Fedotov, and V. L. Badenko. "Features of Multi-target Detection Algorithm for Automotive FMCW Radar." In: 2019, pp. 355–364. ISBN: 978-3-030-30858-2. DOI: 10.1007/978-3-030-30859-9_30. URL: http://link.springer.com/10.1007/978-3-030-30859-9{_}30.

[89] J. Hussey. "Physiology of the Cardiorespiratory System." In: *Paediatric Respiratory Care*. Boston, MA: Springer US, 1995, pp. 13–24. DOI: 10.1007/978-1-4899-4469-6_2. URL: http://link.springer.com/10.1007/978-1-4899-4469-6{_}2.

[90] J. E. Hall. *Guyton and Hall Textbook of Medical Physiology E-Book*. Guyton Physiology. Elsevier Health Sciences, 2010. ISBN: 9781437726749. URL: https://books.google.pt/books?id=Po0zyO0BFzwC.

[91] Tommasin, Caenen, Verhegghe, Greenwald, and Segers. "Physics of Within-Tissue Wave Propagation Generated by Pulse Propagation in the Carotid Artery." In: *Applied Sciences* 9.14 (2019), p. 2878. ISSN: 2076-3417. DOI: 10.3390/app9142878. URL: https://www.mdpi.com/2076-3417/9/14/2878.

[92] L. S Costanzo. *Physiology Seventh Edition*. Philadelphia, United States: Cambridge University Press, 2019.

[93] V. Zakeri, A. Akhbardeh, N. Alamdari, R. Fazel-Rezai, M. Paukkunen, and K. Tavakolian. "Analyzing Seismocardiogram Cycles to Identify the Respiratory Phases." In: *IEEE Transactions on Biomedical Engineering* 64.8 (2017), pp. 1786–1792. ISSN: 0018-9294. DOI: 10.1109/TBME.2016.2621037. URL: http://ieeexplore.ieee.org/document/7707393/.

[94] A. Sapra, A. Malik, and P. Bhandari. "Vital Sign Assessment- PMID: 31985994." In: 2019.

[95] A. Droitcour. "Non-contact measurement of heart and respiration rates with single chip microwave Doppler radar." In: (2006).

[96] M. I. Skolnik. *Radar Handbook, Third Edition*. Electronics electrical engineering. McGraw-Hill Education, 2008. ISBN: 9780071485470. URL: https://books.google.nl/books?id=76uF2Xebm-gC.

[97] M. I. Skolnik. *Introduction to Radar Systems*. Electrical engineering series. McGraw-Hill, 2001. ISBN: 9780071181891. URL: https://books.google.nl/books?id=Y6-APwAACAAJ.

[98] H Nikookar and R Prasad. *Introduction to Ultra Wideband for Wireless Communications*. Signals and Communication Technology. Springer Netherlands, 2008. ISBN: 9781402066337. URL: https://books.google.nl/books?id=6ico-tJpmcYC.

[99] P. Dabove, V. Di Pietra, M. Piras, A. A. Jabbar, and S. A. Kazim. "Indoor positioning using Ultra-wide band (UWB) technologies: Positioning accuracies and sensors' performances." In: *2018 IEEE/ION Position, Location and Navigation Symposium (PLANS)*. IEEE, 2018, pp. 175–184. ISBN: 978-1-5386-1647-5. DOI: 10.1109/PLANS.2018.8373379. URL: https://ieeexplore.ieee.org/document/8373379/.

[100] J. H. Reed. *An Introduction to Ultra Wideband Communication Systems*. Prentice Hall communications engineering and emerging technologies series. Prentice Hall PTR, 2005. ISBN: 9780131481039. URL: https://books.google.nl/books?id=TwgfAQAAIAAJ.

[101] B. Dewberry, S. Huseth, and R. McCroskey. *Pulsed-RF ultrawideband ranging for the GLANSER GPS-denied emergency responder navigation system*. Vol. 1. 2011.

[102] C. Iovescu and S. Rao. "The fundamentals of millimeter wave sensors." In: *Texas Instruments, SPYY005* (2017).

[103] G. Brooker. "Understanding millimetre wave FMCW radars." In: *1st International Conference on Sensing Technology* (2005).

[104] A Christ, A Klingenbock, T Samaras, C Goiceanu, and N Kuster. "The dependence of electromagnetic far-field absorption on body tissue composition in the frequency range from 300 MHz to 6 GHz." In: *IEEE Transactions on Microwave Theory and Techniques* 54.5 (2006), pp. 2188–2195. ISSN: 0018-9480. DOI: 10.1109/TMTT.2006.872789. URL: http://ieeexplore.ieee.org/document/1629062/.

[105] C. G. Rowbottom and S. Webb. "Configuration space analysis of common cost functions in radiotherapy beam-weight optimization algorithms." In: *Physics in Medicine and Biology* 47.1 (2002), pp. 65–77. ISSN: 0031-9155. DOI: 10.1088/0031-9155/47/1/305. URL: https://doi.org/10.1088{\%}2F0031-9155{\%}2F47{\%}2F1{\%}2F305https://iopscience.iop.org/article/10.1088/0031-9155/47/1/305.

[106] B Górka, B Nilsson, J. M. Fernández-Varea, R Svensson, and A Brahme. "Influence of electrodes on the photon energy deposition in CVD-diamond dosimeters studied with the Monte Carlo code PENELOPE." In: *Physics in Medicine and Biology* 51.15 (2006), pp. 3607–3623. ISSN: 0031-9155. DOI: 10.1088/0031-9155/51/15/001. URL: https://doi.org/10.1088{\%}2F0031-9155{\%}2F51{\%}2F15{\%}2F001https://iopscience.iop.org/article/10.1088/0031-9155/51/15/001.

[107] E. Pancera. "Medical applications of the Ultra Wideband technology." In: *2010 Loughborough Antennas & Propagation Conference*. IEEE, 2010, pp. 52–56. ISBN: 978-1-4244-7304-5. DOI: 10.1109/LAPC.2010.5666802. URL: http://ieeexplore.ieee.org/document/5666802/.

[108] O Aardal, Y Paichard, S Brovoll, T Berger, T. S. Lande, and S.-E. Hamran. "Physical Working Principles of Medical Radar." In: *IEEE Transactions on Biomedical Engineering* 60.4 (2013), pp. 1142–1149. ISSN: 0018-9294. DOI: 10.1109/TBME.2012.2228263. URL: http://ieeexplore.ieee.org/document/6357226/.

[109] E. Staderini. "UWB radars in medicine." In: *IEEE Aerospace and Electronic Systems Magazine* 17.1 (2002), pp. 13–18. ISSN: 08858985. DOI: 10.1109/62.978359. URL: http://ieeexplore.ieee.org/document/978359/.

[110] *X4 - Datasheet*. Novelda AS. 2017.

[111] *IWR1843 Single-Chip 76- to 81-GHz FMCW mmWave Sensor datasheet*. SWRS228. Texas Instruments. 2019.

[112] H. A. Hjortland, D. T. Wisland, T. S. Lande, C. Limbodal, and K. Meisal. "Thresholded samplers for UWB impulse radar." In: *2007 IEEE International Symposium on Circuits and Systems*. IEEE, 2007, pp. 1210–1213. ISBN: 1-4244-0920-9. DOI: 10.1109/ISCAS.2007.378326. URL: http://ieeexplore.ieee.org/document/4252861/.

[113] N. Andersen et al. "A 118-mW Pulse-Based Radar SoC in 55-nm CMOS for Non-Contact Human Vital Signs Detection." In: *IEEE Journal of Solid-State Circuits* 52.12 (2017), pp. 3421–3433. ISSN: 0018-9200. DOI: 10.1109/JSSC.2017.2764051. URL: https://ieeexplore.ieee.org/document/8106658/.

[114] M. H. Weik. "Nyquist theorem." In: *Computer Science and Communications Dictionary*. Boston, MA: Springer US, 2000, pp. 1127–1127. ISBN: 978-1-4020-0613-5. DOI: 10.1007/1-4020-0613-6_12654. URL: https://doi.org/10.1007/1-4020-0613-6{_}12654http://link.springer.com/10.1007/1-4020-0613-6{_}12654.

[115] R. Lyons. "Quadrature signals: complex, but not complicated." In: ().

[116] *Novelda AS*. XeThru Sensor Emissions. 2016.

[117] D. M. Mark Frimann. *EU Declaration of Conformity*. Texas Instruments. Texas, USA, 2019.

[118] G. van Rossum and F. L. Drake. *The Python Language Reference Manual*. Network Theory Ltd., 2011. ISBN: 1906966141. DOI: 10.5555/2011965.

[119] P. H. Charlton, M. Villarroel, and F. Salguiero. "Waveform Analysis to Estimate Respiratory Rate." eng. In: *Secondary Analysis of Electronic Health Records*. Cham: Springer International Publishing, 2016, pp. 377–390. ISBN: 978-3-319-43740-8. DOI: 10.1007/978-3-319-43742-2_26. URL: http://link.springer.com/10.1007/978-3-319-43742-2{_}26.

[120] I. Antelmi, R. S. De Paula, A. R. Shinzato, C. A. Peres, A. J. Mansur, and C. J. Grupi. "Influence of age, gender, body mass index, and functional capacity on heart rate variability in a cohort of subjects without heart disease." In: *The American Journal of Cardiology* 93.3 (2004), pp. 381–385. ISSN: 0002-9149. DOI: https://doi.org/10.1016/j.amjcard.2003.09.065. URL: http://www.sciencedirect.com/science/article/pii/S0002914903015054.

[121] R. Herzi, H. Zairi, and A. Gharsallah. "Antipodal Vivaldi antenna array with reduced mutual coupling for UWB radar applications." In: *2014 15th International Conference on Sciences and Techniques of Automatic Control and Computer Engineering (STA)*. IEEE, 2014, pp. 1024–1027. ISBN: 978-1-4799-5907-5. DOI: 10.1109/STA.2014.7086789. URL: http://ieeexplore.ieee.org/document/7086789/.

[122] A. Mesaros, T. Heittola, and T. Virtanen. "Metrics for Polyphonic Sound Event Detection." In: *Applied Sciences* 6.6 (2016), p. 162. ISSN: 2076-3417. DOI: 10.3390/app6060162. URL: http://www.mdpi.com/2076-3417/6/6/162.

[123] A. Alba, M. O. Mendez, M. E. Rubio-Rincon, and E. R. Arce-Santana. "A consensus algorithm for approximate string matching and its application to QRS complex detection." In: *International Journal of Modern Physics C* 27.03 (2016), p. 1650029. ISSN: 0129-1831. DOI: 10.1142/S0129183116500297. URL: https://www.worldscientific.com/doi/abs/10.1142/S0129183116500297.

[124] B. Wiechern, K. A. Liberty, P. Pattemore, and E. Lin. "Effects of asthma on breathing during reading aloud." In: *Speech, Language and Hearing* 21.1 (2018), pp. 30–40. ISSN: 2050-571X. DOI: 10.1080/2050571X.2017.1322740. URL: https://www.tandfonline.com/doi/full/10.1080/2050571X.2017.1322740.

[125] B.-K. Park, O. Boric-Lubecke, and V. M. Lubecke. "Arctangent Demodulation With DC Offset Compensation in Quadrature Doppler Radar Receiver Systems." In: *IEEE Transactions on Microwave Theory and Techniques* 55.5 (2007), pp. 1073–1079. ISSN: 0018-9480. DOI: 10.1109/TMTT.2007.895653. URL: http://ieeexplore.ieee.org/document/4195675/.

[126] F. Khan and S. Cho. "A Detailed Algorithm for Vital Sign Monitoring of a Stationary/Non-Stationary Human through IR-UWB Radar." In: *Sensors* 17.2 (2017), p. 290. ISSN: 1424-8220. DOI: 10.3390/s17020290. URL: http://www.mdpi.com/1424-8220/17/2/290.

[127] H. Idsoe, L. R. Cenkeramaddi, B. B. Lozano, and J Soumya. "Phase-noise Impact on the Performance of mmWave-radars." In: *2019 IEEE International Conference on Advanced Networks and Telecommunications Systems (ANTS)*. IEEE, 2019, pp. 1–6. ISBN: 978-1-7281-3715-5. DOI: 10.1109/ANTS47819.2019.9117975. URL: https://ieeexplore.ieee.org/document/9117975/.

[128] *XeThru X4 Phase Noise Correction*. SA Novelda. 2018.

[129] M. R. Khanzadi, A. Panahi, D. Kuylenstierna, and T. Eriksson. "A model-based analysis of phase jitter in RF oscillators." In: *2012 IEEE International Frequency Control Symposium Proceedings*. IEEE, 2012, pp. 1–4. ISBN: 978-1-4577-1820-5. DOI: 10.1109/FCS.2012.6243677. URL: http://ieeexplore.ieee.org/document/6243677/.

[130] A. Gadiyar, K. Subburaj, and S. Bhatara. "Self-Calibration in TI's mmWave Radar Devices (app note)." In: (2018). URL: https://www.ti.com/lit/an/spracf4/spracf4.pdf?ts=1606898788276{\&}ref{_}url=https://www.ti.com/product/AWR1843.

[131] K. Shi et al. "Contactless Carotid Pulse Measurement Using Continuous Wave Radar." In: *2018 Asia-Pacific Microwave Conference (APMC)*. IEEE, 2018, pp. 569–571. ISBN: 978-4-9023-3945-1. DOI: 10.23919/APMC.2018.8617522. URL: https://ieeexplore.ieee.org/document/8617522/.

[132] C. Gouveia, J. Vieira, and P. Pinho. "A Review on Methods for Random Motion Detection and Compensation in Bio-Radar Systems." eng. In: *Sensors* 19.3 (2019), p. 604. ISSN: 1424-8220. DOI: 10.3390/s19030604. URL: http://www.mdpi.com/1424-8220/19/3/604.

[133] M. Elliott. "Why is Respiratory Rate the Neglected Vital Sign? A Narrative Review." In: *International Archives of Nursing and Health Care* 2.3 (2016), pp. 1–4. ISSN: 24695823. DOI: 10.23937/2469-5823/1510050. URL: https://clinmedjournals.org/articles/ianhc/international-archives-of-nursing-and-health-care-ianhc-2-050.php?jid=ianhc.

Appendix A

Tables

Appendix A presents the tables with the metrics extracted from cardiorespiratory radar signals and described in Chapter 6: Event-Based Respiratory Classification, Respiratory Rate Estimation and Heartbeat Rate Estimation.

Table A.1 presents all the metrics extracted from the event-based classification described in Subsection 5.7.2: the total number of real (REAL) events from audio reference, estimated (EST) events detected by the peak finding algorithm and the total number of True Positive (TP), False Positive (FP) and False Negative (FN) metrics obtained per recording (Subject + Range + Radar).

Table A.2 shows the reference (REF) and estimated (EST) respiratory rate (RR) values obtained applying M1 and M2 methods to R1 and R2 radar signals. M1 and M2 methods were described in Subsections 5.7.3.1 and 5.7.3.2, respectively. Absolute Error (AE) between reference and estimated values per recording is also shown.

Table A.3 shows the reference (REF) and estimated (EST) heart rate (HR) values obtained applying M1 and M2 methods to R1 and R2 radar signals. M1 and M2 methods were described in Subsections 5.8.2.1 and 5.8.2.2, respectively. Absolute Error (AE) between reference and estimated values per recording is also shown.

Table A.1: Event-based respiratory classification results.

		R1					R2				
Subject	Range (m)	REAL	EST	FP	FN	TP	REAL	EST.	FP	FN	TP
S1	2.5	12	12	0	0	12	13	13	0	0	13
	1.0	12	12	0	0	12	12	12	0	0	12
	0.5	12	12	0	0	12	12	12	0	0	12
S2	2.5	11	9	0	2	9	9	9	1	1	8
	1.0	10	10	0	0	10	12	12	0	0	12
	0.5	8	9	1	0	8	10	10	0	0	10
S3	2.5	9	9	0	0	9	10	10	0	0	10
	1.0	11	11	0	0	11	11	11	0	0	11
	0.5	11	11	0	0	11	11	11	1	1	10
S4	2.5	12	12	0	0	12	9	8	1	2	7
	1.0	6	5	0	1	5	6	7	2	1	5
	0.5	8	8	0	0	8	11	11	0	0	11
S5	2.5	9	9	0	0	9	9	9	0	0	9
	1.0	10	10	0	0	10	10	9	6	7	3
	0.5	11	11	0	0	11	8	10	2	0	8
S6	2.5	9	10	1	0	9	11	10	1	2	9
	1.0	12	12	0	0	12	9	10	1	0	9
	0.5	12	12	0	0	12	9	9	0	0	9
S7	2.5	9	9	0	0	9	9	13	6	2	7
	1.0	7	7	0	0	7	8	8	0	0	8
	0.5	12	12	0	0	12	10	10	1	1	9
S8	2.5	15	15	0	0	15	15	8	1	8	7
	1.0	14	14	0	0	14	14	14	0	0	14
	0.5	16	16	0	0	16	14	14	0	0	14
S9	2.5	9	9	0	0	9	7	8	1	0	7
	1.0	8	8	0	0	8	9	10	1	0	9
	0.5	9	9	0	0	9	9	9	0	0	9
S10	2.5	9	9	0	0	9	11	11	0	0	11
	1.0	11	11	0	0	11	10	10	0	0	10
	0.5	9	9	0	0	9	11	11	1	1	10
Total		313	312	2	3	310	309	309	26	26	283

Table A.2: Estimated Respiratory Rate (RR) results.

		R1 (RPM)					R2 (RPM)				
			M1		M2			M1		M2	
Subj.	Range(m)	REF	EST	AE	EST	AE	REF	EST	AE	EST	AE
S1	2.5	17	17	0	17	0	20	20	0	18	2
	1.0	19	19	0	19	0	19	19	0	18	1
	0.5	20	20	0	18	2	18	18	0	17	1
S2	2.5	16	15	1	15	1	14	14	0	12	2
	1.0	16	16	0	14	2	18	18	0	17	1
	0.5	12	13	1	14	2	15	15	0	15	0
S3	2.5	14	13	1	12	2	15	15	0	14	1
	1.0	17	16	1	17	0	17	17	0	15	2
	0.5	17	18	1	17	0	17	17	0	15	2
S4	2.5	18	18	0	18	0	14	13	1	11	3
	1.0	9	10	1	12	3	8	10	2	14	6
	0.5	11	11	0	15	4	17	17	0	14	3
S5	2.5	14	14	0	12	2	14	13	1	12	2
	1.0	15	15	0	14	1	15	13	2	12	3
	0.5	16	16	0	14	2	13	17	4	12	1
S6	2.5	15	16	1	12	3	16	15	1	15	1
	1.0	18	18	0	17	1	14	15	1	17	3
	0.5	18	18	0	17	1	14	14	0	11	3
S7	2.5	14	14	0	14	0	14	19	5	18	4
	1.0	12	11	1	11	1	12	12	0	11	1
	0.5	18	18	0	17	1	15	15	0	18	3
S8	2.5	22	22	0	21	1	23	13	10	20	3
	1.0	20	21	1	20	0	21	21	0	18	3
	0.5	26	25	1	23	3	22	22	0	20	2
S9	2.5	14	14	0	14	0	11	12	1	9	2
	1.0	13	13	0	12	1	14	15	1	14	0
	0.5	14	14	0	12	2	14	13	1	12	2
S10	2.5	14	14	0	12	2	16	16	0	15	1
	1.0	16	16	0	15	1	16	16	0	14	2
	0.5	13	13	0	11	2	17	18	1	14	3

AE: Absolute Error (RPM)

Table A.3: Estimated Heart Rate (HR) results.

		R1 (BPM)					R2 (BPM)				
			M1		M2			M1		M2	
Subj.	Range(m)	REF	EST	AE	EST	AE	REF	EST	AE	EST	AE
S1	2.5	89	85	4	88	1	89	87	2	N	-
	1.0	92	83	9	84	8	94	88	6	86	8
	0.5	91	85	6	88	3	90	92	2	90	0
S2	2.5	76	80	4	73	3	79	88	9	N	-
	1.0	76	76	0	N	-	71	83	12	71	0
	0.5	73	77	4	73	0	70	72	2	68	2
S3	2.5	74	78	4	N	-	75	81	6	N	-
	1.0	70	80	10	70	0	73	75	2	67	6
	0.5	71	84	13	71	0	72	81	9	N	-
S4	2.5	84	85	1	83	1	83	85	2	83	0
	1.0	84	83	1	85	1	84	83	1	84	0
	0.5	83	83	0	85	2	83	83	0	84	1
S5	2.5	71	81	10	65	6	72	82	10	N	-
	1.0	70	75	5	N	-	73	78	5	72	1
	0.5	73	76	3	73	0	72	77	5	70	2
S6	2.5	77	82	5	N	-	84	88	4	84	0
	1.0	78	83	5	N	-	79	83	4	80	1
	0.5	78	87	9	N	-	81	82	1	83	2
S7	2.5	80	82	2	76	4	83	87	4	81	2
	1.0	82	79	3	N	-	83	81	2	85	2
	0.5	83	68	15	N	-	83	91	8	79	4
S8	2.5	61	88	27	N	-	66	84	18	N	-
	1.0	66	79	13	N	-	68	77	9	68	0
	0.5	66	80	14	N	-	67	78	11	67	0
S9	2.5	73	82	9	70	3	73	83	10	77	4
	1.0	75	78	3	75	0	71	76	5	69	2
	0.5	71	76	5	71	0	72	74	2	71	1
S10	2.5	86	85	1	N	-	86	86	0	N	-
	1.0	85	78	7	N	-	87	84	3	N	-
	0.5	85	77	8	N	-	89	88	1	N	-

AE: Absolute Error (BPM) N: NULL

Appendix B

Research Methodology Flow-Chart

In this dissertation, signal processing methods for the acquisition, analysis and extraction of cardiorespiratory parameters, acquired with two different radars, were described in Chapter 4 and Chapter 5. Regardless of the programming systems used for radar signals processing (inline embedded on radars chips or offline using python environment), all the employed methods can be grouped in a general signal processing chain reported in Figure B.1. Although the first signal processing methods were applied in an embedded environment, those can be replicated in offline processing. The same is valid for the methods applied in offline mode, which can also be implemented in embedded platforms. Hence, this flow-chart diagram aims to give an overview of the developed work, helping readers and facilitating the replication of this work in future studies.

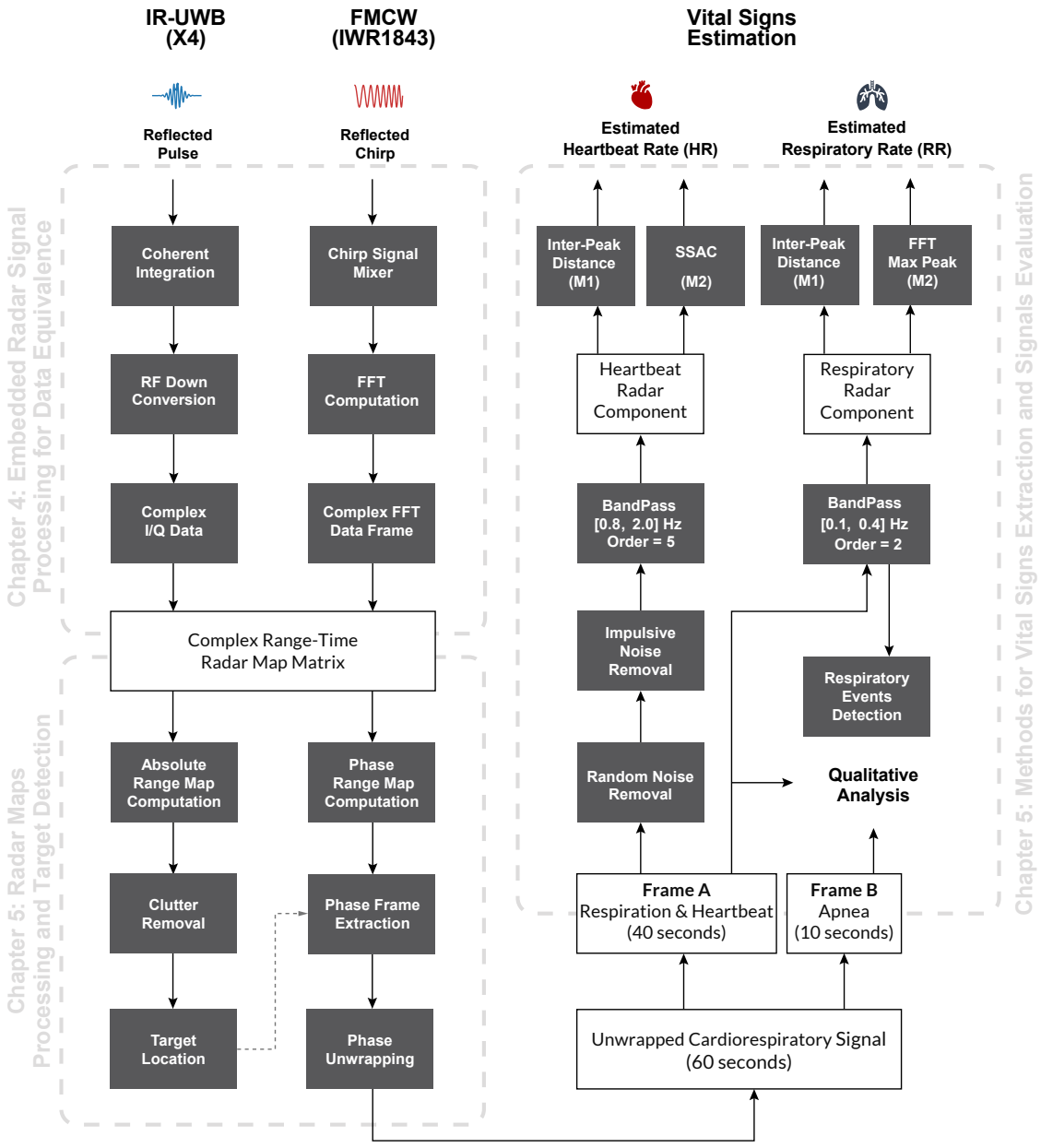

Figure B.1: General flow-chart diagram of the signal processing techniques developed and employed in methodology. Dark boxes are signal processing methods, white boxes represent data structures resulted from applied methods, and dashed grey boxes informs where these steps were described in the document.

Appendix C

Short Commercial Report

The choice of what radar could be used in a commercial product should not be based only on their performance, but also on other key factors. Figure C.1 resumes the weighting factors that were taken into account in this commercial analysis. Individual sensor parameters can be reviewed on Chapter 4. The checkmark (✓) means an advantage that one sensor has about each other and the line (-) means a parameter that should be taken into account during the product life cycle but from which no relevant conclusion was achieved.

	Performance	Range	Antennas	Intelligence	Autonomy	Price	Support	Certification
X4 IR-UWB	✓	✓			✓			—
IWR1843 FMCW			✓	✓		✓	✓	—

Figure C.1: Commercial comparison between the key factor of each radar.

Perfomance: This study proved that both sensors are capable of monitoring cardiorespiratory activity up to a distance of 2.5 meters. However, FMCW presented a lower performance compared to IR-UWB. Notwithstanding, FMCW accuracy may be improved in the future with the development of more specialized algorithms for FMCW operation mode and type of data returned.

Range: Is is a metric correlated to the resolution that each sensor can support. Undoubtedly, IR-UWB wins in this criteria. A good radar resolution allows for better target tracking. Otherwise, this feature can add more value to the product, since the radar can

be exclusively used for human target detection, and also used for multi-target vital signs sensing.

Antennas: An important component that can have a more significant influence in the quality of the TX and RX radar signal, and the size of the final product. The FMCW chip used in this application is advantageous in this aspect since it integrates multiple TX/RX antennas pairs against a unique pair in the IR-UWB chip used. MIMO antennas, allow signals to be emitted and recognised from multiple directions providing extra functionalities to the radar, for example as accurate angle measurements for localization. Additionally, the FMCW sensor antennas are relatively smaller than IR-UWB sensors due to the shorter wavelength, allowing for a more ergonomic and discrete product.

Intelligence (or Processing Power): The double MCU incorporated in the FMCW sensor allows the possibility of making all the signal processing inside the chip which can be very useful in real-time monitoring application or logging applications, since data can be processed in real-time before being sent to the main MCU. In fact, a part of these capabilities was already used in this study, where FFT-range computation was done inside the chip. In the contrast, IR-UWB have a unique and less potent MCU that is mainly used for the transmission of data.

Autonomy: This parameter is related to the power of devices. In the future, the radar should be fully wireless, and an external battery should be added to power the radar. Therefore, this value should be taken into account when choosing between the two radars. The size and autonomy of the module will depend on the battery size, with longer autonomy devices will needing larger batteries with bigger sizes, leading to larger modules.

Price: This parameter is perhaps the second most important, after radar performance, when choosing any component for a product. The IR-UWB (X4) costs 4 times more than FMCW (IWR1843). Notwithstanding, this price is summed to the costs of all extra modules that will be needed to be incorporated, such as antennas, PCB, enclosure and others.

Certification: As configurable RF devices both radars must comply with the regulation needs, regardless of the sensor used. These rules are defined by regulatory bodies (e.g. ETSI, FCC) in specified zones of the world and therefore, some frequencies allowed in some regions are prohibited in others. This is a fact that may have an influence in the choice of commercial radars since the choice of a not universal radar frequency band, limits the market size.

Support: is the last but not the least. The primary seller of the chip should be taken into consideration since it is an essential factor when using a module for the first time

during the development of new product. Household brands often have a bigger support network, which can be very useful. In this field, Texas Instruments is a more prominent company, with larger experience and support than the most recent Xenthru.

It is important to notice that this analysis is not about the operation modes used by radar since the features added depends on the manufacturing branding and models design. Thus, the points discussed above are comparing the features of the off-the-shelf radar used (X4 and IWR) and not their technology. In fact, a direct comparison between the commercial use of general IR-UWB or FMCW radars is not possible due to the wide range of variables that these can feature such as different frequencies, different antennas, different hardware architectures etc.

Hence, considering all the above parameters, for a single application, Texas Instruments could be considered as the best option for the new PLUX Bio-Radar, mainly because of its lower price and better support.

APPENDIX D

WIRELESS BIO-RADAR: A FIRST CONCEPT

One of the biggest motivations for the development of this work was the idea of implementing a future and completely innovator Wireless Bio-Radar system, based on the algorithms developed and results achieved in this dissertation. One of the initial appointed problems was the uncertainties about the viability of transmitting large amounts of radar data through a wireless protocol. Thus, to show the viability of this concept, a small prototype was developed using low-cost materials and signal processing techniques developed in this work. A brief overview of the implemented methods used in the development of this fully wireless bio-radar sensor is given below.

D.1 Materials and Hardware Components Integration

For the development of this system the following material were used:

- X4M03 IR-UWB Radar;
- HC-05 Bluetooth Module;
- LiPo Battery;
- Genuino Board;
- Breadboard and Jump Wires.

The HC-05 module is a very low-cost component commonly used for *Arduino* applications and learning. For fast prototyping, this module was adapted to communicate with X4M03 board via UART. A brief description of this process is given below:

X4M03 Setup: As mentioned before in Chapter 4, the XEP firmware allows communications via USB (default mode and previously used in this study) and UART. Since HC-05 uses this last protocol to transmit data, the XEP firmware was used in UART mode where IR-UWB radar was interfaced with the BLE module, using the standard serial pins connectors: TX, RX, GND and VCC. Moreover, additional pins were needed to be set as HIGH (logical level) for UART mode activation by XEP. All the pins connections for UART mode can be easily found in X4M03 and XEP documentation. Another important value to take into account is the velocity of data transmission. XEP is set with a default baud rate value of 115200 that was maintained for this application.

HC-05 Setup: HC-05 embedded Bluetooth module was configured by default, with a baud rate of 9600. For the correction transmission and reception of serial data between radar and host system, the HC-05 and the X4M03 must be set with the same baud rate values. Hence, it was decided to adapt the HC-05 baud rate to XEP default baud rate value of 115200. The choice of configuring HC-05 and not X4M03 was made for two main reasons: first, a baud rate of 9600 is not fast enough to transmit all the raw data sent from radar at the desired transmission speed, second, since HC-05 is a very popular and user-friendly module, the reprogramming of this parameters is easier than in X4M03, which requires complex modifications of XEP code. Moreover, as 115200 is sufficient to transmit all the necessary radar data, there is no problem in maintaining this value. Finally, for the configuration of HC-05 baud rate, a *Genuino* Board and default open-source libraries developed for HC-05 module by Arduino community were used - see Figure D.1 (a). At last, all the schema of wireless radar sensor was mounted in a breadboard for preliminary tests - Figure D.1 (b).

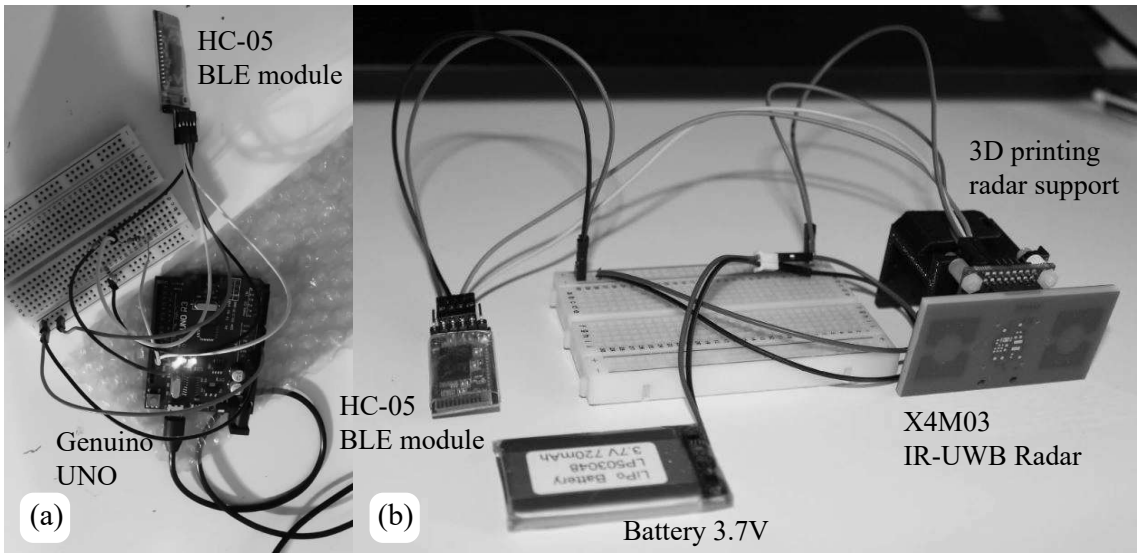

Figure D.1: Experimental setup used to configure and integrate bluetooth and radar modules: (a) Setting baud rate of HC-05 with a genuino board and (b) Experimental setup of the full wireless Bio-Radar developed system.

Data transmission and communication with the host system: After the integration of modules, the BLE module should be paired with the host system (a computer). For communication and configuration of X4, the same python function developed in Subsection 4.2.3 was used. This is only possible due to the XEP firmware used, which allows the use of the same APIs commands using either USB or UART protocols. Notwithstanding, this new setup imposes some restrictions in the amount of transferred data that should be balanced between the number of data bits emitted the radar per second and the baud rate used. In this application, the X4 was set to output frame data in a range frame of 0.5 to 3.0 meters at 10 FPS.

Black Box Finally, the components of the wireless set tested and presented in Figure D.1, were placed inside a small box simulating a fully wireless bio-radar system.

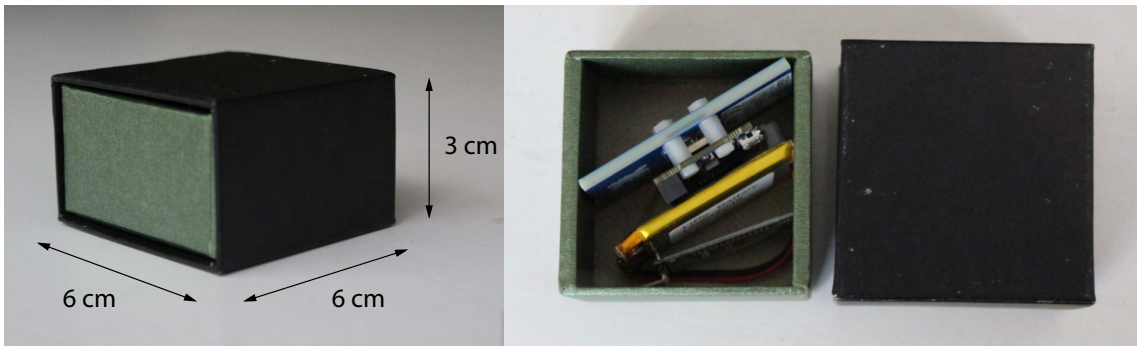

Figure D.2: Wireless bio-radar black box. Components inside the box are not wired for a better visualization of elements arrangement inside the small box.

D.2 Real-Time Algorithm

Considering the analysis made in Subsection 6.2, the respiratory patterns can also be easily observed in the amplitude of X4 data. Hence, to simplify the real-time signal processing methods used in this wireless application, the amplitude of signals was used to track the respiratory radar signals in time-domain. Additionally, target location and respiratory rate (RR) estimation were also computed over time. Once again, the extraction of the RR parameter was based in one of the development methods of this study: the spectral analysis using the FFT method.

Hence, a recursive spectral method was used, where FFT computations are made over the slow-time direction of dynamic matrices containing the last 60-seconds frames emitted by the radar. This process is very common in radar applications being known as *pulse-doppler processing*. From this radar-doppler matrices, the maximum peak could be used to obtain information about the target location and the respiratory frequency of this target.

D.3 Results

Finally, joining the two above described methods, enabled the development of the wireless bio-radar, which is demonstrated in Figure D.3. As illustrated in this figure, this wireless bio-radar is acquiring physiological signals, when the person is reading a book. This could be one of the possible applications of the developed bio radar, suited for occasions that involve little body movements. Once again, this radar prototype was exclusively projected with the topics studied in this dissertation, showing the utility of the developed methods and results achieved for the development of more complex bio-radar systems in the future.

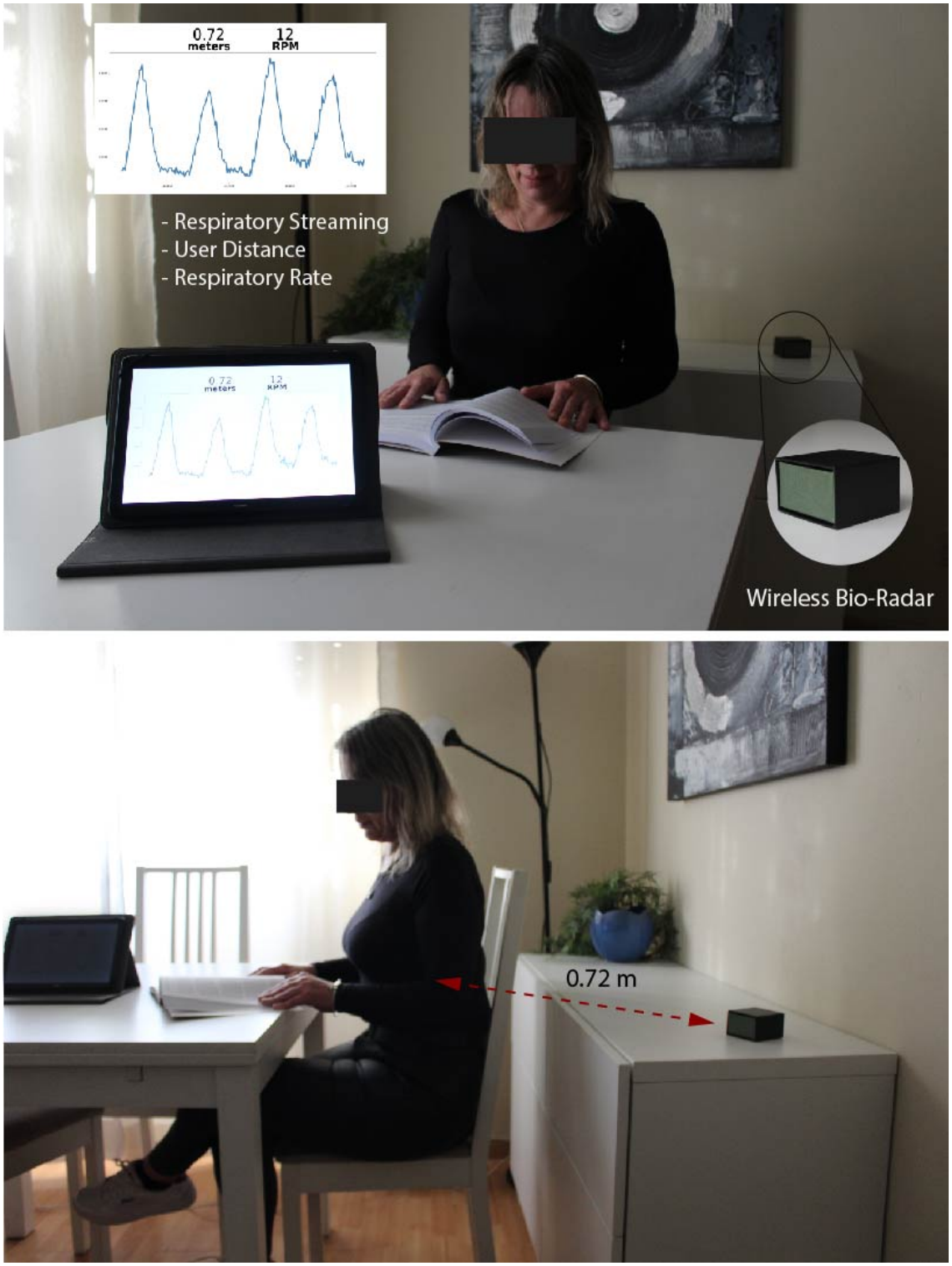

Figure D.3: Developed wireless bio-radar prototype in a home-monitoring scenario. The transmission of data between radar and interface is fully wireless. Due to the reduced dimensions of the sensors and their capacities to see through objects, radars could be used in the future as contactless vital signs monitoring tools inserted in discrete environments.